Functional molecular imaging of cancer development and stem cell regeneration in the nervous system

van Rijn, S.

2016

document version
Publisher's PDF, also known as Version of record

FUNCTIONAL MOLECULAR IMAGING OF CANCER DEVELOPMENT AND STEM CELL REGENERATION IN THE NERVOUS SYSTEM

Sjoerd van Rijn

ISBN: 978-94-6182-638-1
Layout and printing: Off Page, www.offpage.nl
Cover design by Sjoerd van Rijn

VRIJE UNIVERSITEIT

FUNCTIONAL MOLECULAR IMAGING OF CANCER DEVELOPMENT AND STEM CELL REGENERATION IN THE NERVOUS SYSTEM

ACADEMISCH PROEFSCHRIFT

ter verkrijging van de graad Doctor aan
de Vrije Universiteit Amsterdam,
op gezag van de rector magnificus
prof.dr. V. Subramaniam,
in het openbaar te verdedigen
ten overstaan van de promotiecommissie
van de Faculteit der Geneeskunde
op dinsdag 19 januari 2016 om 15.45 uur
in de aula van de universiteit,
De Boelelaan 1105

door

Sjoerd van Rijn

geboren te Leiden

promotor	prof.dr. W.P. Vandertop
copromotoren	prof.dr. T. Würdinger dr. D.P. Noske

TABLE OF CONTENTS

1

FUNCTIONAL MOLECULAR IMAGING OF CANCER DEVELOPMENT AND STEM CELL REGENERATION IN THE NERVOUS SYSTEM

INTRODUCTION

Because of the complexity, plasticity and heterogeneity of malignant brain tumors such as glioblastoma and medulloblastoma, successful treatment of patients remains a challenge. While the 5-years' survival of medulloblastoma is around 60% in adults and 75% in children, these patients do suffer from treatment-related side effects (*1*). Glioblastoma patients usually die within 18 months after diagnosis, despite optimal surgery, followed by chemoradiation therapy (*2*).

In order to improve the treatment of brain tumors, we need to improve our understanding of their basic biology and to identify the molecular mechanisms that underlie brain tumor formation and initiation. Functional bioluminescence imaging is a tool that is able to study molecular regulatory processes in cells (*3*). We aimed to adapt this tool to image and quantify tumor heterogeneity and brain tumor cells in order to discover novel molecular pathways. In addition, we explored the possibility of using this method for the imaging of normal stem cell regeneration, using an explant model of spinal degeneration.

BRAIN TUMORS

Glioblastoma multiforme

In The Netherlands, almost 1000 patients per year present themselves with a malignant glioma. Until now, gliomas where classified according to a World Health Organization (WHO) classification system based on classical phenotypic characteristics as observed in microscopic Hematoxilin-Eosin stained tissue sections (*4*). Adult gliomas have an incidence of 1000-1200 patients per year in The Netherlands of which glioblastoma multiforme (GBM), a WHO grade IV glioma, is the most common type (60% of gliomas). Glioblastoma therapy consists of surgery followed by radiotherapy and temozolomide chemotherapy, and increases life expectancy with 2-3 months (*2*) to a median survival of approximately 14.6 months and a two-years' survival of 30% (*2*). Glioblastomas also arise in children, be it far less frequently, and are histologically indistinguishable from their adult counterparts, although they tend to do better than adults with a five-years' survival of 25%. Despite this histological similarity, the genetic background of pediatric glioblastoma is often very different (*5*).

In recent years, molecular classification has become more important as tumors are increasingly being classified by their genetic profile. Using genetic profiling, it has become clear that glioblastoma multiforme can be classified into four subtypes: The classical, mesenchymal, proneural and neural subtype (*6*). This has led to targeted therapies arising from functional analysis of cellular gene expression and protein contents (*7–10*).

The molecular heterogeneity of glioblastoma may be the result of the transformation of aberrant neural precursor cells that function as brain cancer stem cells (*11*) or of dedifferentiation of cancerous glial cells or neurons (*12*). The clonal evolution of these mutated neural stem cells results in heterogeneous glioblastomas in which cells of all subtypes of GBM can arise (*13*). Despite recent advances in our knowledge of

the molecular mechanisms of glioblastoma and its oncogenesis, there is still a need for tools to study functional and molecular tumor biology. Increased molecular understanding of glioblastoma can provide us with better treatment modalities.

Medulloblastoma

While glioblastoma is the most common brain malignancy in adults, medulloblastoma tops the ranking of most common malignant brain tumor in children with a five-years' survival rate between 50% and 80%, depending on the subtype (*14*). This tumor originates in the cerebellum, often near the fourth ventricle. Common treatment includes surgery, radiotherapy and chemotherapy, but the relatively hopeful survival rates are overshadowed by complications and long-term sequelae which significantly reduce the quality of life (*15*). Currently medulloblastomas are classified based on their morphology and histopathology, such as desmoplastic or nodular medulloblastoma, MBEN (medulloblastoma with extensive nodularity) or classic, large cell and anaplastic medulloblastoma (*1*). However recently, molecular investigations of medulloblastoma have resulted in a molecular classification into four subgroups: a Wnt gene pathway associated subgroup (Wnt group), a Sonic Hedge hock gene (Shh) pathway associated subgroup (Shh group), a subgroup containing MYC gene amplifications and photoreceptor/GABAergic gene expression (group 3), and a subgroup which has MYCN/CDK6 gene amplifications and neuronal or glutamatergic gene expression (group 4) (*1*). These molecular subgroups have different clinical outcomes and react distinctively different to current treatment modalities. It is therefore, a necessity to further analyze these subgroups independently to improve outcome. As with glioblastoma, it is currently unknown whether these subgroups also arise from distinct subsets of progenitor cells.

STEM CELLS AND TISSUE REGENERATION

Stem cells

Stem cells are undifferentiated cells that have the capability to divide limitless and to self-renew while the undifferentiated state is maintained (*16*). Stem cells therefore, play a role in development and in tissue repair and regeneration, and are invaluable for the maintenance of life. The most fundamental stem cells are totipotent zygotes and have the capacity to eventually differentiate into all types of cells that are necessary for the embryonic development. These stem cells are often referred to as embryonic stem cells. When pluripotent stem cells further differentiate, they form multipotent stem cells that are dedicated to form cells that are derived of one germ layer. When multipotent cells lose the capacity of unlimited growth, they are referred to as progenitor cells (*17*). Multipotent progenitor cells are often referred to as adult or somatic stem cells and their function is to replenish dying cells or to regenerate damaged tissues.

Stem cells can either divide symmetrically, for self-renewal and maintenance of the stem cell pool, or divide asymmetrically to form a daughter cell that can differentiate

into a more specialized precursor of tissues. The bone marrow is an important source of stem cells. It contains hematopoietic stem cells that are the progenitor cells of all types of blood cells and it contains mesenchymal stem cells that have the potential to differentiate in chondrocytes, adipocytes or osteoblasts. There are many indications that a population of these bone marrow-derived mesenchymal stem cells may be able to replenish many types of cells after damage, such as muscle tissue, liver hepatocytes, lung tissue and neural cells (*18*).

Stem cell tissue regeneration

As mentioned previously, stem cells have the ability to self renew and differentiate to regenerate damaged tissues. Depending on the stem cell origin, they can differentiate into a specific cell type. Embryonic stem cell transplantation in rats has shown to assist in repair of spinal cord injuries (*19*)(*20*). With the identification of adult stem cells, the use of embryonic stem cells, which are difficult to obtain, was circumvented. Adult stem cells are populations of multipotent stem cells that can be found in almost all tissues, and mesenchymal stem cells can be easily obtained from adipose tissue and bone marrow (*21*, *22*). Adipose-derived mesenchymal stem cells have been shown to restore heart function, to form osteoid tissue, the precursor tissue of bone formation, and to produce cartilage matrix molecules, suggesting potential restoration of cartilage tissue, making it a promising novel therapy for chronic low back pain due to age-related intervertebral disc degeneration (*23*)(*24*)(*25*)(*26*).

Cancer stem cells

Accumulation of genetic aberrations in differentiated cells does not result in tumor formation unless the cells regain their self-renewal potential. One strategy to obtain this capacity is to transform towards a more stem-like type of cell: the cancer stem cell. After consecutive genetic aberrations, epithelial cells can transform towards a mesenchymal cell genotype and phenotype showing expression of stem cell markers (Mani et al., 2008). In essence, tumor cells have the potential to revert from differentiated, more specialized cells towards a more primordial cancer stem cell type with unlimited renewal capacity and a more dynamic, adaptable genotype and phenotype.

Cancer stem cells have been identified in multiple types of tumors and recently it has become clearer that they contribute to increased drug and radiation resistance, and tumor progression and recurrence after surgical resection (*28*). It has been proposed that gliomas arise from dedifferentiation of glia cells, or from undifferentiated neural progenitor cells (*12*, *29*). Early glioblastoma development analysis suggests that they arise in the subventricular zone, where the neural progenitors reside.

There is still debate about the actual existence of cancer stem cells or about the specifications, differences and similarities between cancer stem cells and other cancer cells (*30*). Despite this debate recent research reveals that also in tumors, like in other tissues, differentiated cells can regain stem cell markers and properties such as self-

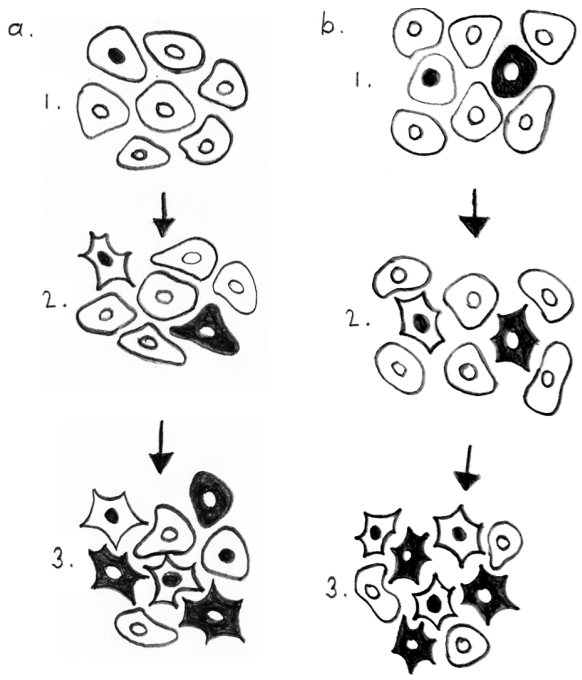

Figure 1. Tumor heterogeneity can be the result of individual cells obtaining mutations and aberrations of time or of different cancer stem cells, each producing different tumor cells. a: Clonal selection theory: A cell obtains mutations and aberrations and proliferates (1.). Over time, each individual cell obtains more, exclusive aberrations (2.) providing a selection advantage for certain cells and resulting in a heterogeneous tumor that contains many different tumor cells (3.). b: Cancer stem cell theory: Self renewing stem cells might obtain aberrations (1.) resulting in cell tumorigenic stem cells (2.). The cancer stem cells proliferate and each cancer stem cell provides bulk tumor cells of a single type, resulting in heterogeneous tumors (3.). Tumorigenesis is most like a result of a combination of both theories.

renewal. Only recently it has been shown that tumor cells can switch between the epithelial state and the stem-like mesenchymal state (*31*).There are also indications that the cancer stem cell population that resides in a tumor could contain a drug-resistant stem cell that repopulates the tumor after initial drug-mediated tumor regression. It is not yet resolved whether resistant cells are present in heterogeneous tumors or whether stem cells acquire resistance after drug treatment but it is speculated that stem cells are more quiescent and therefore less affected by growth-inhibiting drugs (*32*).

FUNCTIONAL MOLECULAR IMAGING

Bioluminescence and fluorescence

Molecular imaging techniques such as bioluminescence or fluorescence provide scientists with quantitative methods for functional cell studies, and many adaptations of these methods in functional molecular biology assays have been developed (*3*)(*33*).

In order to study stem cells and cancer cells, imaging methods to study the behavior and cellular properties of these cells are indispensible to obtain more insight into their molecular mechanisms. Molecular imaging involves the localization and quantification of biomarkers or bioreporters using electromagnetic wave detection such as light, radio waves and radioactivity. In the clinical setting, tumors are often imaged using magnetic resonance imaging (MRI), single photon emission computed tomography (SPECT) or positron emission tomography (PET). For patient safety, these methods may only use transient, biomarker-targeted contrast agents to image tissue-specific or process-specific markers. These biomarkers can be radiolabelled molecules such as antibodies, peptides or aptamers (*34*, *35*). SPECT and PET use radioactive probes for imaging.

In preclinical research, target-specific probes, such as antibodies or complementary DNA, can be fused to fluorophores in order to detect their location within cells and follow molecular movement. Genetic reporters are proteins that are expressed in cells to detect the cells in their environment and to distinguish them from other cells. These bioreporter proteins can be fluorescent or luminescent. Green fluorescent protein (GFP) was the first fluorescent protein used as a bioreporter (*36*) and its importance for molecular imaging and biology has been acknowledged by awarding its discoverers the 2008 Nobel price for chemistry (*37*)(*38*). Since then, many derivatives with different colors have been developed (*39*) and named accordingly, such as cyan or cerulean fluorescent protein, yellow fluorescent protein and red fluorescent protein (*40*).

Bioluminescent proteins are luciferase enzymes that degrade a substrate into products and thereby produce detectable photons. Examples of bioluminescent reporters are Firefly luciferase (*41*), Renilla luciferase (*42*) and the cell-secreted Gaussia luciferase (*43*). Recently, a new firefly luciferase, Luciola italica, was discovered,

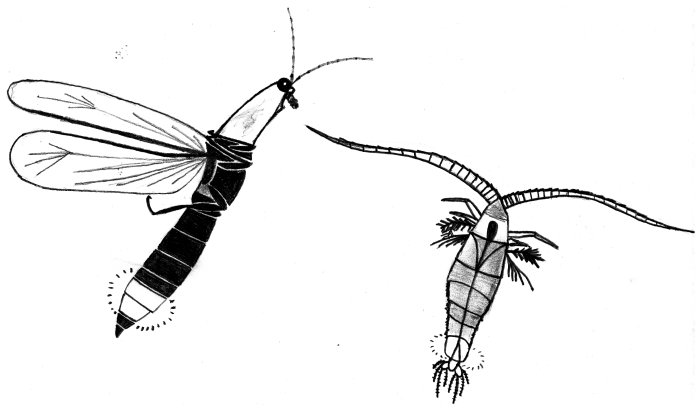

Figure 2. Luciferase enzymes are derived from organisms that use light production to communicate or as a mechanism of defense to distract predators. a: Photinus pyralis, the common eastern or big dipper firefly, uses light flashes to attract a mate. b: Gaussia princeps is an ocean dwelling copepod that uses bioluminescence as a defense mechanism against predators.

increasing the range of reporter luciferases with varying properties(*44*). One property of luciferases is their ability to degrade substrates. Firefly luciferases degrade luciferin, while Gaussia luciferase and Renilla luciferase degrade coelenterazine. The wavelength of the emitted photon also varies, depending on the luciferase type.

Functional bioreporters

Bioreporters are artificial genes that can be expressed constitutively active or under regulation of a specific promoter to make transcriptionally conditional. Also, the gene can be equipped with post-transcriptional or post-translational regulatory elements such as a 3'-UTR for microRNA degradation, a protease cleavage site or a localization domain. Using these methods (and combinations of these methods), different cellular mechanisms can be studied. When the firefly luciferase (Fluc) bioluminescent reporter under control of the constitutively active cytomegalovirus (CMV) promoter, is transplanted into tumor cells, they can be followed *in vivo* over time and viability or growth can be quantified (*45*) after injection of the Fluc substrate d-luciferin using a cooled charged-coupled device (CCD) camera. An alternative for the Fluc bioreporter is the secreted Gaussia luciferase (Gluc) bioreporter, that eliminates the need for an *in vivo* CCD camera and only requires a luminometer to detect gli36 human glioma cells in mice, since the reporter can be detected in collected mouse blood or urine (*46*). The obtained bioluminescent signal is representative for tumor growth and can be used to *ex vivo* determine *in vivo* processes. Gaussia luciferase is actively secreted out of the cells via the endoplasmic reticulum (ER)-related secretory pathways and therefore

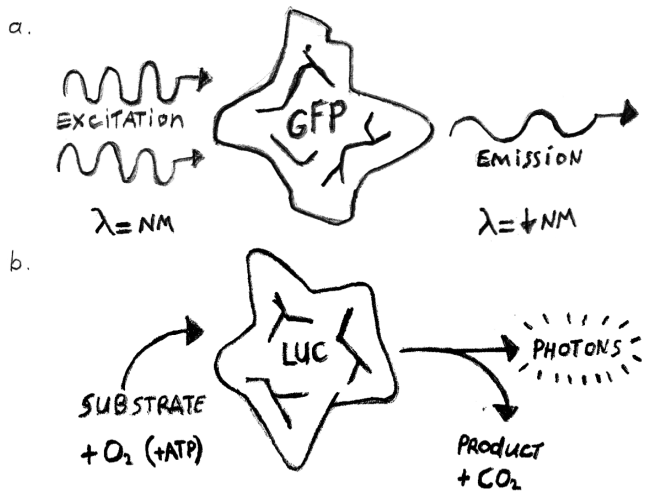

Figure 3. Fluorescence and luminescence are distinct processes. a: Fluorescent proteins such as green fluorescent protein (GFP) require light excitation from its ground state to enable it so return to its ground state and thereby emit a photon with lower wavelength. B: Luciferases such as Gaussia or Firefly luciferase (Gluc or Fluc) are enzymes that require a substrate to catalyse the reaction into a product and photons.

constitutive Gluc expression is used as a secretory pathway reporter (*47*). Upon induced ER stress, Gluc secretion from cells is considerably decreased, making Gluc a suitable reporter to study secretory pathway-related diseases. Fluc is located within the cell, making it ideal to visualize tumors. When a tumor is not contained in a well-defined bulk, is of a more diffuse nature, or when the bulk tumor is surgically removed but small number of residual cells are left over or metastasized to other locations in the body, it can be difficult to determine cancer cell load and to determine treatment effects. In the pre-clinical experimental setting Gluc may be a good option to measure tumor load since it is released into the blood and therefore small metastasis of breast cancers can be detected, even when the location cannot be determined using a CCD camera (*48*). Also, Gluc blood monitoring may reveal a more specific quantification of viable tumor burden as compared to localized reporters, such as Fluc, since the total viable tumor secretes Gluc into the blood while Fluc can become confined, also in a less viable tumor mass. The Gluc reporter is used in glioma high-throughput drug screens to identify potential new drugs. For example, lanatoside C has been shown to sensitize glioblastoma cells to TNF-related apoptosis-inducing ligand (TRAIL)-induced apoptosis (*49*) and only recently Gluc has also been used to identify inhibitors of Marburg and Ebola virus. Bioreporters under a conditional promoter can provide insight into transcriptional activity of genes or transcription factors. Transcription factors bind the double stranded DNA of a gene promoter in the genome and thereby positively or negatively regulate gene expression. Transcription factors have preferred DNA sequences to which they bind and these consensus sequences can be used to construct transcription factor activity bioreporters

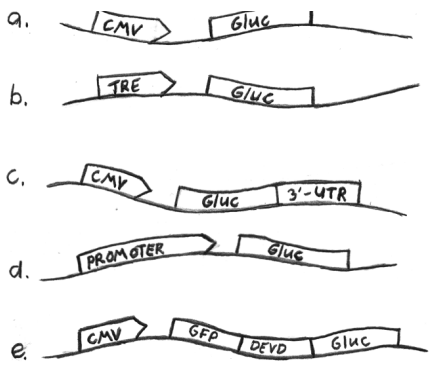

Figure 4. Functional bioluminescent reporters can be designed in to report different properties. a: The Gluc reporter is under control of a constitutively active cytomegalovirus (CMV) promoter to report cell viability and proliferation. b: The Gluc reporter is under control of a transcription recognition element (TRE) to report specific transcription factor activity. C: The Gluc reporter is under control of a CMV promoter but contains a specific 3'-UTR region downstream so it can be recognized and postranslationally repressed by a specific microRNA. d: The Gluc reporter is under control of a specific gene promoter region to report (tissue specific) gene expression. e: A constitutively active promoter drives a fusion gene of intracellular GFP linked to Gluc by a protease cleavage sequence (DEVD). When a protease is active, Gluc is released from the intracellular GFP, allowing detectable Gluc secretion.

that regulate reporter gene activity (*50*). In another study microRNA 23a (miR-23a) maturation and activity was assessed, by using the Fluc reporter under transcriptional control of the miR-23a promoter and the Gluc reporter, fused to miR-23a 3′-UTR target sequences, to quantify miR-23a post-transcriptional activity (*51*). Since Fluc and Gluc use the luciferase substrate luciferin and coelenterazine respectively, this dual reporter system can be used to simultaneously study primary miR-23a expression by detection of miR-23a promoter activity represented by the Fluc reporter and mature miR-23a silencing activity by binding of the miRNA to the Gluc-3′-UTR fusion reporter. In order to analyze cell apoptosis and caspase proteolytic activity, Niers et al. (*52*) designed a caspase 3 activity reporter. Therefore, they fused the recreated Gluc reporter to intracellular GFP with a caspase 3 cleavage site (DEVD). The intracellular GFP prohibited Gluc to exit the cell. When caspase 3 becomes active, it cleaved the DEVD linker between GFP and Gluc, allowing detectable Gluc secretion outside the cell.

Functional molecular imaging of stem cells

Stem cells have been often studied using bioluminescent reporters (*53*). These methods have been extensively used to reveal the temporal behavior and spatial localization of stem cells, but also for functional research and even therapeutic modalities. There are many studies that have used bioluminescent reporters based on luciferases. The most widely used luciferase is the cell localized Fluc.

For example, Fluc imaging can follow neural progenitor cells after injection into mouse ventricles and they have been proposed to migrate towards sites of brain infarction (*54*). Also using Fluc, systemically injected neural precursor cells, modified to express therapeutic molecules such as TRAIL, have been shown to selectively deliver these molecules to gliomas, inflicting tumor regression (*55*). Similar results were obtained by using the Gluc reporter blood-based assay and treatment combined with the previously mentioned TRAIL-sensitizing compound lanatoside C (*56*).

In another example, to study glioma-initiating stem cells the Fluc reporter was put under control of the plagl1 gene promoter to correlate Sox11 expression with neural differentiation. It was shown that upon loss of Sox11 expression plagl1 was overexpressed, resulting in loss of neural differentiation commitment and tumorigenesis *in vivo* (*57*). The construction of a RTVP-1 3′-UTR reporter, a target of microRNA-137, which is down-regulated in glioblastoma by promoter hypermethylation, resulted in decreased degradation of RTVP-1 and increase of self-renewal potential of glioma stem cells (*58*).

To study rat intervertebral disc degeneration, Fluc has been used to image mesenchymal stem cell fate and viability (*59*). The use of Gluc in regenerative medicine, and specifically in intervertebral disc regeneration, is still limited and the functionality of Gluc in this research is largely unexplored. In a study on mesenchymal stem cell biodistribution in mice, the stem cells were equipped with Fluc using non-viral sleeping beauty transposons. After injection of these stem cells the mice developed increasing Fluc signal, suggesting an increase in transplanted mesenchymal stem cells and post-

mortem analysis of the mice revealed sarcomas in the lungs and the researchers were able to grow malignant lesions in secondary mouse recipients (*60*).

The secreted Gluc is a relatively new 'kid on the block' (*43*) and therefore is less well-known and used. This also accounts for even more recently discovered luciferases. The secreted luciferases have certain advantages such as the relative ease of use without CCD equipment, the possibility to measure cell viability without the need to know a near location and the ability to measure relatively diffuse cells in tissues and organisms. Downsides may be that cell secretion might lead to higher background signals in organisms when using CCD imaging to localize cells or the relative stability of Gluc *in vitro*, although efforts are made to identify mutants that harbor other specifications. There is no better or worse luciferase; the luciferase of choice depends on the application and therefore the options available should always be considered.

AIMS AND OUTLINE OF THIS THESIS

The aim of this thesis is to develop a novel application of Gaussia luciferase bioluminescence imaging and to apply bioluminescent imaging to discover functional molecular mechanisms in nervous system pathologies. Functional bioluminescent imaging is a tool that can be adapted for many types of research in many diseases. In our research we mainly focused on malignant brain tumors but in chapter six we also explored spine intervertebral disc stem cell regeneration imaging as another example of functional bioluminescent imaging in the nervous system. In **Chapter 2** we aim to develop a novel multiplex bioluminescence assay, based on the secreted Gluc fused to an epitope tag. This method would enable us to identify and functionally analyze multiple types cells, each expressing Gluc with a different epitope tag, and to follow the performance of each type of cell within a heterogeneous tumor cell population *in vitro* and *in vivo*. This opens up the possibility to study a variety of cell subpopulations in heterogeneous tumors and tissues. In **Chapter 3** we provide an extensive protocol, with tips & tricks and troubleshooting, for the multiplex reporter assay described in chapter 2. In **Chapter 4** we conduct a comprehensive meta-analysis of gene expression studies of mouse and human medulloblastoma to identify novel mechanisms in medulloblastoma development. **Chapter 5** also aims at identifying novel tumor suppressor genes by an *in silico* analysis of GBM gene expression data. In **Chapter 6** we explore luciferase-mediated bioluminescence imaging of adipose-derived mesenchymal stem cells in an intervertebral disc model in order to study stem cell regenerative biology. A general discussion and future considerations are presented in **Chapter 7**, followed by an English summary in **Chapter 8** and a Dutch summary in **Chapter 9**.

REFERENCES

1 M. D. Taylor *et al.*, Molecular subgroups of medulloblastoma: the current consensus. *Acta Neuropathol.* **123**, 465–72 (2012).

2 R. Stupp *et al.*, Radiotherapy plus concomitant and adjuvant temozolomide for glioblastoma. *N. Engl. J. Med.* **352**, 987–96 (2005).

3 C. E. Badr, B. a. Tannous, Bioluminescence imaging: progress and applications. *Trends Biotechnol.* **3**, 1–10 (2011).

4 D. N. Louis *et al.*, The 2007 WHO classification of tumours of the central nervous system. *Acta Neuropathol.* **114**, 97–109 (2007).

5 B. S. Paugh *et al.*, Integrated molecular genetic profiling of pediatric high-grade gliomas reveals key differences with the adult disease. *J. Clin. Oncol.* **28**, 3061–8 (2010).

6 R. G. W. Verhaak *et al.*, Integrated genomic analysis identifies clinically relevant subtypes of glioblastoma characterized by abnormalities in PDGFRA, IDH1, EGFR, and NF1. *Cancer Cell.* **17**, 98–110 (2010).

7 E. Yeoh, M. Ross, S. Shurtleff, Classification, subtype discovery, and prediction of outcome in pediatric acute lymphoblastic leukemia by gene expression profiling. **1**, 133–143 (2002).

8 K. Berns, H. M. Horlings, B. T. Hennessy, A functional genetic approach identifies the PI3K pathway as a major determinant of trastuzumab resistance in breast cancer. **12**, 395–402 (2007).

9 M. Moroni, S. Veronese, S. Benvenuti, Gene copy number for epidermal growth factor receptor (EGFR) and clinical response to antiEGFR treatment in colorectal cancer: a cohort study. **6**, 279–286 (2005).

10 H. Ohgaki, P. Kleihues, Genetic pathways to primary and secondary glioblastoma. **170**, 1445–1453 (2007).

11 N. Sanai, A. Alvarez-Buylla, M. S. Berger, Neural stem cells and the origin of gliomas. *N. Engl. J. Med.* **353**, 811–22 (2005).

12 D. Friedmann-Morvinski *et al.*, Dedifferentiation of neurons and astrocytes by oncogenes can induce gliomas in mice. *Science.* **338**, 1080–4 (2012).

13 C. W. Brennan *et al.*, The somatic genomic landscape of glioblastoma. *Cell.* **155**, 462–77 (2013).

14 M. Kool, J. Koster, J. Bunt, Integrated Genomics Identifies Five Medulloblastoma Subtypes with Distinct Genetic Profiles, Pathway Signatures and Clinicopathological Features. **3** (2008) (available at http://apps.isiknowledge.com/full_record.do?product=UA&search_mode=GeneralSearch&qid=11&SID=Z2NsKIGhlYsYOB8ICiV&page=1&doc=6).

15 N. V Batora *et al.*, Transitioning from genotypes to epigenotypes: why the time has come for medulloblastoma epigenomics. *Neuroscience.* **264**, 171–85 (2014).

16 J. A. Thomson, Embryonic Stem Cell Lines Derived from Human Blastocysts. *Science (80-.).* **282**, 1145–1147 (1998).

17 K.-I. Yoshioka, Y. Atsumi, H. Nakagama, H. Teraoka, Development of cancer-initiating cells and immortalized cells with genomic instability. *World J. Stem Cells.* **7**, 483–9 (2015).

18 J. E. Grove, E. Bruscia, D. S. Krause, Plasticity of bone marrow-derived stem cells. *Stem Cells.* **22**, 487–500 (2004).

19 J. McDonald, X. Liu, Y. Qu, Transplanted embryonic stem cells survive, differentiate and promote recovery in injured rat spinal cord. **5**, 1410–1412 (1999).

20 F. Erdo, C. Buhrle, J. Blunk, Host-dependent tumorigenesis of embryonic stem cell transplantation in experimental stroke. **23**, 780–785 (2003).

21 P. Zuk, M. Zhu, H. Mizuno, Multilineage cells from human adipose tissue: Implications for cell-based therapies. **7**, 211–228 (2001).

22 Y. Jiang, B. Jahagirdar, R. Reinhardt, Pluripotency of mesenchymal stem cells derived from adult marrow. **418**, 41–49 (2002).

23 M. N. Helder, M. Knippenberg, J. Klein-Nulend, P. I. J. M. Wuisman, Stem cells from adipose tissue allow challenging new concepts for regenerative medicine. *Tissue Eng.* **13**, 1799–808 (2007).

24 Y. Miyahara, N. Nagaya, M. Kataoka, Monolayered mesenchymal stem cells repair scarred myocardium after myocardial infarction. **12**, 459–465 (2006).

25 G. Erickson, J. Gimble, D. Franklin, Chondrogenic potential of adipose tissue-derived stromal cells in vitro and in vivo. **290**, 763–769 (2002).

26 K. Hicok, T. Du Laney, Y. Zhou, Human adipose-derived adult stem cells produce osteoid in vivo. **10**, 371–380 (2004).

27 S. A. Mani, W. Guo, M.-J. Liao, The epithelial-mesenchymal transition generates cells with properties of stem cells. **133**, 704–715 (2008).

28 J. Chen *et al.*, A restricted cell population propagates glioblastoma growth after chemotherapy. *Nature*. **488**, 522–6 (2012).

29 S. Alcantara Llaguno *et al.*, Malignant astrocytomas originate from neural stem/progenitor cells in a somatic tumor suppressor mouse model. *Cancer Cell*. **15**, 45–56 (2009).

30 P. B. Gupta, C. L. Chaffer, R. A. Weinberg, Cancer stem cells: mirage or reality? *Nat. Med.* **15**, 1010–2 (2009).

31 C. L. Chaffer *et al.*, Poised chromatin at the ZEB1 promoter enables breast cancer cell plasticity and enhances tumorigenicity. *Cell*. **154**, 61–74 (2013).

32 J. E. Visvader, G. J. Lindeman, Cancer stem cells: current status and evolving complexities. *Cell Stem Cell*. **10**, 717–28 (2012).

33 B. N. G. Giepmans, S. R. Adams, M. H. Ellisman, R. Y. Tsien, The fluorescent toolbox for assessing protein location and function. *Science*. **312**, 217–24 (2006).

34 S. Lee, J. Xie, X. Chen, Peptide-Based Probes for Targeted Molecular Imaging. **49**, 1364–1376 (2010).

35 C. Lee, L. Farde, Using positron emission tomography to facilitate CNS drug development. **27**, 310–316 (2006).

36 R. Y. Tsien, The green fluorescent protein. *Annu. Rev. Biochem.* **67**, 509–44 (1998).

37 A. Roda, Discovery and development of the green fluorescent protein, GFP: the 2008 Nobel Prize. *Anal. Bioanal. Chem.* **396**, 1619–22 (2010).

38 M. Zimmer, GFP: from jellyfish to the Nobel prize and beyond. *Chem. Soc. Rev.* **38**, 2823–32 (2009).

39 S. R. McRae, C. L. Brown, G. R. Bushell, Rapid purification of EGFP, EYFP, and ECFP with high yield and purity. *Protein Expr. Purif.* **41**, 121–7 (2005).

40 R. Lansford, G. Bearman, S. E. Fraser, Resolution of multiple green fluorescent protein color variants and dyes using two-photon microscopy and imaging spectroscopy. *J. Biomed. Opt.* **6**, 311–8 (2001).

41 S. J. Gould, S. Subramani, Firefly luciferase as a tool in molecular and cell biology. *Anal. Biochem.* **175**, 5–13 (1988).

42 W. W. Lorenz, R. O. McCann, M. Longiaru, M. J. Cormier, Isolation and expression of a cDNA encoding Renilla reniformis luciferase. *Proc. Natl. Acad. Sci. U. S. A.* **88**, 4438–42 (1991).

43 B. A. Tannous, D.-E. Kim, J. L. Fernandez, R. Weissleder, X. O. Breakefield, Codon-optimized Gaussia luciferase cDNA for mammalian gene expression in culture and in vivo. *Mol. Ther.* **11**, 435–43 (2005).

44 C. A. Maguire, J. C. van der Mijn, M. H. Degeling, D. Morse, B. A. Tannous, Codon-optimized Luciola italica luciferase variants for mammalian gene expression in culture and in vivo. *Mol. Imaging*. **11**, 13–21 (2012).

45 L. Zhang, K. E. Hellström, L. Chen, Luciferase activity as a marker of tumor burden and as an indicator of tumor response to antineoplastic therapy in vivo. *Clin. Exp. Metastasis*. **12**, 87–92 (1994).

46 T. Wurdinger *et al.*, A secreted luciferase for ex vivo monitoring of in vivo processes. *Nat. Methods*. **5**, 171–3 (2008).

47 C. E. Badr, J. W. Hewett, X. O. Breakefield, B. A. Tannous, A highly sensitive assay for monitoring the secretory pathway and ER stress. *PLoS One*. **2**, e571 (2007).

48 E. Chung *et al.*, Secreted Gaussia luciferase as a biomarker for monitoring tumor progression and treatment response of systemic metastases. *PLoS One*. **4**, e8316 (2009).

49 C. E. Badr *et al.*, Lanatoside C sensitizes glioblastoma cells to tumor necrosis factor-related apoptosis-inducing ligand and induces an alternative cell death pathway. *Neuro. Oncol.* **13**, 1213–24 (2011).

50 C. E. Badr, J. M. Niers, D. P. Noske, T. Wurdinger, Real-Time Monitoring of Nuclear Factor κB Activity in Cultured Cells and in Animal Models. **8**, 278–290 (2009).

51 J. Y. Lee *et al.*, Development of a dual-luciferase reporter system for in vivo visualization of MicroRNA biogenesis and posttranscriptional regulation. *J. Nucl. Med.* **49**, 285–94 (2008).

52 J. M. Niers, M. Kerami, L. Pike, G. Lewandrowski, B. A. Tannous, Multimodal in vivo imaging and blood monitoring of intrinsic and extrinsic apoptosis. *Mol. Ther.* **19**, 1090–6 (2011).

53 Z. Lee, J. E. Dennis, S. L. Gerson, Imaging stem cell implant for cellular-based therapies. *Exp. Biol. Med. (Maywood).* **233**, 930–40 (2008).

54 D.-E. Kim, D. Schellingerhout, K. Ishii, K. Shah, R. Weissleder, Imaging of stem cell

recruitment to ischemic infarcts in a murine model. *Stroke*. **35**, 952–7 (2004).

55 K. Shah *et al.*, Glioma therapy and real-time imaging of neural precursor cell migration and tumor regression. *Ann. Neurol.* **57**, 34–41 (2005).

56 J. Teng, S. Hejazi, C. E. Badr, B. A. Tannous, Systemic anticancer neural stem cells in combination with a cardiac glycoside for glioblastoma therapy. *Stem Cells.* **32**, 2021–32 (2014).

57 T. Hide *et al.*, Sox11 prevents tumorigenesis of glioma-initiating cells by inducing neuronal differentiation. *Cancer Res.* **69**, 7953–9 (2009).

58 A. Bier *et al.*, MicroRNA-137 is downregulated in glioblastoma and inhibits the stemness of glioma stem cells by targeting RTVP-1. *Oncotarget.* **4**, 665–676 (2013).

59 N. Kimelman *et al.*, 455. Genetically Engineered Adult Stem Cells and Hybrid Scaffolds as a Platform for Intervertebral Disc Regeneration. *Mol. Ther.* **13**, S175–S176 (2006).

60 J. Tolar *et al.*, Sarcoma derived from cultured mesenchymal stem cells. *Stem Cells.* **25**, 371–9 (2007).

2

FUNCTIONAL MULTIPLEX REPORTER ASSAY USING TAGGED GAUSSIA LUCIFERASE

Sjoerd van Rijn, Jonas Nilsson, David P. Noske, W. Peter Vandertop,
Bakhos A. Tannous, and Thomas Würdinger

Scientific Reports 3:1046 (2013)

ABSTRACT

We have developed a multiplex reporter system to monitor multiple biological variables in real-time. The secreted *Gaussia* luciferase was fused to ten different epitope tags ($Gluc_{tag}$), each expressed in different tumor cells. By immunobinding of the tags followed by $Gluc_{tag}$ detection, this system allowed the independent and real-time monitoring of mixed cell cultures *in vitro* and of mixed subcutaneous and intracranial tumor subpopulations *in vivo*.

INTRODUCTION

To study complex processes in systems biology, tools are needed that give insight into multiple molecular and cellular interactions simultaneously and in real-time[1]longitudinal studies of dynamic biological processes in vivo. The most common reporters include firefly luciferase (bioluminescence imaging[2]. Several cellular reporter systems are in use to shed light on biological processes, many based on luciferase enzymes and their photon production upon luciferin substrate addition, including Firefly luciferase (Fluc)[3], *Renilla* luciferase (Rluc)[4], and *Gaussia* luciferase (Gluc)[5]nontoxic, and novel reporters can serve to expand this potential. Here we describe the properties of a luciferase from the copepod marine organism Gaussia princeps. It is a monomeric protein composed of 185 aa (19.9 kDa[6]. These bioluminescent reporters have been used to monitor biological processes such as cellular proliferation and differentiation[7], transcription factor activity[8], translational repression by miRNA[9,10], and intercellular interactions[11], reviewed in[12]. Other commonly used reporters are based on the green fluorescent protein (GFP), the red fluorescent protein (RFP) and, more recently, near infra-red fluorescent proteins[13,14] which can be multiplexed together to monitor several processes simultaneously using spectral unmixing in conjunction with fluorescence molecular tomography[15]. These reporters have several disadvantages including low sensitivity due to autofluorescence, complexity, and the requirement of expensive instrumentation. Further, similar to bioluminescence, limited numbers of variables can be monitored simultaneously, limiting their use in multiplex screening assays and cellular heterogeneity studies. Here, we developed a multiplex bioluminescence assay that allows monitoring of many variables in real-time within the same biological system. This assay is based on Gluc since this reporter is highly sensitive, naturally secreted, and can be detected in the conditioned medium of cells in culture as well as in the blood of animals *ex vivo*, allowing real-time monitoring of cellular variables[5]nontoxic, and novel reporters can serve to expand this potential. Here we describe the properties of a luciferase from the copepod marine organism Gaussia princeps. It is a monomeric protein composed of 185 aa (19.9 kDa[6].

RESULTS

We constructed a library of lentiviral vectors consisting of the Gluc cDNA fused to ten different epitope tags at its C-terminus, under the constitutively active cytomegalovirus (CMV) promoter resulting in $Gluc_{Flag}$, $Gluc_{His}$, $Gluc_{HA}$, $Gluc_{AcV5}$, $Gluc_{V5}$, $Gluc_{Glu}$, $Gluc_{Myc}$, $Gluc_{Kt3}$, $Gluc_{Au1}$, $Gluc_{E2}$, and the control reporter construct without tag, $Gluc_{Ctrl}$. These lentiviral vectors also express cerulean fluorescent protein (CFP) separated from $Gluc_{tag}$ by an internal ribosomal entry site (IRES) element as a marker for transduction efficiency (Fig. 1a and Methods section). We employed human U87 glioblastoma cells stably expressing Fluc and the mCherry fluorescent protein[6] (U87-FM) for validation of the $Gluc_{tag}$ multiplex system. These cells were transduced with each of the lentiviral vectors to produce ten different cell lines, each stably expressing a different $Gluc_{tag}$ and CFP

(U87-FM-$Gluc_{tag}$-CFP). Fluorescent microscopy analysis for mCherry and CFP showed that these cells were nearly 100% transduced with the reporter vectors (Fig. 1b). We first demonstrated that all of the individual U87-FM-$Gluc_{tag}$-CFP cells expressed the corresponding tags by immunostaining using specific antibodies, except for $Gluc_{Au1}$ that was not detectable by immunostaining attributed to anti-Au1 antibody properties (Fig. 1c). As a control we stained cells expressing $Gluc_{ctrl}$ with the different tag antibodies, which did not show any staining (data not shown). We confirmed $Gluc_{tag}$ expression by Western blot using anti-tag antibodies (Sup. Fig. 1a) and RT-PCR of the tag region (Sup. Fig. 1b and c). Next, we determined the effect of the tags on Gluc by measuring luciferase activity at different time points in an aliquot of conditioned medium from U87-FM cells expressing each $Gluc_{tag}$ reporter construct using the Gluc substrate coelenterazine. We demonstrated that fusion of epitope tags to Gluc does not dramatically affect the expression, secretion or activity of Gluc (Fig. 1d and supplemental Fig. 1a-c). We then used the conditioned media containing the different $Gluc_{tag}$ constructs to optimize antibody-tag immunobinding in a 96-well plate format (Methods). Plates were first coated with monoclonal antibodies against the different tags and incubated with different amounts of conditioned medium allowing $Gluc_{tag}$ immunobinding. Subsequently, the wells were washed to remove unbound $Gluc_{tag}$ and subjected to the Gluc assay by direct addition of coelenterazine to the wells and measuring photon counts using a plate luminometer. As a control, an aliquot of conditioned medium was assayed directly for total Gluc activity. We determined that six of the ten individual $Gluc_{tag}$ constructs, i.e. $Gluc_{Flag}$, $Gluc_{His}$, $Gluc_{HA}$, $Gluc_{AcV5}$, $Gluc_{V5}$, $Gluc_{Glu}$, reported with high-efficiency after immunobinding in the antibody-coated wells, as compared to total $Gluc_{tag}$ activity (Fig. 1e). The $Gluc_{Myc}$, $Gluc_{Kt3}$, $Gluc_{Au1}$, and $Gluc_{E2}$ reporters showed lower activity upon immunobinding, attributed to suboptimal antibody-tag interactions. In order to demonstrate the use of the $Gluc_{tag}$ system for multiplex applications, we mixed equal numbers of the ten different U87-FM-$Gluc_{tag}$-

Figure 1. $Gluc_{tag}$ multiplex assay development and validation *in vitro*. (a) Schematic of the lentiviral vector constructs encoding the luciferase reporters. (b) Fluorescence microscopy analysis of a representative U87-FM-$Gluc_{tag}$-CFP cells (using $Gluc_{Flag}$ reporter) showing mCherry levels (in red; marker for tumor cells) and CFP expression (in blue; marker for transduction efficiency). (c) Immunostaining against the various tags in U87-FM cells expressing different $Gluc_{tag}$. (d) Gluc activity in U87 cells expressing different $Gluc_{tag}$ with respect to cell proliferation over time and cell number. The dashed line represents $Gluc_{Ctrl}$ activity. (e) $Gluc_{tag}$ immunobinding assay versus total Gluc activity using serial dilutions of the conditioned medium from a 1-day culture of U87-FM cell lines expressing the individual $Gluc_{tag}$ reporters. . (f-g) Equal mixture of ten cell lines each expressing a different $Gluc_{tag}$ reporter. (f) Immunobinding assay of $Gluc_{tag}$ from a mixed population. (g) Immunostaining for the ten different tags expression in the mixed population of U87-FM cell culture. (h-i) U87-FM cells expressing all ten different $Gluc_{tag}$ reporters. (h) Immunostaining for the ten different tags in one cell line. The insert panels show staining of control parental cells. Percentages of positively stained cells are indicated. (i) Immunobinding assay of all ten $Gluc_{tag}$ reporters in one cell line after TMZ treatment (black bars) compared to untreated control (white bars). (j) CFP fluorescence microscopy of cells in (h-i) with or without 600 μM TMZ. Size bar (in b,c, g and h) = 200 μm. Size bar (i) = 400 μm. N.d. = not detectable. ►

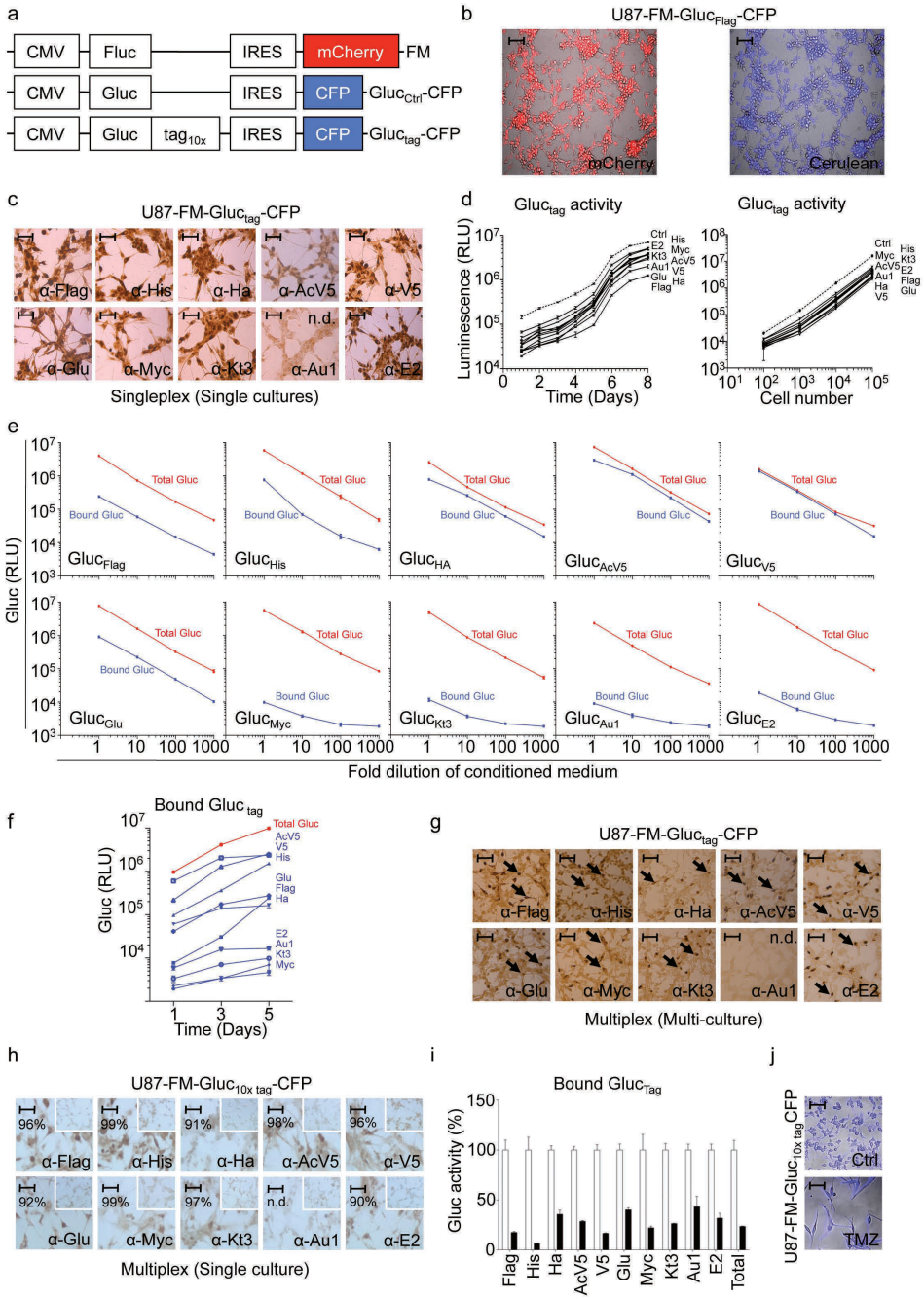
a
CMV
Fluc
IRES
mCherry
FM
CMV
Gluc
IRES
CFP
Gluc$_{Ctrl}$-CFP
CMV
Gluc
tag$_{10x}$
IRES
CFP
Gluc$_{tag}$-CFP
b
U87-FM-Gluc$_{Flag}$-CFP
αCherry
Cerulean
c
U87-FM-Gluc$_{tag}$-CFP
α-Flag
α-His
α-Ha
α-AcV5
α-V5
α-Glu
α-Myc
α-Kt3
n.d.
α-Au1
α-E2
Singleplex (Single cultures)
d
Gluc$_{tag}$ activity
Luminescence (RLU)
Time (Days)
Gluc$_{tag}$ activity
Cell number
e
Gluc (RLU)
Total Gluc
Bound Gluc
Gluc$_{Flag}$
Gluc$_{His}$
Gluc$_{HA}$
Gluc$_{AcV5}$
Gluc$_{V5}$
Gluc$_{Glu}$
Gluc$_{Myc}$
Gluc$_{Kt3}$
Gluc$_{Au1}$
Gluc$_{E2}$
Fold dilution of conditioned medium
f
Bound Gluc $_{tag}$
Gluc (RLU)
Time (Days)
g
U87-FM-Gluc$_{tag}$-CFP
α-Flag
α-His
α-Ha
α-AcV5
α-V5
α-Glu
α-Myc
α-Kt3
n.d.
α-Au1
α-E2
Multiplex (Multi-culture)
h
U87-FM-Gluc$_{10x\ tag}$-CFP
96%
99%
91%
98%
96%
α-Flag
α-His
α-Ha
α-AcV5
α-V5
92%
99%
97%
n.d.
90%
α-Glu
α-Myc
α-Kt3
α-Au1
α-E2
Multiplex (Single culture)
i
Bound Gluc$_{Tag}$
Gluc activity (%)
Flag
His
Ha
AcV5
V5
Glu
Myc
Kt3
Au1
E2
Total
j
U87-FM-Gluc$_{10x\ tag}$-CFP
Ctrl
TMZ

CFP cells and plated them in a single well. One, three and five days later, we measured the total Gluc level in aliquots of the conditioned medium. The levels of the individual $Gluc_{tag}$ reporters in the mixed culture medium were analyzed by immunobinding with the different tag specific antibodies. We were able to monitor in real-time the growth of the individual U87-FM-$Gluc_{tag}$-CFP cell populations in the mixed culture (Fig. 1f). Immunostaining confirmed the expression of each tag in the corresponding cells in the mixed culture, again except for $Gluc_{Au1}$ (Fig. 1g). In order to determine whether we can measure the activity of ten different $Gluc_{tag}$ constructs in the same cell, we transduced U87-FM cells with all ten different lentiviral $gluc_{tag}$ reporters. Immunostaining of the U87-FM-$Gluc_{10x\ tag}$CFP glioblastoma cells with tag specific antibodies showed that almost all cells expressed all ten different $Gluc_{tag}$ constructs (Fig. 1h). The tag expression as demonstrated by immunostaining is less intens in Fig. 1h as compared to Fig. 1c, which we attribute to the transduction pool of ten different lentivectors used in Fig. 1h. We used these cells to monitor cell viability in the presence and absence of the alkylating agent temozolomide (TMZ), the standard chemotherapy for glioblastoma patients. $Gluc_{tag}$ immunobinding assays were used to determine the expression of all ten reporters in the presence or absence of TMZ. We treated the U87-FM-$Gluc_{10x\ tag}$CFP cells with TMZ and measured $Gluc_{tag}$ activity after six days (Fig. 1i). Precipitation of all ten different $Gluc_{tag}$ reporters showed a ~75% decrease in Gluc bioluminescence signal after TMZ treatment, similar to the total Gluc signal and confirmed by CFP immunofluorescence analysis (Fig. 1j). Altogether, these results demonstrate that we can measure biologically relevant differences using our multiplex $Gluc_{tag}$ system.

In order to determine the *in vivo* applicability of the $Gluc_{tag}$ reporter assay, we injected the ten individual U87-FM cell cultures expressing either one of the $Gluc_{tag}$ or $Gluc_{Ctrl}$ reporters subcutaneously in nude mice for singleplex application. In another set, we injected mice with PBS as a negative control (12 groups; n=3/group). Tumor growth was monitored over time by calliper measurement, and Fluc bioluminescence imaging (Fig. 2a,b). Blood was collected from mice at different time points and 5 µl of whole blood (optimum amount for Gluc blood assay[16]) was assayed for total Gluc activity. At the same time, 25 µl of blood was analyzed for Gluc activity after immunobinding on wells coated with the corresponding tag antibody (Fig. 2b). All of the $Gluc_{tag}$ reporters, except $Gluc_{E2}$, allowed blood monitoring of tumor growth over time in a singleplex assay. We compared the tumor growth as measured by calliper, Fluc imaging and Gluc blood assay to signals obtained from the ten different $Gluc_{tag}$ reporters after immunobinding (Fig. 2b). The six $Gluc_{tag}$ reporters $Gluc_{Flag}$, $Gluc_{His}$, $Gluc_{HA}$, $Gluc_{AcV5}$, $Gluc_{V5}$, $Gluc_{Glu}$ were more sensitive in detecting tumor growth than the others, possibly due to a higher affinity of the antibodies to these tags. To demonstrate the use of the $Gluc_{tag}$ system for multiplex applications, we mixed equal numbers of U87-FM cells expressing the ten different $Gluc_{tag}$ and implanted the heterogeneous cell pool subcutaneously in nude mice (n=5). We monitored tumor growth by Fluc bioluminescence imaging and total Gluc blood assay (Fig. 2c,d). Importantly, we were

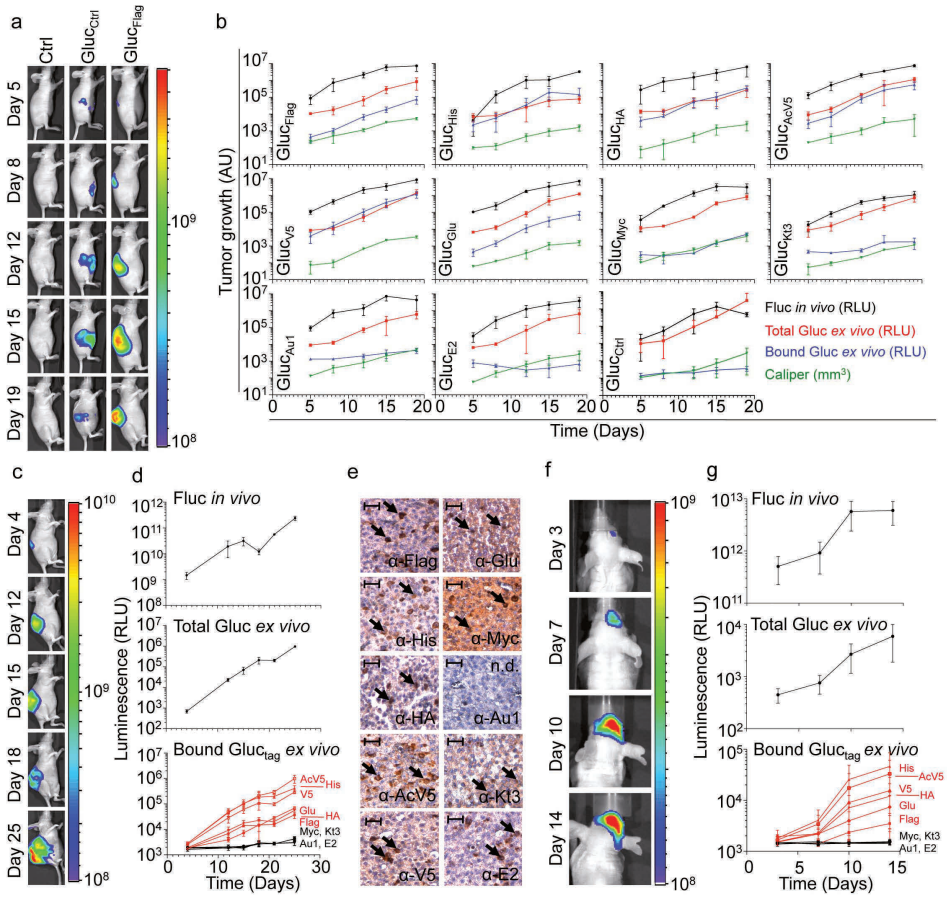

Figure 2. $Gluc_{tag}$ multiplex assay *in vivo*. (a) U87-FM cells expressing different $Gluc_{tag}$ were implanted subcutaneously in nude mice (n=3) and tumor growth was monitored overtime. Shown are representative Fluc bioluminescence images of the U87-FM-$Gluc_{tag}$-CFP tumors expressing the $Gluc_{Flag}$ reporter. (b), Quantitation of the different U87-FM tumors expressing different $Gluc_{tag}$ reporters; Fluc activity (black), calliper measurement (green), total $Gluc_{tag}$ activity in the blood (red), and bound $Gluc_{tag}$ activity after immunobinding (blue). (c-d) U87-FM cells expressing the different $Gluc_{tag}$ reporters were mixed in equal amounts and injected subcutaneously in the same mouse (n=5). Tumor growth was monitored using Fluc imaging and total Gluc blood assay as in (a-b). Individual cells subpopulation within the same tumor were monitored using the multiplex $Gluc_{tag}$ immunobinding assay. (e) Immunostaining for the ten different tags expression in the mixed U87-FM-$Gluc_{tag}$-CFP tumor. Black arrows indicate positive staining for cells expressing the corresponding $Gluc_{tag}$. Size bar = 200 µm. N.d. = not detectable. (f-g) Mixed population of U87-FM cells expressing all ten different tags were implanted intracranially in the brain of nude mice (n=5). Tumor growth was monitored with Fluc imaging and Gluc total blood assay, and different tumor cell subpopulations were monitored using the multiplex $Gluc_{tag}$ assay as in (c-d). Fluc bioluminescence imaging of a representative mouse is shown in (f). Data shown in (b,d, and g) as average relative light units (RLU) ± standard deviation. Heatscales in (a, c and f) indicate relative photon levels (photons/sec) as measured by the CCD camera.

able to efficiently monitor the growth of the individual subpopulation of the U87-FM cells expressing the different high-efficiency $Gluc_{tag}$ reporters ($Gluc_{Flag}$, $Gluc_{His}$, $Gluc_{HA}$, $Gluc_{AcV5}$, $Gluc_{V5}$, $Gluc_{Glu}$) in the same tumor over time (Fig. 2d). We confirmed the expression of all tags (except for $Gluc_{Au1}$) in the same tumor by immunostaining (Fig. 2e). To determine the applicability of the $Gluc_{tag}$ multiplex system in deep tissues, the mixture of the ten different U87-FM-$Gluc_{tag}$-CFP cells were implanted orthotopically in the brain of nude mice (n=5). We monitored tumor growth by Fluc bioluminescence imaging and total Gluc blood assay (Fig. 2f,g). Again, we were able to monitor the intracranial growth of the individual subpopulations of U87-FM cells expressing the high-efficiency $Gluc_{tag}$ reporters within the same brain tumor in real-time, by blood sampling and the application of the $Gluc_{tag}$ multiplex reporter system (Fig. 2g).

DISCUSSION

Here we demonstrated the functionality of the $Gluc_{tag}$ multiplex reporter system by the parallel monitoring of mixed cell cultures *in vitro*, and of subpopulations in mixed subcutaneous and intracranial tumors *ex vivo*. The individual epitope tags could also be employed to localize expression by immunostaining. We used ten different $Gluc_{tag}$ reporters, but this tag library can be readily extended allowing for increased multiplexing. In addition, antibody binding of the low-efficiency tags in the $Gluc_{tag}$ immunobinding assay might be further optimized to achieve higher sensitivity since these tags, except for $Gluc_{AU1}$, were efficiently detected by immunostaining. Real-time monitoring of individual cells in a heterogeneous mixture may allow, for instance, multiplexed RNAi screening or measurement of drug responses of multiple cell populations in parallel. The $Gluc_{tag}$ multiplex system might be extended to monitor different variables in a single cell type. For instance, engineering each individual $Gluc_{tag}$ under the control of different transcription response elements for multiplex transcription factor activity measurements[7], constructing microRNA (miRNA)-binding sequences in the 3'-UTR of the $Gluc_{tag}$ constructs for multiplex monitoring of miRNA activity[10] or by inserting different protease cleavage sites into the $Gluc_{tag}$ gene for multiplex protease activity measurement[17]. This reporter assay provides a versatile tool to study complex processes with different variables in systems biology.

METHODS

Cells. For *in vitro* and *in vivo* validation, we used the glioblastoma cell line U87, stably co-expressing Firefly luciferase and mCherry fluorescent protein. Cell lines were maintained in DMEM high glucose complemented with sodium pyruvate, stable glutamine, 10% FBS and pen/strep (all PAA), incubated under standard cell culture conditions of 37°C and 5% CO_2.

Lentivirus vector construction and transduction. First, we amplified Gluc by PCR using Accuprime Pfx DNA polymerase (Life Technologies) from CSCW-Gluc-IRES-CFP[6]

with specific primers that incorporate an XbaI site downstream of the Gluc cDNA (Forward primer: 5'- GCGTGTACGGTGGGAGGTCT-3', reverse primer: 5'-TCTCGA GTAGAGATCTGTCACCACCGGCCCCCTT-3'). The reverse primer also covers the original stop-codon that is thereby removed. The Gluc cDNA, now containing a unique XbaI site, was ligated back into the CSCW-Gluc-IRES-CFP vector with T4 DNA ligase (Life Technologies), after removal of the wild-type Gluc using NheI and XhoI (Life Technologies). Plasmid DNA was transformed in XL-10 Gold ultracompetent cells (Agilent Technologies), cultured overnight in LB agar containing 50 µg/ml Ampicillin. We isolated DNA using a DNA plasmid mini kit (Qiagen) and verified successful transformation by XbaI restriction analysis. The Gluc construct was then digested with XbaI and XhoI to insert the different epitope tags. The epitope tags were designed with an XbaI site upstream, a stop codon and XhoI site downstream. A total of 20 µM of both single strand oligonucleotides of the acquired tag DNA (Life Technologies, see Table S1 for sequences) was annealed in annealing buffer (100 mM Tris-HCl pH 7.5, 1 M NaCl and 10 mM EDTA) by heating to 65°C for 10 minutes and slow cooling to room temperature. The epitope tag was then inserted into the vector using T4 DNA ligase and transformed in XL-10 Gold ultracompetent cells. Bacteria were cultured and DNA was isolated. We verified the $Gluc_{tag}$ constructs by sequencing using BigDye Terminator v3.1 Cycle Sequencing kit (Life Technologies, primer: 5'-GCCAACGTGCAGTGTTC-3'). The $Gluc_{tag}$ construct was co-transfected with a third generation lentiviral packaging mix (pMDLg/pRRE, pRSV-Rev and pMD2.G, Addgene) in HEK293T cells using Lipofectamine 2000 (Life Technologies). Virus was harvested two and three days after transfection and cell debris was spun down for five minutes at 1,000 x g. U87 cells were transduced overnight with lentivirus using a multiplicity of infection of 100 transducing units per cell in the presence of 8 µg/ml polybrene in standard culture conditions.

Fluorescence microscopy. Successful transduction was verified by visualizing CFP (co-expressed with the $Gluc_{tag}$ construct) and mCherry fluorescent protein (co-expressed with Fluc) using fluorescent microscopy (Leica).

Immunostaining and antibodies. For *in vitro* immunostaining, cells were fixed in 3.7% formaldehyde for 20 minutes, washed with PBS and permeabilized with PBS containing 0.1% Triton X-100. Cells were then washed three times in PBS containing 5% FBS and blocked with PBS containing 5% FBS. Primary mouse-anti-tag monoclonal antibody (10 µg/ml in 100 µl of PBS, Table S1) was added and incubated for one hour at room temperature. Cells were washed again and incubated with 1:100 goat-anti-mouse horseradish peroxidase (HRP) conjugate (Dako) for one hour. After washing, cells were stained with DAB+ (Life Technologies). For mouse tissue staining, tumors were removed and embedded in paraffin. Microtome sections of 5 micron on glass slides were deparaffinized in xylene and rehydrated in ethanol series of 100%, 96%, and 70% ethanol. Endogenous peroxide was blocked with 0.3% H_2O_2 in methanol for 30 minutes. After rinsing with water, antigens were retrieved with citrate buffer (pH 6) with 0.05%

Tween 20 using a microwave (Bosch, five minutes 900 watt, 10 minutes 360 watt). After slowly cooling, tissues were washed three times with PBS and incubated with primary antibody (10 µg/ml), for one hour at room temperature. After washing three times again, tissues were incubated with REAL Envision Rabbit anti-mouse (Dako and REAL DAB+ stained (Dako). Tissue sections were dehydrated with ethanol series as before and fixed in xylene. Cells and sections were imaged and photographed by light microscopy (Leica).

Western blot. U87-FM-$Gluc_{tag}$-CFP cells were lysed in RIPA buffer and mixed with Laemli buffer containing ß-mecaptoethanol (80µl/ml). The samples were separated using a 10% SDS-PAGE gel and the XCell-II blot module (Invitrogen). Primary antibodies (Table S1) were used in a 1:3,000 dilutions and goat-anti-mouse HRP immunoglobuline (Dako) secondary antibody was used in a 1:2,000 dilution. Incubation times were 1 hour at room temperature.

RT-PCR. U87-FM-$Gluc_{tag}$-CFP RNA was isolated using Trizol (Invitrogen) according to manufacturer's guidelines. cDNA was generated using Omniscript RT kit (Qiagen) and PCR was performed in triplo using FastStart SYBR Green Master (Rox) mix (Roche). As a forward primer we used 5'- GCCAACGTGCAGTGTTC-'3, which is located in the Gluc gene. We used the tag antisense oligonucleotides as tag specific reverse primers (Table S1).

In vitro Gluc activity assay. For $Gluc_{tag}$ activity measurement over time, 50,000 cells were plated in a 24-well plate and incubated overnight. A total of 10 µl conditioned medium was harvested from cells and Gluc activity was measured by adding 50 µl (5 µg/ml) coelenterazine (Nanolight Technologies) in PBS and 0.1% Triton X-100). Before addition to the sample, the substrate was incubated at room temperature for 30 minutes for stabilization. Photon counts were determined over 10 seconds in a luminometer (Berthold Technologies). For the measurement of $Gluc_{tag}$ activity with respect to cell number, indicated numbers of cells were plated in a 24-well plate and incubated overnight. $Gluc_{tag}$ activity in medium was determined as described above.

$Gluc_{tag}$ immunobinding assay. White goat-anti-mouse-coated 96-well plates (Thermo Scientific) were washed three times with PBS containing 0.05% Tween 20 and incubated with 50 µl (10 µg/ml) of each of the mouse monoclonal antibody directed against the specific epitope tags (Table S1). Incubation time was two hours while centrifuging at 500 x g at 4°C. Wells were washed and blocked three times with PBS containing 5% FBS and 0.05% Tween 20 on a plate shaker at 65-75 rpm. A total of 30 µl of $Gluc_{tag}$ conditioned medium or $Gluc_{tag}$ mouse blood was added to the well and incubated for two hours at room temperature on a microplate shaker at 65-75 rpm. Wells were washed five times for five minutes on a plate shaker at 65-75 rpm. A total of 50 µl Gluc substrate (5 µg/ml coelenterazine in PBS and 0.1% Triton X-100) was added to the well and photon counts were determined in a microplate luminometer (Tecan) at 0.1 second per well. For the comparison of the bound Gluc to the total Gluc activity, aliquots of conditioned medium or 5 µl mouse blood were transferred to a white 96-wells microplate and assayed using 50 µl (5 µg/ml) coelenterazine in PBS and 0.1% Triton X-100.

In vivo experiments. All *in vivo* experiments were subject to ethical committee approval and are in accordance with VU University Medical Center and national regulations. For subcutaneous tumor xenograft model, six weeks old athymic Nude-Foxn1^{nu} mice (Harlan) were implanted with 5 x 10^5 U87-FM-Gluc$_{tag}$-CFP cells in 50 µl DMEM and 50 µl Matrigel (BD Biosciences). For intracranial tumor implantation, a stereotactic frame (Harvard Biosciences) was used to inject cells vertically into the right hemisphere. General anesthesia was induced by subcutaneous injection of buprenorphine hydrochloride (0.1 mg/kg). The mice were further anesthetized with oxygen containing 2.5% isofluorane. After skin incision, lidocaine drops (5 mg/ml in PBS) were administered topically. A small drill was used to drill a hole into the skull. Coordinates used for injection were X = 0.5 mm, Y = 2 mm, Z = -2 mm from the bregma. A total of 2 x 10^5 cells in 5 µl of DMEM was injected vertically. On indicated days after injection, tumor size was monitored using a calliper (for subcutaneous) and bioluminescence *in vivo* Fluc imaging, by injecting $_D$-luciferin (100 mg/kg) intraperitoneally. Imaging was performed with an IVIS CCD camera and analyzed with Living Image software (Caliper Life Sciences). We collected 300 µl mouse blood aliquots from the tail vein in Microvette CB300 EDTA capillary tubes (Sarstedt) for *ex vivo* whole Gluc measurements and Gluc immunobinding assays.

ACKNOWLEDGEMENTS

This work was supported partly by grants from NWO-VIDI (TW), and NIH/NINDS P30NS045776 and R01NS064983 (BAT). SVR and JN are supported by CCA/VICI Fellowships. We are thankful to Priscilla Jainandunsing, Laura Jonkman, Stephanie van Hoppe, Tonny Lagerweij and Laurine Wedekind for technical support

AUTHOR CONTRIBUTIONS STATEMENT

JN and TW conceived this study and SVR, BAT, JN and TW designed the experimental setup, with help of DN and WPV. SVR performed most of the experiments. SVR, JN, and TW wrote the manuscript, which was edited and reviewed by all the authors.

COMPETING FINANCIAL INTERESTS STATEMENT

All authors declare no competing financial interests.

REFERENCES

1 Gross, S. & Piwnica-Worms, D. Spying on cancer: molecular imaging in vivo with genetically encoded reporters. *Cancer cell* **7**, 5-15 (2005).

2 Pittet, M.J. & Weissleder, R. Intravital Imaging. *Cell* **147**, 983-991 (2011).

3 Contag, C.H. & Ross, B.D. It's not just about anatomy: in vivo bioluminescence imaging as an eyepiece into biology. *Journal of magnetic resonance imaging : JMRI* **16**, 378-87 (2002).

4 Bhaumik, S. & Gambhir, S.S. Optical imaging of Renilla luciferase reporter gene expression in living mice. *Proceedings of the National Academy of Sciences of the United States of America* **99**, 377-82 (2002).

5 Tannous, B.A., Kim, D.-E., Fernandez, J.L., Weissleder, R. & Breakefield, X.O. Codon-optimized Gaussia luciferase cDNA for mammalian gene expression in culture and in vivo. *Molecular therapy : the journal of the American Society of Gene Therapy* **11**, 435-43 (2005).

6 Wurdinger, T. *et al.* A secreted luciferase for ex vivo monitoring of in vivo processes. *Nature methods* **5**, 171-3 (2008).

7 Bhang, H.-eun C., Gabrielson, K.L., Laterra, J., Fisher, P.B. & Pomper, M.G. Tumor-specific imaging through progression elevated gene-3 promoter-driven gene exp ression. *Nature medicine* **17**, 123-9 (2011).

8 Badr, C.E., Hewett, J.W., Breakefield, X.O. & Tannous, B.A. A highly sensitive assay for monitoring the secretory pathway and ER stress. *PloS one* **2**, e571 (2007).

9 Lee, J.Y. *et al.* Development of a dual-luciferase reporter system for in vivo visualization of MicroRNA biogenesis and posttranscriptional regulation. *Journal of nuclear medicine : official publication, Society of Nuclear Medicine* **49**, 285-94 (2008).

10 Tian, W. *et al.* High-Throughput Functional MicroRNAs Profiling by Recombinant AAV-Based MicroRNA Sensor Arrays. *PloS one* **7**, e29551 (2012).

11 McMillin, D.W. *et al.* Tumor cell-specific bioluminescence platform to identify stroma-induced changes to anticancer drug activity. *Nature medicine* **16**, 483-9 (2010).

12 Badr, C.E. & Tannous, B.A. Bioluminescence imaging: progress and applications. *Trends in Biotechnology* **29**, 624-33 (2011).

13 Shaner, N.C., Steinbach, P.A. & Tsien, R.Y. A guide to choosing fluorescent proteins. *Nature methods* **2**, 905-9 (2005).

14 Filonov, G.S. *et al.* Bright and stable near-infrared fluorescent protein for in vivo imaging. *Nature biotechnology* **29**, 757-61 (2011).

15 Deliolanis, N.C. *et al.* In vivo tomographic imaging of red-shifted fluorescent proteins. *Biomedical optics express* **2**, 887-900 (2011).

16 Tannous, B. a Gaussia luciferase reporter assay for monitoring biological processes in culture and in vivo. *Nature protocols* **4**, 582-91 (2009).

17 Niers, J.M., Kerami, M., Pike, L., Lewandrowski, G. & Tannous, B.A. Multimodal in vivo imaging and blood monitoring of intrinsic and extrinsic apoptosis. *Molecular therapy : the journal of the American Society of Gene Therapy* **19**, 1090-6 (2011).

Supplementary table S1. Sequence for different epitope tags and an9bodies used in this study.

Tag name	Sequence of oligonucleotides 1: sense, 2: antisense 5'-3'	Antibody Clone	Company Cat#
Flag	1: CTAGAGACTACAAAGACCATGACGGTGATTATAAAGATCATGACATCGACTACAAGGATGACGATGACAAGTGAC 2: TCGAGTCACTTGTCATCGTCATCCTTGTAGTCGATGTCATGATCTTTATAATCACCGTCATGCTGTTTGTAGTCT	Anti-Flag M2	Sigma-Aldrich F1804
His	1: CTAGACATCATCACCATCACCACTGAC 2: TCGAGTCAGTGGTGATGGTGATGATGT	6xHis tag AD1.1.10	Abcam ab81663
HA	1: CTAGATATCCGTATGATGTGCCGGATTATGCGTGAC 2: TCGAGTCACGCATAATCCGGCACATCATACGGATAT	Hemagglutinin HA.C5	Abcam ab59076
AcV5	1: CTAGAAGCTGGAAGGACGCCAGCGGCTGGAGCTGAC 2: TCGAGTCAGCTCCAGCCGCTGGCGTCCTTCCAGCTT	AcV5 tag AcV5	Abcam ab49581
V5	1: CTAGAGGCAAGCCTATCCCTAACCCTCTGCTGGGCCTGGACAGCACCTGAC 2: TCGAGTCAGGTGCTGTCCAGGCCCAGCAGAGGGTTAGGGATAGGCTTGCCT	V5 tag SV5-Pk1	Abcam ab27671
Glu	1: CTAGATGCGAGGAAGAGGAATACATGCCTATGGAGTGAC 2: TCGAGTCACTCCATAGGCATGTATTCCTCTTCCTCGCAT	Glu-Glu tag Glu-Glu	Abcam Ab24627
Myc	1: CTAGAGAACAAAAACTCATCTCAGAAGAGGATCTGTGAC 2: TCGAGTCACAGATCCTCTTCTGAGATGAGTTTTTGTTCT	Anti-c-Myc 9E10	Sigma-Aldrich M 4439
Kt3	1: CTAGAAAGCCTCCAACACCTCCACCTGAGCCTGAGACCTGAC 2: TCGAGTCAGGTCTCAGGCTCAGGTGGAGGTGTTGGAGGCTTT	KT3 tag KT3	Abcam ab24739
Au1	1: CTAGAGACACCTACAGATACATCTGAC 2: TCGAGTCAGATGTATCTGTAGGTGTCT	Au1 tag AU1	Covance MMS-130P
E2	1: CTAGAAGCAGCACCAGCAGCGACTTCAGAGACAGATGAC 2: TCGAGTCATCTGTCTCTGAAGTCGCTGCTGGTGCTGCTT	E2 tag 5E11	Abcam ab977

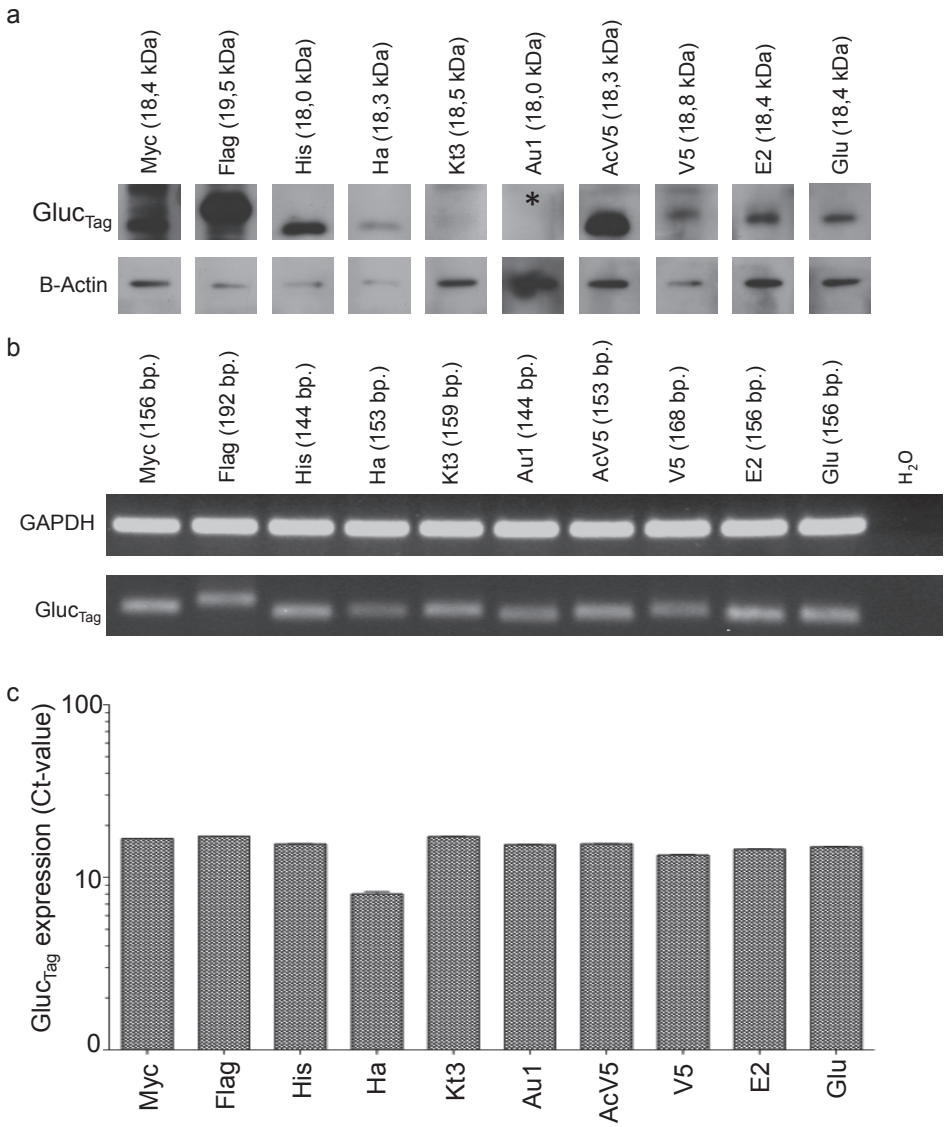

Fig. S1. Gluc$_{tag}$ expression in the ten U87-FM-Gluc$_{tag}$CFP. (a) Western blot, * = not detected. (b) RT-PCR. (c) RT-qPCR.

3

MULTIPLEX FUNCTIONAL BIOLUMINESCENT REPORTERS USING GAUSSIA LUCIFERASE FUSED TO EPITOPE TAGS IN AN IMMUNOBINDING ASSAY

Sjoerd van Rijn, Thomas Würdinger and Jonas Nilsson

Methods in Molecular Biology 1098, 231-47 (2014)

SUMMARY/ABSTRACT

The use of *Gaussia* luciferase in a multiplex assay can have several advantages over the singleplex method for an experimental setup. Issues such as intersample variability, screening purposes, efficiency and *in vivo* applications can be addressed using a multiplex assay. Here we describe a functional reporter multiplex method using *Gaussia* luciferase fused to epitope tags to identify the different reporters that are expressed. Tag specific antibodies are used to bind and separate the tagged luciferase reporters.

Key words: *Gaussia* luciferase, optical imaging, bioluminescent imaging, multiplex assay, epitope tag, antibody binding assay

INTRODUCTION

Bioluminescent reporters can be used to non-invasively detect and quantify biological processes in vitro and in vivo[1]. By engineering the reporter gene under the control of genetic promoters or other gene regulatory elements, the resulting reporter protein reflects the regulation of these elements. Examples of these regulatory elements can be constitutively active promoters to analyse cell survival and proliferation (e.g. CMV promoter) or specific promoters containing transcription factor regulatory elements (TREs) to analyse transcription factor activities[2,3]. Other examples are 3'-UTR regions to analyse miRNA activities[4] and protease cleavage sites (PCSs) to analyse protease activities[5]. Regularly used bioluminescent reporter genes are *Firefly* luciferase[6] (Fluc) and *Renilla* luciferase[7] (Rluc). After translation these luciferases are localised inside the cell's cytoplasm and *ex vivo* detection can therefore be a challenge. The enzyme *Gaussia* luciferase[8] (Gluc) is secreted into the extracellular fluids such as culture medium, animal blood and urine and can therefore be readily non-invasively detected in these fluids enabling serial sampling over time in a single experiment.

One major disadvantage of luciferase reporters is the difficulty to use a multiplicity of luciferase reporters in combination in a single experiment. This limits the use of luciferase reporters in multiplex assays. Attempts are made to use a range of reporters using modified luciferases, each producing light with a different wavelength in order to discriminate between the different parameters they represent. The downside of this strategy is the need for sophisticated equipment to separate the different signals. Also, overlap in the light spectra might make signal separation a challenge and the number of reporters limited.

Another strategy to analyse multiple reporters in a single assay is to use luciferases that need different enzyme substrates to produce light[9]. A regularly used example is *firefly* luciferase, which needs D-luciferin as a substrate, in combination with *Renilla* luciferase, which needs coelenterazine. The disadvantage of this method is the limited number of luciferase substrate combinations currently known.

We aimed to develop an easily adaptable method for multiplexing a secreted luciferase reporter in order to perform broad range screening of biologically relevant processes *in vitro* or *in vivo*. Therefore, we engineered a range of fusion gene reporters consisting of the Gluc gene, each coupled to a different epitope tag[10] (see figure 1). By this method we engineered the ten $Gluc_{Tag}$ reporters $Gluc_{Flag}$, $Gluc_{His}$, $Gluc_{HA}$, $Gluc_{AcV5}$, $Gluc_{V5}$ and $Gluc_{Glu}$, $Gluc_{Myc}$, $Gluc_{Kt3}$, $Gluc_{Au1}$ and $Gluc_{E2}$. Epitope tags[11] are peptide sequences usually derived from viral or bacterial genes, giving them a high affinity to mammalian antibodies. Coupling the Gluc gene to a range of different epitope tags enables us to design a large number of different $Gluc_{Tag}$ reporters. Using the corresponding tag specific antibodies to selectively immunobind the different $Gluc_{Tag}$ makes it possible to separate the different $Gluc_{Tag}$ reporters and individually quantify them by reading out the light production after addition of substrate[10](see figure 3). As a proof of concept we designed ten different $Gluc_{Tag}$ based reporters, each coupled to a different epitope tag, under the control of the constitutively active

Figure 1. Overview of the $Gluc_{Tag}$ construct. We constructed ten $Gluc_{Tag}$ constructs, each with a different tag: $Gluc_{Flag}$, $Gluc_{His}$, $Gluc_{HA}$, $Gluc_{AcV5}$, $Gluc_{V5}$ and $Gluc_{Glu}$, $Gluc_{Myc}$, $Gluc_{Kt3}$, $Gluc_{Au1}$ and $Gluc_{E2}$.

cytomegalovirus (CMV) promoter. After lentiviral transduction[12] we produced ten U87 glioma cell lines, each stably expressing one $Gluc_{Tag}$ reporter and used these cells to collect $Gluc_{Tag}$ conditioned cell culture medium or mouse blood to monitor *in vitro* and *in vivo* tumor cell growth by measuring $Gluc_{Tag}$ activity *ex situ*, after tag specific antibody immunobinding (see figure 3). In this chapter the proof of concept of the multiplex Gaussia luciferase-based functional reporter assays *in vivo* is described[10].

MATERIALS

Construction and development of $Gluc_{Tag}$ reporter cell lines

1. The CSCW-Gluc-IRES-CFP lentiviral vector DNA (see note 1). This lentiviral vector co-expresses the Gluc bioluminescent reporter and the cerulean fluorescent protein (CFP) control. The internal ribosomal entry site (IRES) allows co-expression of both proteins using the same cytomegalovirus (CMV) promoter. The vector is designated CSCW-Gluc-CFP in this protocol.
2. AccuPrime Pfx DNA polymerase (Life Technologies, see note 2). It is provided with a 10 x AccuPrime reaction mix and separate $MgSO_4$ (50 mM).
3. PCR amplification primer oligonucleotides (10 µM, see note 1):
   - Forward: 5'-GCG TGT ACG GTG GGA GGT CT-3'
   - Reverse: 5'-T CTC GAG TAG TCT AGA GTC ACC ACC GGC CCC CTT-3'.
4. PCR thermocycler.
5. Restriction enzymes NheI, XbaI and XhoI (New England Biolabs, see note 3).
6. Heat block.
7. DNA gel electroforesis system.
8. 0.5 % agarose (v/w) DNA gel with ethidium bromide (10 µg/ml final concentration). The total volume depends on the DNA gel electroforesis system used (7.). Add e.g. 0.5 g agarose to 100 ml TAE buffer (9.) and cook it in a microwave for 2 minutes at the highest power (~900 watts). Be careful to make sure that the agarose has melted completely. Cool down the gel to ~65˚C, add ethidium bromide (10 µg/ml final concentration, see note 4) and swirl gel well. Pour gel in a DNA gel cast with a DNA gel slot comb and let it solidify for 30 minutes. Remove the DNA gel slot comb carefully.
9. 1 x TAE buffer (40 mM Tris, 20 mM acetic acid and 1 mM EDTA in dH_2O). Make a 50 x TAE stock solution by dissolving 242 g Tris base in dH_2O. Add 57.1 ml glacial

acetic acid and add 100 ml 0.5 M EDTA (pH 8.0). Add the volume up to 900 ml with dH_2O and set the pH to 8.5 using HCl or NaOH. Bring the total volume to 1000 ml with distilled H_2O and autoclave the TAE buffer for 20 minutes at 121˚C. Dilute 20 ml 50 x TAE stock solution in 980 ml distilled H_2O to prepare 1000 ml 1 x TAE buffer.

10. DNA gel loading dye and a broad range (100 bp – 10.000 bp) DNA gel molecular weight marker. Use the loading dye and the weight marker according to the manufacturers guidelines.
11. DNA gel extraction kit (Qiagen).
12. T4 DNA ligase (Life Technologies).
13. XL10-Gold ultracompetent cells (Agilent Technologies) for large or ligated DNA.
14. LB + ampicillin (50 µg/ml) bacteria selection and propagation plates. To make LB, measure 10 g of peptone, 5 g yeast extract and 10 g NaCl and suspend in 1000 ml distilled H_2O and autoclave the suspension for 20 minutes at 121˚C. Let the LB cool down to ~65˚C and add ampicillin to a final concentration of 50 µg/ml and briefly swirl. Pour 20 ml of LB + ampicillin per plate (Ø 100 mm).
15. 37˚C bacteria incubator.
16. QIAfilter plasmid kit.
17. Epitope tag sense and antisense oligonucleotides with appropriate ligation overhangs (See table 1 and note 1) in a concentration of 100 µM.
18. 10 x Oligonucleotide annealing buffer. To prepare a 50 ml stock solution, mix 5 ml 1 M Tris-HCl (pH 7.5, final concentration 100 mM) with 10 ml 5 M NaCl (final concentration 1 M) and 1 ml 0.5 M EDTA (final concentration 10 mM) and add 34 ml ultrapure H_2O.
19. Human embryonic kidney cell line HEK293T.
20. Human glioblastoma cell line U87.
21. Dulbecco's modified Eagle's medium (DMEM) containing 4.5 g/l glucose, 110 mg/l sodium pyruvate and 584 mg/l L-glutamine. To make DMEM complete culture medium, add 10% Fetal bovine serum and penicillin/streptomycin.
22. Phosphate buffered saline (PBS).
23. Trypsin (0.5 mg/ml) + EDTA (0.22 mg/ml) in PBS.
24. A cell culture incubator at 37˚C and with 5% CO_2.
25. Third generation lentiviral packaging plasmid pRRE, packaging plasmid pRSV/Rev and envelope plasmid pMD2.G (Addgene).
26. 3 M Calcium chloride (CaCl). to make 100 ml of 3 M CaCl solution, dissolve 33.3 g CaCl x $2H_2O$ in 95 ml ultrapure H_2O. Set the pH to 7.2 and fill the solution up to 100 ml. Sterile filter the 3 M CaCl solution.
27. 2x HEPES buffered saline (HEBS). Dissolve 8 g NaCl (final concentration 273.7 mM), 0.37 g KCl (final concentration 9.9 mM), 1 g Na_2HPO_4 (1.4 mM), 1 g dextrose

(final concentration 11.1 mM) and 5 g HEPES (42 mM) in 450 ml ultrapure H_2O. Set the pH to 7.2 and then fill up the solution to 500 ml with ultrapure H_2O. Autoclave the 2x HEBS for 15 minutes at 121˚C.

$Gluc_{Tag}$-CFP multiplex assay application

$Gluc_{Tag}$ immunobinding assay in vitro

1. 6-well cell culture plates.
2. A cell culture incubator at 37˚C and with 5% CO_2.
3. Wash buffer. Add 0.5 ml Tween-20 (0.05%) to 1 l of phosphate buffered saline (PBS) to make the PBS + 0.05% Tween-20 wash buffer solution.
4. White goat anti-mouse IgG coated 96-well microplates (Thermo Scientific, see note 5).
5. Mouse monoclonal anti-Tag IgG (see Table 1, see note 6).
6. Microplate centrifuge.
7. Microplate shaker.
8. Block buffer. Add 0.5 ml Tween-20 (0.05%) and 10 g bovine serum albumin (BSA, 1% v/w) in 1 l of phosphate buffered saline (PBS) to make the PBS + 0.05% Tween-20 + 1% BSA block buffer solution.
9. Coelenterazine Gluc substrate. Dilute coelenterazine in methanol (5 mg/ml) to make a stock solution. Before use, dilute the stock solution coelenterazine 1 µl per 1000 µl PBS + Triton X-100. Incubate the final user solution coelenterazine (5 µg/ml) 30 minutes at room temperature.
10. Microplate luminometer.

$Gluc_{Tag}$ immunostaining in vitro

1. 24-well plates.
2. Phosphate buffered saline (PBS).
3. 3.7% formaldehyde fixative solution.
4. Block buffer. Add 10 g bovine serum albumin (BSA) to 1 L of PBS to make a PBS + 1% BSA block buffer solution.
5. Permeabilization buffer. Add 1 ml Triton X-100 to 1 l of PBS to make a PBS + 0.1% Triton X-100 permeabilization buffer solution.
6. Mouse monoclonal anti-Tag IgG (see Table 1, see note 6).
7. Goat polyclonal anti-mouse-HRP Ig (Dako).
8. DAB substrate kit.
9. Light microscope.

Gluc$_{Tag}$ immunobinding assay in vivo

1. Athymic nude-foxn1^{nu} mice.
2. Isoflurane anaesthesia system.
3. Temgesic (Buprenorfinehydrochloride) analgesia in PBS.
4. Small animal stereotaxic frame.
5. Surgical scalpel.
6. Microsyringe (Hamilton).
7. Microdrill 0.8 mm.
8. Capillary collection and sample container (Sarstedt, see note 7).
9. Blood dilution buffer. Add 0.8 g EDTA (0.8% v/w) to 100 ml PBS to make PBS + 0.8% EDTA blood dilution buffer solution.
10. White goat anti-mouse IgG coated 96-well microplates (Thermo Scientific, see note 5).
11. Wash buffer. Add 0.5 ml Tween-20 (0.05%) to 1 l of phosphate buffered saline (PBS) to make the PBS + 0.05% Tween-20 wash buffer solution.
12. Mouse monoclonal anti-Tag IgG (see Table 1, see note 6).
13. Microplate centrifuge.
14. Block buffer. Add 0.5 ml Tween-20 (0.05%) and 10 g bovine serum albumin (BSA, 1% v/w) in 1 l of phosphate buffered saline (PBS) to make the PBS + 0.05% Tween-20 + 1% BSA block buffer solution.
15. Microplate shaker.
16. Coelenterazine Gluc substrate. Dilute coelenterazine in methanol (5 mg/ml) to make a stock solution. Before use, dilute the stock solution coelenterazine 1 µl per 1000 µl PBS + Triton X-100. Incubate the final user solution coelenterazine (5 µg/ml) 30 minutes at room temperature.
17. Microplate luminometer.

Gluc$_{Tag}$ immunostaining in vivo

1. Formaldehyde 3.7% in PBS. To make 100 ml of 3.7% formaldehyde in PBS, add 10 ml of 37% stock solution formaldehyde to 90 ml of phosphate buffered saline (PBS) and mix.
2. Microtome.
3. Glass microscope slides.
4. Xylene.
5. Ethanol series. Make 3 ethanol solutions of 100%, 97% and 75% ethanol in H_2O. To make 100 ml of 97% ethanol solution, add 97 ml ethanol in 3 ml H_2O and mix. To make 100 ml of 75% ethanol solution, add 75 ml ethanol to 25 ml H_2O and mix.

6. 0.3% H_2O_2 in methanol. To make a 0.3% hydrogen peroxide (H_2O_2) in methanol solution, add 1 ml of 30% H_2O_2 stock solution to 100 ml of methanol and mix.
7. Antigen retrieval citrate buffer. To make the antigen retrieval citrate buffer, add 1.92 g anhydrous citric acid (final concentration 10 mM) to 950 ml of H_2O and mix. Set the pH to 6 and fill up the solution to 1 l. Finally, add 0.5 ml of Tween-20 and mix well.
8. Microwave.
9. Mouse monoclonal anti-Tag IgG (see Table 1, see note 6).
10. Antibody diluent (Dako).
11. Phosphate buffered saline (PBS).
12. Goat polyclonal anti-mouse-HRP Ig (Dako).
13. DAB substrate kit.
14. Haematoxyline staining solution.
15. Light microscope.

3 METHODS

Construction and development of $Gluc_{Tag}$ reporter cell lines

1. Construct the $Gluc_{modified}$ gene by amplifying the $Gluc_{parental}$ gene from lentiviral vector CSCW-Gluc-CFP (see figure 2 and note 1) making a PCR reaction mix of 20 µl using primers that exclude the STOP codon and add the unique restriction site XbaI downstream. Use a high fidelity proof reading DNA polymerase and follow the manufacturer's guidelines to amplify the $Gluc_{modified}$ gene (633 bp) in thermal cycler by 1: denature the plasmid DNA for 2 minutes at 95˚C. Then 2: denature for 30 seconds at 95˚C, 3: anneal primers for 30 seconds at 62˚C and 4: elongate DNA for 1 minute at 72˚C and cycle sequence 2, 3, 4 for 35 times. Allow 5: final elongation of DNA for 2 minutes at 72˚C.
2. To form sticky ends to the $Gluc_{modified}$ gene in order to clone it back into the CSCW lentiviral backbone to replace the $Gluc_{parental}$ gene, restrict the $Gluc_{modified}$ gene with restriction enzyme NheI upstream, and restriction enzyme XhoI downstream. Restrict the total volume of the PCR reaction from (1.) by making a double digestion using high fidelity enzymes (see note 3), according to the manufacturer's guidelines in a total volume of 50 µl. Incubate the restriction mix for 2 hours at 37˚C to ensure complete restriction. Also, create the CSCW lentiviral backbone by restricting 2 µg of the parental CSCW-Gluc-CFP lentiviral vector with NheI and XhoI as described to restrict out the $Gluc_{parental}$ gene.
3. Isolate and purify the $Gluc_{modified}$ gene from (2.) and the CSCW lentiviral backbone from (2.) on a 0.5% (w/v) agarose DNA gel. Add DNA loading buffer (final concentration is 1x DNA loading buffer) to the $Gluc_{modified}$ gene and CSCW lentiviral backbone

Table 1. Epitope sequences and antibodies used in the immunobinding assays and immunostainings. The epitope tag oligonucleotides are designed to complement each other and to create the proper ligation overhang (XbaI-tag sequence-XhoI). The assay is optimised for use with epitope tag Flag, His, HA, AcV5, V5 and Glu. They show a high binding and assay performance *in vitro* and *in vivo*. Epitope tag combinations Myc, Kt3, Au1 and E2 show a low binding and assay performance due to a lower antibody affinity. Conditions for use of these epitope tags or other tags in the assay need to be optimised.

Tag	Oligonucleotide sequence (sense, antisense, 5'-XbaI-Tag-XhoI-3')	Antibody
Flag	CTAGAGACTACAAAGACCATGACGGTGATTATAAAGATCATGACATCGACTACAAGGATGACGATGACAAGTGAC	Sigma-Aldrich
	TCGAGTCACTTGTCATCGTCATCCTTGTAGTCGATGTCATGATCTTTATAATCACCGTCATGGTCTTTGTAGTCT	F1804
His	CTAGACATCATCACCATCACCACTGAC	Abcam
	TCGAGTCAGTGGTGATGGTGATGATGT	ab81663
HA	CTAGATATCCGTATGATGTGCCGGATTATGCGTGAC	Abcam
	TCGAGTCACGCATAATCCGGCACATCATACGGATAT	ab59076
AcV5	CTAGAAGCTGGAAGGACGCCAGCGGCTGGAGCTGAC	Abcam
	TCGAGTCAGCTCCAGCCGCTGGCGTCCTTCCAGCTT	ab49581
V5	CTAGAGGCAAGCCTATCCCTAACCCTCTGCTGGGCCTGGACAGCACCTGAC	Abcam
	TCGAGTCAGGTGCTGTCCAGGCCCAGCAGAGGGTTAGGGATAGGCTTGCCT	ab27671
Glu	CTAGATGCGAGGAAGAGGAATACATGCCTATGGAGTGAC	Abcam
	TCGAGTCACTCCATAGGCATGTATTCCTCTTCCTCGCAT	ab24627
Myc	CTAGAGAACAAAAACTCATCTCAGAAGAGGATCTGTGAC	Sigma-Aldrich
	TCGAGTCACAGATCCTCTTCTGAGATGAGTTTTTGTTCT	M4439
Kt3	CTAGAAAGCCTCCAACACCTCCACCTGAGCCTGAGACCTGAC	Abcam
	TCGAGTCAGGTCTCAGGCTCAGGTGGAGGTGTTGGAGGCTTT	ab24739
Au1	CTAGAGACACCTACAGATACATCTGAC	Covance
	TCGAGTCAGATGTATCTGTAGGTGTCT	MMS-130P
E2	CTAGAAGCAGCACCAGCAGCGACTTCAGAGACAGATGAC	Abcam
	TCGAGTCATCTGTCTCTGAAGTCGCTGCTGGTGCTGCTT	ab977

restriction mixtures from (2.) and load both the samples into a separate gel well. Also load a separate well with a DNA molecular weight marker to identify the product and confirm product sizes. Run the gel in 1 x TAE buffer at 100 volts until the $Gluc_{parental}$ gene (718 bp) has separated properly from the CSCW lentiviral backbone (9408 bp).

4. Extract the $Gluc_{modified}$ gene construct (570 bp) and the CSCW lentiviral backbone (9408 bp) using a DNA gel extraction kit according to manufacturer's protocol. After elution with 50 µl elution buffer, heat both the DNA extractions in an open tube to 60˚C for 5 minutes to completely evaporate any residual ethanol.
5. To clone the $Gluc_{modified}$ gene into the CSCW lentiviral backbone, ligate 100 ng CSCW lentiviral backbone from (4.) with 57 ng $Gluc_{modified}$ gene from (4.) (($Gluc_{modified}$ gene):(CSCW lentiviral backbone) is 10:1 molar ratio, see note 8) using a T4 DNA ligase according to the manufacturer's guidelines. Use a total reaction volume of 20 µl.
6. Transform the resulting ligation product CSCW-$Gluc_{modified}$-CFP lentiviral vector in ultracompetent bacterial cells for ligated DNA according to the manufacturer's guidelines in order to make bacterial clones for CSCW-$Gluc_{modified}$-CFP lentiviral vector production. Plate the bacterial cells on a LB + ampicillin (50 µg/ml) bacteria selection and propagation plate and grow the bacterial colonies overnight at 37˚C.
7. Amplify and isolate the CSCW-$Gluc_{modified}$-CFP lentiviral vector using a DNA plasmid kit following the manufacturer's guidelines.
8. Construct epitope tag inserts by annealing the corresponding epitope tag sense and antisense oligonucleotides (see Table 1). Mix 50 µl of H_2O with 10 µl of the 10x annealing buffer, 20 µl of the sense oligonucleotide (100 µM) and 20 µl of the antisense oligonucleotide (100 µM). Heat the annealing mixture in a heat block for 10 minutes at 65˚C, then take out the metal heat block insert to very slowly cool down the annealing mixture to room temperature.
9. Restrict 2 µg of the CSCW-$Gluc_{modified}$-CFP using restriction enzymes XbaI and XhoI to open up the CSCW lentiviral backbone in order to insert the epitope tag from (8.). Make a 20 µl double digestion using high fidelity restriction enzymes and follow manufacturer's guidelines.
10. Isolate and purify the CSCW lentiviral backbone as described in (3.) and clone the epitope tag insert into the CSCW lentiviral backbone as described in (5.). Use a molar ratio (epitope insert):(CSCW lentiviral vector, see note 8) of 10:1 and a total volume of 20 µl. Transform the resulting CSCW-$Gluc_{Tag}$-CFP lentiviral vector ligation product as described in (6.) and amplify the vector as described in (7.).
11. HEK293T and U87 cells are cultured in DMEM complete culture medium at 37˚C and 5% CO_2. The cells are diluted 1/10 when the culture vessel is ~90% confluent. To dilute, aspirate the culture medium and was attached cells with PBS. Shake culture vessel gently and aspirate PBS. Detach the cells by adding 1x Trypsin + EDTA, enough to just cover the surface of the culture vessel. Incubate the cells 5 minutes at

37˚C for 5 minutes. Resuspend the cells in DMEM complete culture medium (>5x the Trypsin + EDTA volume) and aspirate 9/10 of the total volume to discard or collect the suspended cells. Add DMEM complete culture medium to the 1/10 leftover cell suspension up to the final culture volume. Make sure the surface of the culture vessel is covered with ~0.5 cm culture medium. Use room temperature reagents.

12. Produce the lentiviral particles as described in (Ref. Dull et al.). Transiently transfect 5.5 x 10^6 HEK293T cells in a 10 cm^2 culture dish with 3 µg pMD2.G envelope plasmid, 5 µg pMDLg/pRRE and 2.5 µg pRSV/Rev packaging plasmids and 10 µg CSCW-$Gluc_{Tag}$-CFP lentiviral vector using the calcium phosphate transfection method (Ref, see note 9). Harvest the virus-containing medium and spin at 1000 x G for 5 minutes to remove residual cells and debris. Aliquote and store the virus-containing medium at 4˚C for use within a week or at -80˚C for longer periods of time.
13. Make U87 cell lines (see note 10) stably expressing $Gluc_{Tag}$-CFP by lentiviral transduction as described in (Dull et al.). Transduce 2 x 10^5 U87 cells in a 6 well plate with CSCW-$Gluc_{Tag}$-CFP lentivirus (MOI of 5, see note 11) overnight. The following day, replace the virus-containing medium with 2 ml fresh DMEM complete culture medium. Expand and culture the cells as described in (11.). Transduction efficiency can be determined by fluorescence microscopy of CFP (455-480 nm).

$Gluc_{Tag}$-CFP multiplex assay application

$Gluc_{Tag}$ immunobinding assay in vitro

1. Plate U87-$Gluc_{6x\ Tag}$-CFP cells (see note 10) in a 6-well plate in DMEM complete culture medium and culture the cells in 37˚C and 5% CO_2. For a triplo experiment, plate 3 wells of a 6-well plate.
2. At predetermined time points, collect 180 µl (30 µl x 6 Tags) of the $Gluc_{6x\ Tag}$ conditioned culture medium of the 3 wells and store the culture medium at 4˚C (see figure 2).
3. After the final time point collection, Wash 18 wells (6 Tags in triplo) per time point of a goat anti-mouse IgG coated 96-well microplate 3 x with 200 µl wash buffer (see note 5).
4. Per timepoint, prepare 150 µl wash buffer with mouse anti-Tag monoclonal IgG (10 µg/ml, see Table 1, see note 6) for all 6 Tags. Coat the wells with 50 µl anti-Tag monoclonal mixture per well (see figure 2) and incubate for 1 hour at 4˚C spinning at 500 x G followed by 1 hour of incubation at room temperature on a microplate shaker at 65-75 RPM (to create a gentle swirl in the wells).
5. Then, aspirate anti-Tag monoclonal mixture and the wash the wells 3 x with 200 µl of block buffer for 5 minutes on a microplate shaker at 65-75 RPM (to create a gentle swirl in the wells).
6. To bind the $Gluc_{Tag}$ from the conditioned culture medium, add 30 µl of the $Gluc_{6x\ Tag}$ conditioned culture medium to a mouse anti-tag coated well and incubate at room

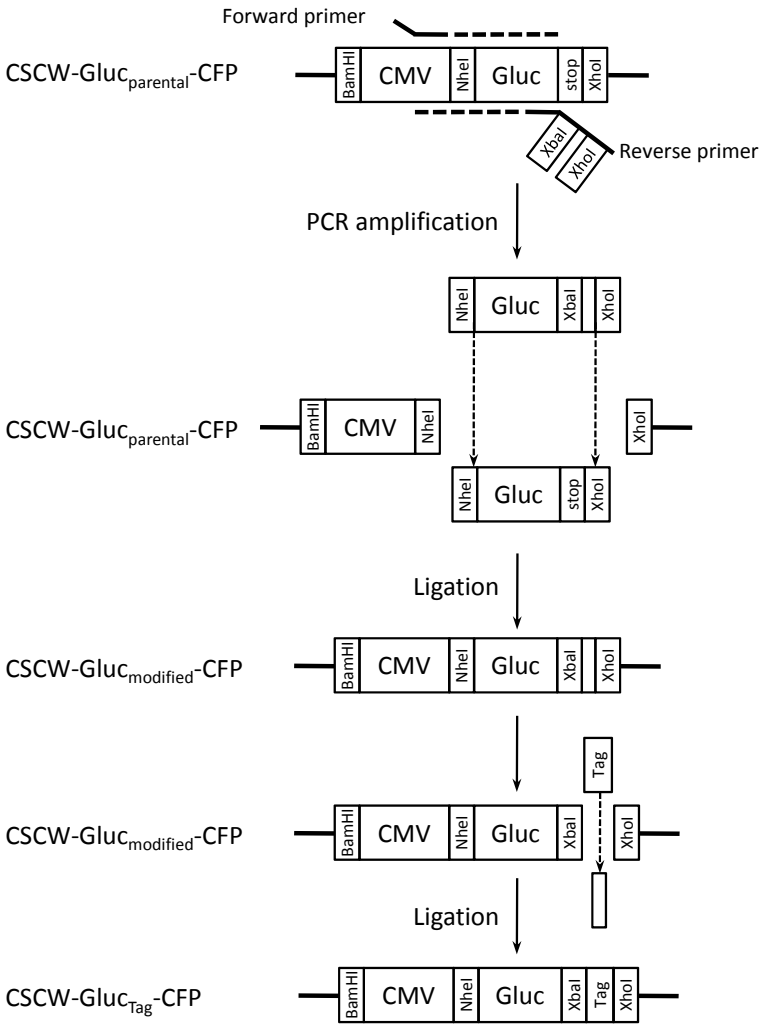

Figure 2. Gluc$_{Tag}$ cloning strategy. The Gluc gene is amplified from the parental vector using primers that amplify Gluc without the tata-box and adding an XbaI and XhoI restriction site downstream. This modified Gluc gene then replaces the original Gluc gene in the parental vector to construct the Gluc$_{modified}$ vector. Then, the vector is restricted with XbaI and XhoI to insert an epitope tag of choice. This Gluc$_{Tag}$ is the final construct.

temperature for 2 hours on a microplate shaker with 65-75 RPM (to create a gentle swirl in the wells).

7. After this, aspirate the culture medium and wash the wells 5 x for 5 minutes with 200 µl wash buffer on a microplate shaker at 65-75 RPM (creating a gentle swirl in the wells).
8. To measure the bound Gluc$_{Tag}$ in the mouse anti-Tag coated wells, aspirate the wash buffer completely and just before measurement add 50 µl coelenterazine

Gluc substrate per well using a multichannel pipette. Immediately insert the plate in the microplate luminometer (see note 11), shake the plate briefly and read out the wells for 0.1 second per well (see figure 3).

$Gluc_{Tag}$ Immunostaining in vitro

1. Plate 10^5 of the U87-$Gluc_{tag}$ cell lines (see note 10) in a 24 well plate overnight in 500 µl DMEM complete culture medium at 37˚C and 5% CO_2.
2. The next day, wash the cells with 200 µl PBS and fix with 100 µl 3.7% formaldehyde fixative solution for 20 minutes.
3. Then, wash and block the cells 3 x 5 minutes with 200 µl block buffer and permeabilize the cells with 100 µl permeabilization buffer for 15 minutes.
4. Next, wash and block the cells 2 x 5 minutes with 200 µl block buffer.
5. Add 100 µl primary mouse anti-tag IgG (2 µg/ml, see note 6) in block buffer to the cells and incubate for 1 hour at room temperature.
6. Subsequently, wash and block the cells 3 x 5 minutes with 200 µl block buffer.
7. Add 100 µl secondary goat anti-mouse-HRP antibody (5 µg/ml, see note 12) in block buffer to the cells and incubate for 1 hour at room temperature.
8. Then, wash the cells 3 x for 5 minutes with 200 µl block buffer and stain the cells with the DAB reagent set according to the manufacturers guidelines. Analyse the immunostaining using light microscopy (see figure 4).

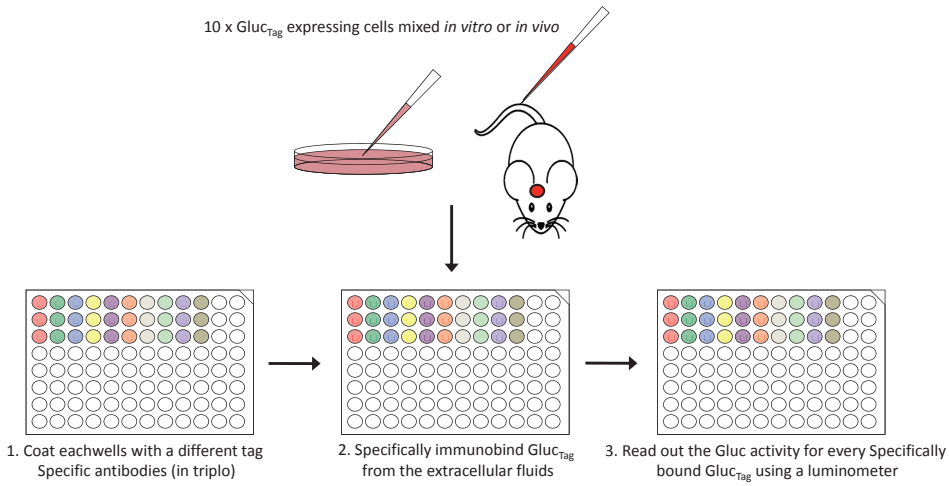

Figure 3. Immunobinding assay. A white 96-well microplate is coated with anti-tag antibodies. Every well contains one antibody specific for one $Gluc_{Tag}$. Cell culture medium or animal blood containing a mix of all ten different $Gluc_{Tags}$ is added to the well to immunobind a specific $Gluc_{Tag}$ reporter. After washing the bioluminescent activity of every specific $Gluc_{Tag}$ reporter is determined using a luminometer.

$Gluc_{Tag}$ immunobinding assay in vivo

1. Culture and collect the U87-$Gluc_{Tag}$-CFP cells as described before. Collect 5 x 10^5 U87-$Gluc_{Tag}$-CFP cells per orthotopical injection in athymic nude-foxn1^{nu} mouse. For a triplo experiment inject 3 mice.
2. 30 minutes before surgery of the mouse, subcutaneously administer Temgesic (Buprenorfinehydrochloride, 0.1 mg/kg) in PBS analgesia and anesthetize the mouse using an isoflurane anaesthesia and fix the mouse in a small animal stereotaxic frame.
3. Incise the head skin with a surgical scalpel and locate the injection site x = 2 mm and y = 0.5 mm from bregma. Drill a hole in the skull and slowly inject the U87-$Gluc_{Tag}$-CFP cell suspension into the brain. Then, cover up the skull with the head skin and stitch the wound.
4. At predetermined time points, collect 100 µl of the $Gluc_{Tag}$ conditioned mouse blood of all the mice using a capillary collection and sample container containing EDTA to prevent blood clotting and store the blood at 4˚C (see note 7).
5. After the final blood sample collection, dilute the blood 1:1 with blood dilution buffer to increase the sample volume to 180 µl.
6. Wash 18 wells (6 Tags in triplo) per time point of a goat anti-mouse IgG coated 96-well microplate (see note 5) 3 x with 200 µl wash buffer.
7. Per timepoint, prepare 150 µl wash buffer with mouse anti-Tag monoclonal IgG (10 µg/ml, see Table 1) for all 6 Tags (see note 13). Coat the wells with 50 µl anti-Tag monoclonal mixture per well and incubate for 1 hour at 4˚C spinning at 500 x G followed by 1 hour of incubation at room temperature.
8. Then, aspirate anti-Tag monoclonal mixture and the wash the wells 3 x with 200 µl of block buffer for 5 minutes on a microplate shaker at 65-75 RPM (to create a gentle swirl in the well).
9. To bind the $Gluc_{Tag}$ from the conditioned mouse blood, add 30 µl of the diluted $Gluc_{6x\,Tag}$ blood samples to a mouse anti-tag coated well and incubate at room temperature for 2 hours on a microplate shaker with 65-75 RPM (to create a gentle swirl in the well).
10. After this, aspirate the diluted $Gluc_{6x\,Tag}$ blood samples and wash the wells 5 x for 5 minutes with 200 µl wash buffer on a microplate shaker at 65-75 RPM (creating a gentle swirl).
11. To measure the bound $Gluc_{Tag}$ in the mouse anti-Tag coated wells, aspirate the wash buffer completely and just before measurement add 50 µl coelenterazine Gluc substrate per well using a multichannel pipette. Immediately insert the plate in the microplate luminometer plate reader, shake the plate briefly and read out the wells for 0.1 second per well (see figure 3 and note 11).

$Gluc_{Tag}$ Immunostaining in vivo

1. After the *in vivo* $Gluc_{Tag}$ assay, collect and fix the mouse brains containing the tumor in 3.7% formaldehyde for at least 48 hours. Then, dehydrate and embed the tissue samples in paraffin.
2. Using a microtome, section the paraffin embedded tissue samples in 5 µm slices and mount the slices on glass slides.
3. Deparaffinise the tissue slices in xylene and rehydrate in a series of 100% ethanol, 96% ethanol and 75% ethanol.
4. Block the endogenous peroxidase with fresh 0.3% H_2O_2 in methanol for 30 minutes at room temperature and rinse the slices with H_2O.
5. Perform antigen retrieval by cooking the slices in citrate buffer (pH 6) using a microwave. Cook the samples 5 minutes at 100% power and 10 minutes at 50% power. Cool the slices down to room temperature in 20 minutes and rinse the slices 3 x 5 minutes with PBS.
6. Incubate the slices with mouse anti-Tag monoclonal IgG (final concentration is 2 µg/ml, see note 6) diluted in in antibody diluent for 1 hour at room temperature. After IgG incubation, rinse the slices 3 x 5 minutes with PBS.
7. Incubate the slices with anti-mouse-HRP (1 in 200) diluted in antibody diluent for 30 minutes at room temperature and rinse the slices 3 x 5 minutes in PBS.
8. Incubate the slices with DAB for 5 to 10 minutes and rinse the slices with H_2O.
9. Counterstain the cell nuclei of the tissue slices with haematoxyline for 30 to 60 seconds and rinse the slices with PBS.
10. Dehydrate the slices in the ethanol series of 75% ethanol, 96% ethanol and 100% ethanol and incubate the slices in xylene for 5 minutes. Let the tissue slices dry and analyse them using a light microscope (see figure 4).

NOTES

1. In the assay described here, we use the CSCW-Gluc-IRES-CFP lentiviral vector DNA as a template to amplify the Gluc reporter gene and to religate our $Gluc_{Tag}$ reporter constructs in. When using other template vectors or reporters, it is necessary do redesign primers, restriction sites and oligonucleotide sequences and PCR programs should be optimised in order to fit the alternative vector DNA or reporter gene.
2. We advise to use a high fidelity proof reading DNA polymerase for the amplification of the Gluc reporter gene. This minimizes optimization and the risk of copy errors due to incorrect basepairing.
3. We advise to use high fidelity restriction enzymes for restriction of the DNA vectors. This increases restriction efficiency and user simplicity since most high fidelity enzymes are optimised in the same restriction reaction buffer. Also, most

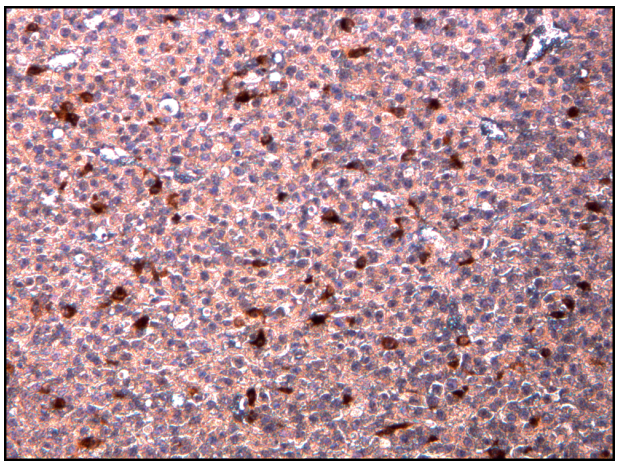

Figure 4. $Gluc_{Tag}$ Immunostaining. Representative immunostaining of ten mixed U87-$Gluc_{Tag}$-CFP cell lines in a mouse xenograft, each expressing another $Gluc_{Tag}$. In this example, an immunostaining against $Gluc_{V5}$ was performed using an anti-V5 mouse immunoglobulin. The $Gluc_{V5}$ expressing U87 cells can be clearly distinguished from the other cells in the tumor.

high fidelity restriction enzymes are optimised to have less star activity, increasing ligation efficiency in later steps of the protocol.

4. There are less hazardous alternatives available for ethidium bromide, such as SYBR safe DNA gel stain (Life Technologies). Besides being less hazardous, these stains can also be used to visualize DNA with non-UV-light, decreasing damage of the DNA due to UV exposure.
5. For luciferase assays it is best to use white microplates to prevent crossover detection of photons between wells. The white goat anti-mouse IgG coated microplates (Thermo Scientific) are pre-coated to improve assay stability but it is also possible to manually coat microplates (e.g. ELISA microplates).
6. The antibodies we used are all mouse monoclonal IgG antibodies. The coated microplates used (see note 5) are optimised to use with mouse IgG antibodies. Using monoclonal antibodies over polyclonal antibodies improves assay stability. We were able to optimize 6 $gluc_{Tag}$ antibody combinations for high performance binding capacity while for $Gluc_{Tag}$ antibody combinations showed low binding capacity due to a lower affinity of the antibody to the epitope tag. When using new antibodes, you should optimize the immunobinding assay by validating the antibody binding capacity to the $Gluc_{Tag}$.
7. The capillary collection and sample container (Sarstedt) we used combines a capillary blood collector with an EDTA coated sample container. This enables fast and easy sample collection and storage. If you collect mouse blood using other methods, make sure you add EDTA to the blood sample to prevent clotting.

8. To quantify the concentration of the DNA gel extracts, we do not recommend the use of spectrophotometry (Nanodrop) since the concentration will usually be low (<100 ng/µl). We advise to quantify the concentrations of the DNA gel extracts by loading a small amount of DNA sample on a gel and quantify the resulting bands by comparing to the molecular marker. We used ImageJ to quantify the DNA sample concentrations and calculate the ligation conditions.
9. Generally, higher virus titers are obtained using other methods of transfection of the plasmids and vectors. Using Lipofectamine 2000 (Life Technologies) or Fugene (Promega) can be beneficial for virus production titres.
10. It is possible to transduce other cell lines of your interest but not all cell lines are equally resistant to lentiviral transduction and therefore the transduction conditions need to be optimized for every cell line. To increase transduction efficiency, it might be beneficial to culture the cells with polybrene (2-10 µg/ml) before transduction. Also using polybrene requires optimization, depending on the cell line of use. Expression of the reporters is also cell line dependent since the CMV promoter is not equally active in all cell lines and therefore also the promoter might be an issue for optimization.
11. Since the Gluc photon signal is degrading over time (~10% per minute), the most stable method of measuring would be to measure Gluc signal directly after coelenterazine substrate addition. A plate reader with a substrate injector would be optimal but it is also an option to use a multichannel pipette. Measuring a 96-well microplate for 0.1 second per well would take about 10 seconds, so the time difference as a result of measuring the first well and the last well would be well within 10% deviation as a result of the Gluc signal degradation.
12. For this assay we used goat anti-mouse secondary Ig. It would also be possible to use other anti-mouse Ig antibodies but optimisation is required.
13. As a negative control for the immunobinding assays and the stainings it is possible to use the CSCW-$Gluc_{ctrl}$-CFP vector. This vector contains the Gaussia luciferase not fused with an epitope tag.

REFERENCES

1 Badr, C. E. & Tannous, B. a. Bioluminescence imaging: progress and applications. *Trends in Biotechnology* **3**, 1–10 (2011).

2 Stratowa, C. & Audette, M. Transcriptional regulation of the human intercellular adhesion molecule-1 gene: a short overview. *Immunobiology* **193**, 293–304 (1995).

3 Wrana, J. L., Attisano, L., Wieser, R., Ventura, F. & Massagué, J. Mechanism of activation of the TGF-beta receptor. *Nature* **370**, 341–7 (1994).

4 Subramaniam, D. *et al*. Translation inhibition during cell cycle arrest and apoptosis: Mcl-1 is a novel target for RNA binding protein CUGBP2. *American journal of physiology. Gastrointestinal and liver physiology* **294**, G1025–32 (2008).

5 Niers, J. M., Kerami, M., Pike, L., Lewandrowski, G. & Tannous, B. A. Multimodal in vivo imaging and blood monitoring of intrinsic and extrinsic apoptosis. *Molecular therapy : the journal of the American Society of Gene Therapy* **19**, 1090–6 (2011).

6 De Wet, J. R., Wood, K. V, DeLuca, M., Helinski, D. R. & Subramani, S. Firefly luciferase gene: structure and expression in mammalian cells. *Molecular and cellular biology* **7**, 725–37 (1987).

7 Loening, A. M., Wu, A. M. & Gambhir, S. S. Red-shifted Renilla reniformis luciferase variants for imaging in living subjects. *Nature methods* **4**, 641–3 (2007).

8 Tannous, B. A., Kim, D.-E., Fernandez, J. L., Weissleder, R. & Breakefield, X. O. Codon-optimized Gaussia luciferase cDNA for mammalian gene expression in culture and in vivo. *Molecular therapy : the journal of the American Society of Gene Therapy* **11**, 435–43 (2005).

9 McNabb, D. S., Reed, R. & Marciniak, R. A. Dual luciferase assay system for rapid assessment of gene expression in Saccharomyces cerevisiae. *Eukaryotic cell* **4**, 1539–49 (2005).

10 Van Rijn, S. *et al*. Functional multiplex reporter assay using tagged Gaussia luciferase. *Scientific reports* **3**, 1046 (2013).
Ford, C. F., Suominen, I. & Glatz, C. E. Fusion tails for the recovery and purification of recombinant proteins. *Protein expression and purification* **2**, 95–107

11 Dull, T. *et al*. A third-generation lentivirus vector with a conditional packaging system. *Journal of virology* **72**, 8463–71 (1998).

4

EZH2-REGULATED DAB2IP IS A MEDULLOBLASTOMA TUMOR SUPPRESSOR AND A POSITIVE MARKER FOR SURVIVAL

Michiel Smits, Sjoerd van Rijn, Esther Hulleman, Dennis Biesmans, Dannis G. van Vuurden, Marcel Kool, Christine Haberler, Eleonora Aronica, W. Peter Vandertop, David P. Noske, and Thomas Würdinger

Clinical Cancer Research 18, 4048-58 (2012)

ABSTRACT

Purpose: Medulloblastoma is the most common malignant brain tumor in children. Despite recent improvements, the molecular mechanisms driving medulloblastoma are not fully understood and further elucidation could provide cues to improve outcome prediction and therapeutic approaches.

Experimental Design: Here, we performed a meta-analysis of mouse and human medulloblastoma gene expression datasets, in order to identify potential medulloblastoma tumor suppressor genes.

Results: We identified DAB2IP, a member of the RAS-GTPase activating protein family (RAS GAP), and demonstrated that DAB2IP expression is repressed in medulloblastoma by EZH2-induced trimethylation. Moreover, we observed that reduced DAB2IP expression correlates significantly with a poor overall survival of medulloblastoma patients, independent of metastatic stage. Finally, we demonstrated that ectopic DAB2IP expression enhances stress-induced apoptotis in medulloblastoma cells and that reduced expression of DAB2IP in medulloblastoma cells conveys resistance to irradiation-induced cell death.

Conclusion: These results suggest that repression of DAB2IP may at least partly protect medulloblastoma cells from apoptotic cell death. Moreover, DAB2IP may represent a molecular marker to distinguish medulloblastoma patients at high risk from those with a longer survival prognosis.

INTRODUCTION

Brain tumors are the most common form of solid tumors in children of which medulloblastoma is the most frequent malignant variant, accounting for 20% of cases [1]. Treatment modalities consist of surgery, radiotherapy and chemotherapy and result in a 5-year survival rate of 40% in high risk patients and 80-90% in low risk patients [2]. Approximately 30% of patients however remain incurable and current intensive treatment protocols cause significant adverse long term effects [3]. Medulloblastomas comprise four subtypes: WNT, SHH, Group 3 and Group 4 which differ regarding histology and clinical outcome [4] and are believed to derive from the deregulation of various signalling pathways in brain development, such as the WNT-pathway and sonic hedgehog (SHH) signalling pathways. Over activation of these pathways leads to a loss of cell cycle control and a dysfunctional apoptosis program, allowing for continued growth and tumorigenesis, predominantly in the cerebellum [5].

DAB2IP - disabled homolog 2-interacting protein, located at chromosome 9q33.1-q33.3 - is a member of the RAS-GTPase activating protein family (RAS GAP) that inactivates RAS by promoting conversion of GTP into GDP [6]. DAB2IP acts as a putative tumor suppressor gene and is down-regulated by epigenetic modification in multiple aggressive cancers. In prostate cancer DAB2IP expression was shown to be repressed by promoter methylation and histone modification [7], while in breast cancer [8], lung cancer [9], and gastrointestinal tumors [10], aberrant promoter hypermethylation was shown to down-regulate DAB2IP. Moreover, it was shown in prostate cancer that down-regulation of DAB2IP expression results in resistance to ionizing radiation [11], it initiates epithelial-to-mesenchymal transition [12] and promotes tumor growth and metastasis [13]. In addition, DAB2IP is involved in TNFα-induced apoptosis in prostate cancer cells by suppressing the ASK1-JNK and PI3-AKT pathway [14], and in endothelial cells via the ASK1-JNK pathway [15].

Apoptosis is a programmed variant of cell death common to all human cells. Defects in the apoptosis program result in an imbalance in the rate of cell proliferation and the rate of cell death thereby contributing to tumor growth and treatment resistance. Essential steps in the apoptotic mechanism are inactivated in medulloblastoma cells, resulting in resistance to apoptosis. A recent *in vivo* study showed that cerebellar stem cells can give rise to medulloblastomas when having acquired an impaired apoptosis mechanism [16]. Consequently, many of the apoptosis mediators are generally considered tumor suppressors [17].

Here, we describe a comprehensive meta-analysis of gene expression studies of mouse and human medulloblastoma [18-23] identifying multiple medulloblastoma tumor suppressor candidates, including DAB2IP. We found DAB2IP expression to be strongly down-regulated in human medulloblastoma cells and in primary human medulloblastoma tissues. We demonstrate that DAB2IP down-regulation is - at least partially - caused by EZH2-mediated repression through histone methylation, conveying apoptosis resistance in immortalized neural precursor and medulloblastoma cells. Furthermore, we show that DAB2IP expression correlates significantly with the overall survival of medulloblastoma patients, independent of metastatic stage.

RESULTS

Meta-analysis of candidate tumor suppressor genes in medulloblastoma

In order to identify candidate tumor suppressor genes in medulloblastoma, we determined transcripts that were down-regulated in medulloblastoma as compared to normal cerebellar precursor cells in seven data sets comparing gene expression of normal cerebellar precursor cells and medulloblastoma in mice. We used mouse studies since that allowed for a comparison between medulloblastoma cells and proliferating progenitor cells. All data sets employed mouse models that mimic the SHH-medulloblastoma subgroup (Supplemental Table S1A, GSE9299, GSE2426, GSE7212, GSE11859, GSE6463) [18-22]. This analysis yielded 56 genes that were significantly down-regulated (>2-fold) in at least five out of the seven mouse medulloblastoma datasets. Subsequently, to increase the relevance of our screen for human medulloblastoma, we compared the expression of the significantly down-regulated mouse genes to a human medulloblastoma gene expression dataset (GSE10327) [23] and an independent gene expression dataset of normal human cerebellum (GSE3526) [24]. We established that 37 genes out of our set of 56 genes were significantly down-regulated in both mouse and human medulloblastoma (Supplemental Table S2A). In addition, we compared genes that were significantly down-regulated in both mouse and human medulloblastoma to a composed list of designated tumor suppressor genes. This resulted in two candidate gene sets, one set of 37 highly deregulated genes that have not before been designated as tumor suppressors (Fig. 1A and Supplemental Table S2A), and one set of 26 genes that have been reported as a tumor suppressor before – mostly in cancers other than medulloblastoma (Fig. 1B and Supplemental Table S2B).

DAB2IP is down-regulated in medulloblastoma and is associated with poor clinical outcome

We focused on the down-regulated medulloblastoma genes with designated tumor suppressor function (Fig. 1B) and analyzed by literature search to which of these genes a pro-apoptotic function could be attributed. This resulted in the emergence of DAB2IP as a potential pro-apoptotic tumor suppressor gene in medulloblastoma, since DAB2IP is the third most differentially expressed transcript in our analysis and literature search suggests its function in apoptosis regulation [14, 15, 25]. To confirm that DAB2IP is down-regulated in medulloblastoma, we first analyzed the DAB2IP expression levels in medulloblastoma cells. qRT-PCR revealed that DAB2IP mRNA expression was down-regulated in medulloblastoma cells D283-med, D556-med, Daoy and in primary human medulloblastoma cells (Fig. 2A), as compared to normal human cerebellar tissue. This was confirmed on protein level by DAB2IP Western blot analysis (Fig. 2B). In order to determine the correlation of DAB2IP down-regulation to clinical outcome, DAB2IP expression was evaluated in mRNA expression datasets of human

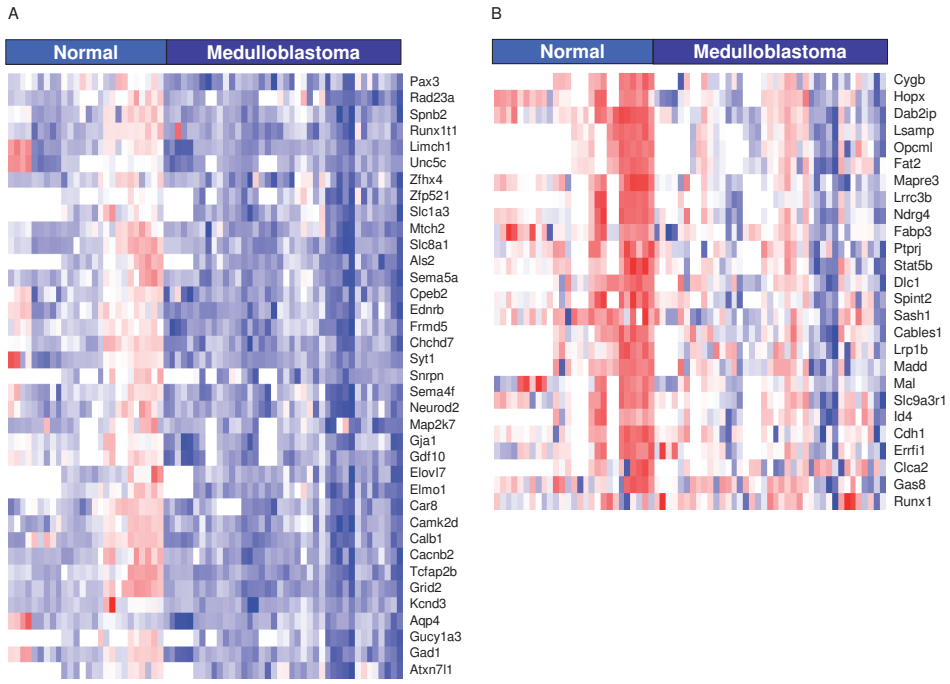

Figure 1. Meta-analysis of potential tumor suppressor genes in medulloblastoma. (A) Down-regulated genes in medulloblastoma versus normal cerebellar precursor cells in at least five out of seven mouse medulloblastoma datasets. The heatmap only represents transcripts that are also down-regulated in human medulloblastoma versus normal cerebellum. (B) Representation of putative tumor suppressor genes down-regulated in at least three out of seven mouse medulloblastoma datasets. The heatmap only represents transcripts that are also down-regulated in human medulloblastoma versus normal cerebellum.

medulloblastoma [23,26], and was correlated to survival (Fig. 2C). The clinical characteristics of the tumors/patients used in the survival analysis are summarized in Table 1A. Kaplan-Meier analysis demonstrates that low DAB2IP mRNA expression correlates significantly with a poor prognosis, as measured by a lower overall survival probability (p=0.010). Multivariate Cox proportional-hazards analysis shows that DAB2IP expression can predict prognosis (Hazard ratio: 3.0, CI 95% = 1.1 – 8.6, p = 0.036), independently of clinical variables such as age, metastatic stage and histology. Medulloblastoma is known to comprise four subtypes: WNT, SHH, Group 3 and Group 4 which differ regarding histology, molecular biology, genetics and clinical outcome [4]. However, we did not find a significant correlation between DAB2IP expression and any specific subtype in our patient series (Supplemental Fig. S1). We also investigated the relation between DAB2IP expression and metastatic stage in our patient group. However we did not find a significant correlation (Fig. 2D). Finally, to further analyze the effects of DAB2IP expression and metastatic stage on prognosis, patients were stratified based

on metastatic stage (Fig. 2D, Supplemental Fig. S2A and S2B). Again Kaplan-Meier analysis demonstrated that low DAB2IP expression correlated with a poor prognosis (p=0.055) both in the metastatic patient and non-metastatic patient groups.

DAB2IP and EZH2 are inversely expressed in medulloblastoma

Previously it was described that DAB2IP expression is epigenetically suppressed by EZH2, a member of the polycomb complex and a histone methylating enzyme [27]. Therefore we determined the EZH2 expression levels in medulloblastoma cells and tissues and compared these to DAB2IP expression. First, DAB2IP and EZH2 expression levels were evaluated in the mRNA expression dataset of 62 human medulloblastoma (9 WNT, 15 SHH, 11 Group 3 and 27 Group 4) [23] and nine normal cerebellum samples [24]. As expected the DAB2IP mRNA levels were significantly down-

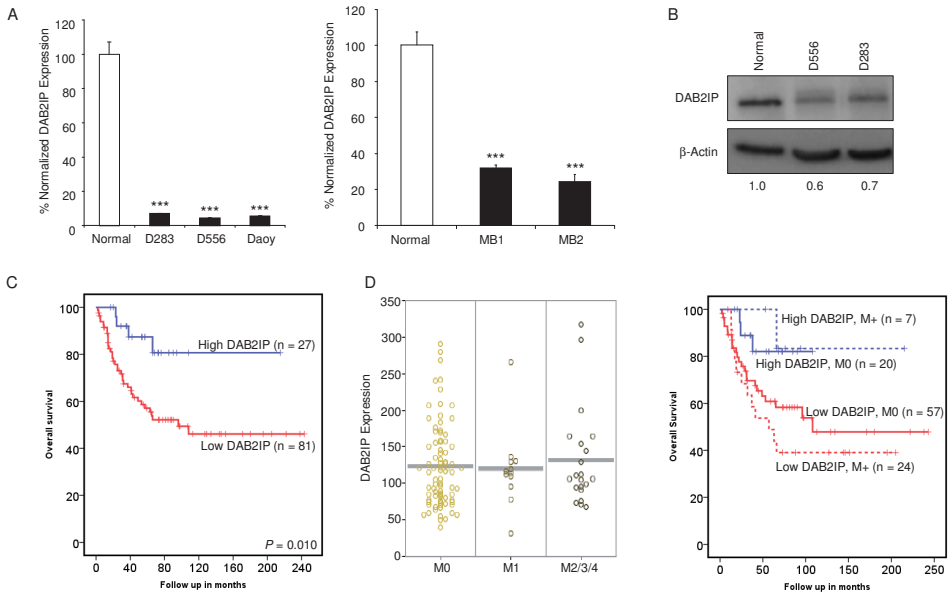

Figure 2. DAB2IP is down-regulated in medulloblastoma and is associated with poor clinical outcome. (A) RNA, extracted from various medulloblastoma cell lines (D283-med, D556-med, Daoy) and non-neoplastic brain cell lines (left panel), and from two primary human medulloblastoma samples and one normal human cerebellum tissue sample (right panel) were analyzed by qRT-PCR for expression levels of DAB2IP. The data were normalized to the levels of GAPDH mRNA in each sample. Error bars indicate s.d. *p<0.05, ***p<0.001, t-test. (B) Protein expression analysis of DAB2IP in various medulloblastoma and non-neoplastic brain cell lines. Numbers indicate relative DAB2IP protein expression normalized against β-Actin expression. (C) Kaplan-Meier analysis shows that individuals with medulloblastoma that have lower expression of DAB2IP have a significantly lower overall survival probability (p= 0.010). Cut-off for high and low expression is based on maximum likelihood. (D) Scatterplot of DAB2IP mRNA expression levels (arbitrary units) in patients based on metastatic stage M0/M1/M2-3-4 shows that average DAB2IP expression does not correlate with metastatic stage in medulloblastoma. (left panel). Kaplan-Meier survival curves of (C) further stratified based on metastatic stage (right panel).

Table 1A. Patient/tumor characteristics of medulloblastoma series used for survival analysis.

	DAB2IP low, M0	DAB2IP low, M+	DAB2IP high, M0	DAB2IP high, M+
Total no cases	57	24	20	7
Gender				
Male	39	16	11	5
Female	18	8	9	2
Age at diagnosis				
Average age	8.0	7.3	8.4	7.8
Median age	7.0	7.6	6.6	8.1
Age range	1.0 - 35.3	2.0 - 16.6	0.8 - 25.6	2.8 - 13.5
Age groups				
Infants (<4)	16	6	2	2
Children (4 - 16)	37	18	17	5
Adults (>16)	4	0	1	0
Histology				
Classic	37	21	16	5
Desmoplastic	13	3	2	2
LCA	4	0	2	0
ND	3	0	0	0
Molecular subgroups				
WNT	4	0	6	0
SHH	21	1	1	0
Group 3	12	10	5	2
Group 4	20	13	8	5

regulated in the medulloblastoma samples as compared to normal human cerebellum (Fig. 3A). In contrast, EZH2 mRNA levels were significantly up-regulated in the medulloblastoma samples as compared to normal human cerebellum (Fig. 3A). There was no significant difference in the expression of DAB2IP between the four subgroups of medulloblastoma, while the expression of EZH2 demonstrated an increasing trend from the WNT and SHH subgroups to Group 3 and 4 (Fig. 3A). In addition we compared DAB2IP and EZH2 expression in individual samples and found a negative correlation between DAB2IP and EZH2 mRNA expression (Supplemental Fig. S3A). This negative correlation was also found on protein level (Supplemental Fig. S3B). In parallel to the DAB2IP expression analysis in medulloblastoma cell lines and primary tissues (Fig. 2A), EZH2 expression analysis was performed using the same samples. This demonstrated an increased EZH2 expression in medulloblastoma cells as compared to normal cerebellum (Fig. 3B), again correlating inversely with DAB2IP expression in these samples. Finally, immunohistochemical analysis on tissue microarrays, composed of 276 pediatric medulloblastoma tissues from 87 patients, showed that EZH2 expression was significantly overexpressed in 30 out of 87 samples. In contrast, DAB2IP protein expression was not detectable in medulloblastoma samples (Fig. 3C). However, in one

patient sample that included adjacent normal cerebellar tissue, the adjacent tissue stained negatively for EZH2 and positively for DAB2IP (Fig. 3C, bottom panel). The clinical characteristics of the tumors/patients are summarized in Table 1B.

Epigenetic modulation of DAB2IP expression in medulloblastoma

In order to determine whether DAB2IP expression in medulloblastoma is regulated by EZH2-mediated epigenetic histone modulation we transfected medulloblastoma cells with siRNAs directed against EZH2 (siEZH2). At 96 h after transfection we observed significantly reduced EZH2 levels by Western blot in medulloblastoma cells

Table 1B: Patient/tumor characteristics of medulloblastoma series on tissue micro array (TMA).

Total no cases	87
Gender	
Male	27
Female	12
Unknown	48
Age at diagnosis	
Average age	14.2
Median age	7.0
Age range	1 - 53
Age groups	
Infants (<4)	7
Children (4 - 16)	19
Adults (>16)	15
Unknown	46
Histology	
Classic	23
LCA	3
ND	8
Unknown	53
Molecular subgroups	
WNT	7
SHH	18
Group 3	14
Group 4	33
Unknown	15
Metastatic Stage	
M0	35
M+	6
Unknown	46
Survival	
Alive	61
Diseased	26

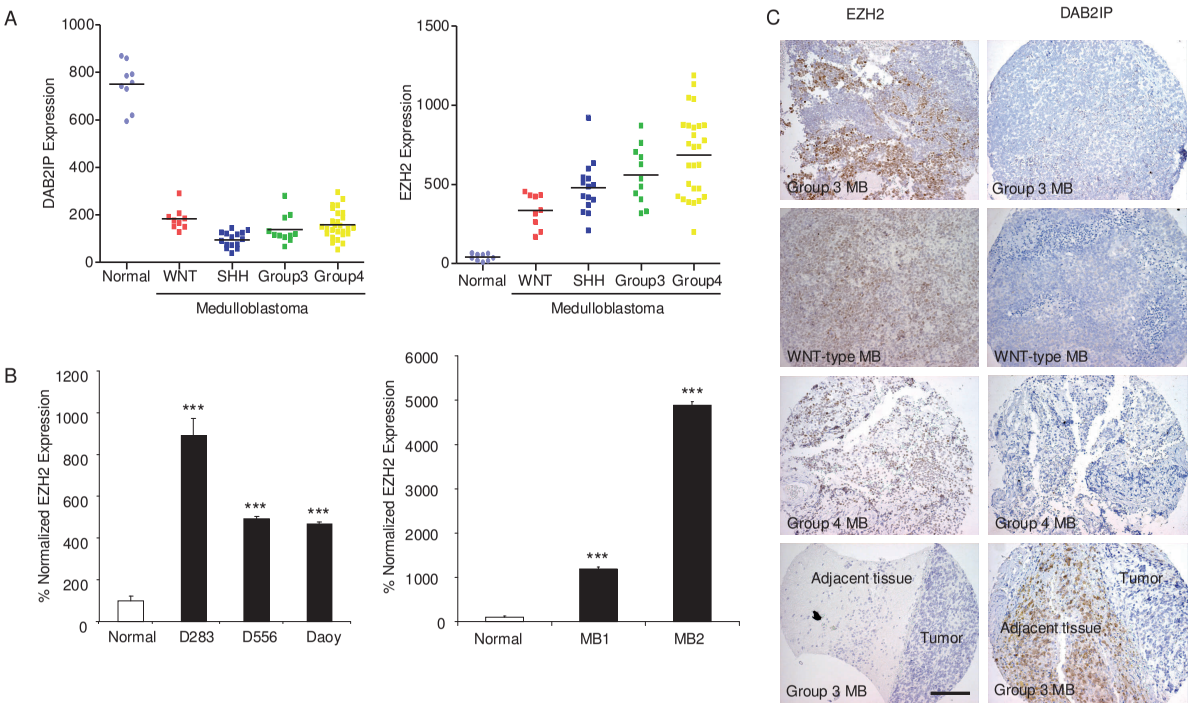

Figure 3. DAB2IP and EZH2 are inversely expressed in medulloblastoma. (A) Microarray analysis of 62 pediatric/human medulloblastoma tissues (9 WNT, 15 SHH, 11 Group 3 and 27 Group 4) and nine normal human cerebellum tissues. (A) Scatterplot of DAB2IP expression, bar represents mean (left panel). Scatterplot of EZH2 expression, bar represents mean (right panel). (B) RNA extracted from various medulloblastoma cell lines (D283-med, D556-med, Daoy) and non-neoplastic brain cell lines (left panel), and two primary human medulloblastoma samples and non-neoplastic brain samples (right panel) was analyzed by qRT-PCR for expression levels of EZH2. The data was normalized to the levels of GAPDH mRNA in each sample. Error bars indicate s.d. *p<0.05, ***p<0.001, t-test. (C) Representative immunohistochemical staining for EZH2 (left) and DAB2IP (right) in human medulloblastoma tissues. Left and right panels belong to the same tumor sample. Tumor samples are from different medulloblastoma subgroups. Bottom panels depict tumor samples with adjacent normal cerebellar tissue that stains negatively for EZH2 and positively for DAB2IP - opposite to the tumor samples. Scale bar = 100 μm.

transfected with siEZH2 (Fig. 4A). In addition, EZH2-mediated histone 3 methylation at lysine 27 was reduced and DAB2IP protein levels increased in the siEZH2 transfected medulloblastoma cells. We also analyzed lysates from medulloblastoma cells treated with the S-adenosylhomocysteine hydrolase inhibitor DZNep, a potent inhibitor of EZH2 histone methyltransferase activity [28-30]. Again a reduction in EZH2 protein levels was observed with a delayed increase in DAB2IP levels (Fig. 4B). Besides histone methylation DAB2IP expression can be altered by histone acetylation [7] and promoter DNA hypermethylation [7-10]. It was previously shown that in various cancer types DAB2IP expression could be restored by treatment with the DNA hypomethylation agent 5-aza-2'-deoxycytidine (DAC). In the medulloblastoma cells used here we could not detect an increase in DAB2IP expression following DAC treatment (Fig. 4C). However, additional treatment with the histone deacetylase inhibitor trichostatin A (TSA) did significantly increase DAB2IP expression (Fig. 4D). This suggests that histone modifications may play a more significant role in suppressing DAB2IP expression in medulloblastoma, as was described also in prostate cancer [7].

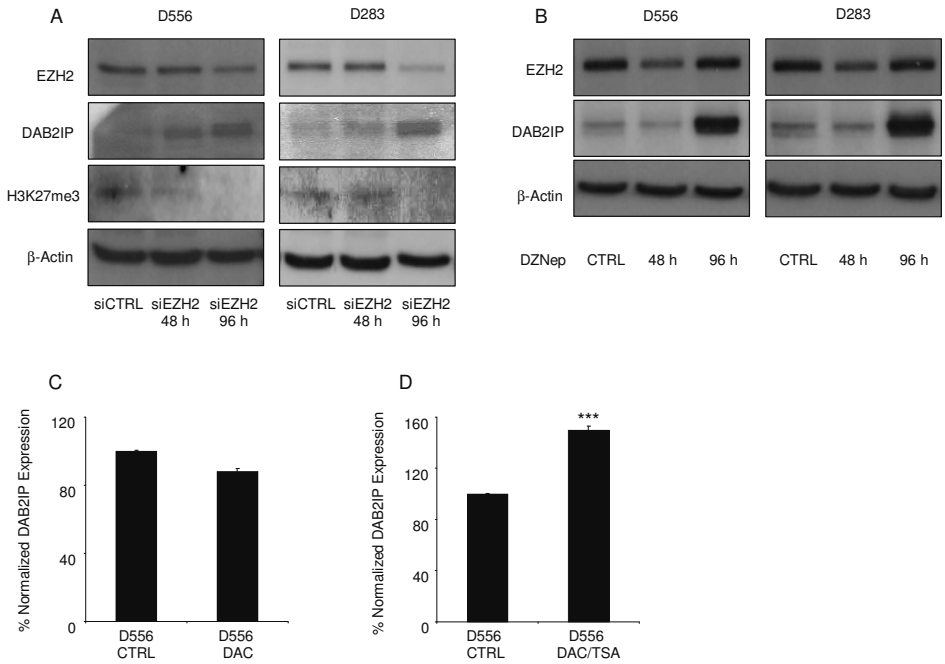

Figure 4. Epigenetic modulation of DAB2IP expression in medulloblastoma cells. (A) D556-med and D283-med protein expression analysis of DAB2IP and EZH2 and H3K27me3 at 48 and 96 h after transfection with EZH2 siRNA, or non-related siRNAs. β-Actin expression was used as normalization control. (B) D556-med and D283-med protein expression analysis of DAB2IP and EZH2 at 48 and 96 h after treatment with DZNep. (C) Effect of 5-aza-2'-deoxycytidine (DAC) treatment on DAB2IP mRNA expression in D556-med cells. (D) Effect of combined DAC and trichostatin-A (DAC-TSA) treatment on DAB2IP mRNA expression in D556-med cells. Error bars indicate s.d. *p<0.05, ***p<0.001, t-test.

DAB2IP promotes stress-induced apoptosis in medulloblastoma

To assess the functional role of DAB2IP in medulloblastoma, we examined the effects of DAB2IP modulation in human medulloblastoma cells and mouse neuronal precursor cells. Since DAB2IP was reported to enhance TNFα-induced apoptotic cell death in endothelial cells [15] and prostate cancer cells [14], we analyzed the effect of DAB2IP overexpression on TNFα-induced apoptotic cell death in medulloblastoma cells. Lentiviral vectors encoding for DAB2IP or LacZ were used to stably transduce Daoy medulloblastoma cells. Treatment with TNFα (100 ng/ml) resulted in a 2-fold increase in caspase activity in Daoy cells overexpressing DAB2IP, as compared to LacZ control cells. This increase was neutralized by simultaneous treatment with the caspase inhibitor z-VAD (20 μM) (Fig. 5A). In addition we measured the cell proliferation rate of Daoy cells overexpressing DAB2IP or LacZ control. Daoy-DAB2IP cells showed a lower proliferation rate as compared to their controls. This result was confirmed in D283-med cells (data not shown). Treatment with a low dose of TNFα (10 ng/ml) - to induce mild cellular stress - impaired proliferation of the DAB2IP-overexpressing cells even further, whereas the proliferation rate of control cells was not significantly inhibited (Fig. 5B). Furthermore, DAB2IP overexpression also inhibited anchorage independent growth following treatment with a low dose of TNFα (10 ng/ml) in Daoy cells (Supplemental Fig. S4). Since ionizing radiation (IR) is an important treatment modality in medulloblastoma and down-regulation of DAB2IP gene expression was related to resistance to IR in prostate cancer cells [11], we studied the effect of DAB2IP modulation on the clonogenic growth of medulloblastoma cells after IR. Daoy-DAB2IP and Daoy-LacZ cells were irradiated with doses of 0, 1, 2, 3, 4 and 5 Gy. DAB2IP overexpression showed an IR dose-dependent reduction in clonogenic survival as compared to LacZ control cells (Fig. 5C). Finally, in order to further study the effect of DAB2IP on TNFα-induced apoptosis, we used a shDAB2IP construct to transiently knock down DAB2IP expression in C17.2 murine cerebellar progenitor cells immortalized by v-myc [31]. Moderate knock down of DAB2IP was confirmed by Western blot analysis. DAB2IP knock down in these immortalized neural precursor cells significantly reduced TNFα-induced caspase activation (Fig. 5D), suggesting that DAB2IP has a pro-apoptotic function in these stressed neural precursor cells. In the absence of TNFα induced stress, caspase activation was similar as was observed for DAB2IP knock down and C17.2 shCTRL cells (Fig. 5D).

DISCUSSION

We performed a meta-analysis of publicly available medulloblastoma gene expression datasets in order to identify potential medulloblastoma tumor suppressor genes. We identified DAB2IP to be strongly down-regulated in medulloblastoma cells and in primary medulloblastoma tissues. Reduced DAB2IP expression was shown to correlate significantly with poor overall survival of medulloblastoma patients, independent of clinical variables such as age, metastatic stage and histology. Moreover DAB2IP was shown to be regulated

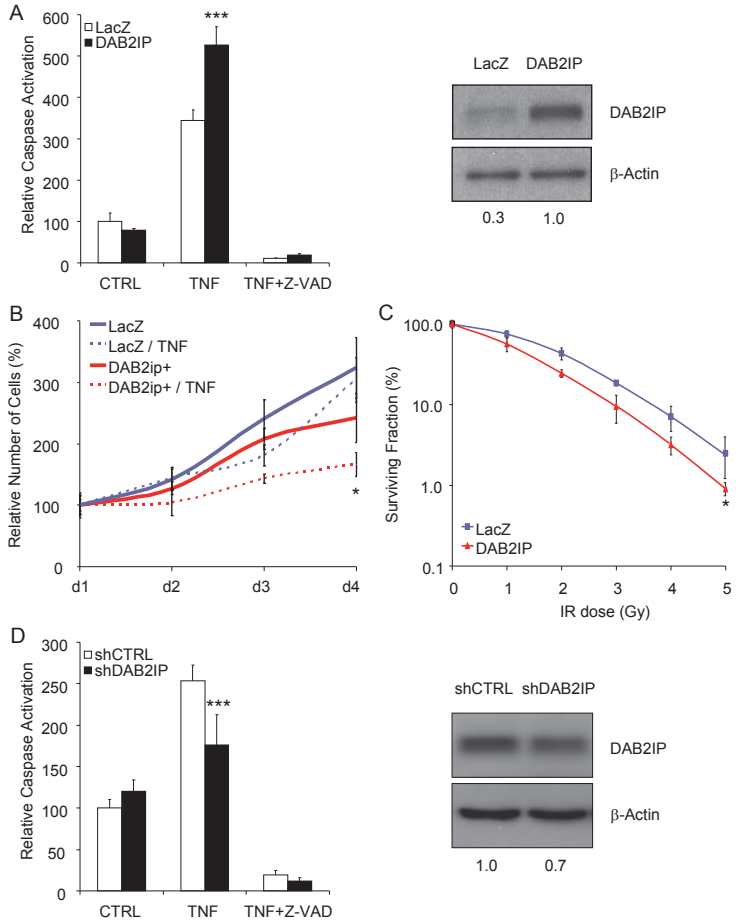

Figure 5. DAB2IP promotes stress-induced apoptosis in medulloblastoma cells. (A) DAB2IP overexpression increased caspase activation in Daoy cells treated with TNFα 6 h after treatment. Overexpression of DAB2IP in Daoy cells was confirmed by Western blot. (B) Acumen proliferation assay of Daoy cells overexpressing DAB2IP following treatment with or without a low dose of TNFα. (C) Colony formation of DAB2IP overexpressing Daoy cells, following exposure to increasing doses of IR. (D) DAB2IP knock down decreased caspase activation in C17.2 neural precursor cells treated with TNFα 6 h after treatment. Knockdown of DAB2IP in C17.2 cells was confirmed by Western blot. Error bars indicate s.d. *p<0.05, ***p<0.001, t test.

by histone modifications, including histone acetylation, and histone methylation by the polycomb group member EZH2. Finally, we demonstrated that ectopic DAB2IP expression enhances stress-induced apoptotis in medulloblastoma cells, and that reduced expression of DAB2IP in medulloblastoma conveys resistance to irradiation-induced cell death.

Medulloblastomas are known to comprise four subtypes: WNT, SHH, Group 3 and Group 4 which differ regarding histology, molecular biology, genetics and clinical outcome [4]. The studies used in our meta-analysis all employed mouse models that

mimic SHH-subgroup medulloblastoma (Supplemental Table S1A). While this article was being revised, the first MYC-based medulloblastoma mouse models that mimic Group 3 were generated [32, 33]. The medulloblastomas generated by one of these MYC models [32] demonstrate a reduced DAB2IP expression in line with our results (Supplemental Fig. S5A). However the medulloblastomas generated by the other model [33] do not show differential DAB2IP expression compared to the control tissue used in that study (Supplemental Fig. S5B). Recently a mouse model that mimics WNT subgroup medulloblastoma was also described [34]. However the small number (three) of samples and the strong variation in their DAB2IP expression preclude making any meaningful comments on DAB2IP expression in this model (Supplemental Fig. S5C). Finally, our human medulloblastoma dataset demonstrates that DAB2IP expression is significantly reduced in all subgroups (Fig. 3A, Supplemental Fig. S1).

To increase the likelihood of identifying tumor suppressors in medulloblastoma we compared the deregulated mRNA transcripts with a composed list of tumor suppressor genes. This list was established by interrogating publicly available gene ontology databases that included transcripts that have been tied to a tumor suppressor function. A number of well-known tumor suppressors in the context of medulloblastoma such as PTCH1, SUFU, APC, AXIN and TP53 [35-41] are not included in our candidate gene sets. This is likely to be caused by our stringent threshold and the various medulloblastoma mouse models used to gather the datasets. For instance, PTCH1 is down-regulated >2-fold in two out of seven medulloblastoma mouse model datasets, thereby not reaching our cut-off of deregulation in at least three out of seven datasets. However in two additional datasets PTCH1 is down-regulated ~1.8 fold. Another well known tumor suppressor, TP53, is down-regulated >2-fold in three out of seven different mouse models datasets. However, TP53 is not differentially expressed between the human medulloblastoma and normal cerebellum dataset, supporting reports that TP53 down-regulating mutations in sporadic human medulloblastoma are not very common [37]. In addition, transcripts can have inactivating mutations without being down-regulated at mRNA level, and are therefore not detected using mRNA expression analysis. Similar observations have also been reported for PTCH1, AXIN2 and TP53 in various subgroups of medulloblastoma [23].

It was previously shown that DAB2IP expression can be silenced by promoter methylation and histone modification [7-10]. Other reported mechanisms for DAB2IP inactivation include one case of a translocation that disrupts DAB2IP expression in acute myeloid leukemia [42], and a single nucleotide polymorphism in the DAB2IP gene in aggressive prostate cancer [43]. LOH at DAB2IP was demonstrated in 20% of cases in hepatocellular carcinoma [44]. In addition, a common sequence variant within DAB2IP associates with the risk of abdominal aortic aneurysm [45] and recently a genetic variant of DAB2IP was also shown to be an independent risk factor for early onset of lung cancer [46]. However, as far as we know in medulloblastoma no such mechanisms of DAB2IP deregulation have been reported yet. Here we show a significant

negative correlation between overexpressed EZH2 and down-regulated DAB2IP in human medulloblastoma samples. Moreover, we show that DAB2IP suppression in medulloblastoma cells can be at least partly reversed by EZH2 inhibition. Treatment with the DNA hypomethylation agent 5-aza-2'-deoxycytidine (DAC) did not affect DAB2IP expression in medulloblastoma cells. However, additional treatment with the histone deacetylase inhibitor trichostatin A (TSA) did significantly increase DAB2IP expression. This may suggest that histone modifications play a significant role in suppressing DAB2IP expression in medulloblastoma cells, however, we do not rule out that DAB2IP expression in medulloblastoma cells may also be impaired by additional mechanisms. Other transcripts in our list of potential medulloblastoma tumor suppressor genes may also be EZH2 targets, this is however only confirmed for CDH1 [47].

We found DAB2IP mRNA expression was reduced in medulloblastoma cell lines and primary tissues. DAB2IP protein levels were also reduced in medulloblastoma cell lines. Immunohistochemistry on the medulloblastoma tissue micro array did not reveal DAB2IP expression in these samples. However, this does not necessarily mean that no protein is present at all. It may well be that small traces of DAB2IP are present in some of the medulloblastoma tissue samples, although undetectable by us in these experiments. Another explanation may be that post-transcriptional events account for the discrepancy between mRNA and protein levels.

Recently, two publications have related the loss of DAB2IP expression to increased epithelial-to-mesenchymal transition (EMT) and metastasis in prostate cancer. Xie et al. show that DAB2IP knock down increases nuclear β-catenin accumulation and trans-activation of target genes involved in EMT by inhibiting GSK3β, indicating an inhibitory function of DAB2IP in WNT/β-catenin signaling [12]. In the context of medulloblastoma this seems paradoxical as metastasis is uncommon in the subgroup of human medulloblastoma in which WNT signaling is active [4]. In our patient series, average DAB2IP expression was slightly higher in the group of WNT associated medulloblastomas (Fig. 3A), however this difference was non-significant. It would be of interest to determine the role of DAB2IP in WNT signaling in the context of medulloblastoma, since a major role in medulloblastoma oncogenesis has been attributed to WNT/β-catenin [48]. Furthermore, it was reported that loss of DAB2IP expression induces the activation of Ras and NF-κB in prostate cancer, where Ras is presumed to play an essential role in primary tumor growth and NF-κB drives prostate cancer metastasis [13]. Therefore, we investigated the relation between DAB2IP expression and metastatic stage. However, we were unable to demonstrate a significant correlation between DAB2IP expression and medulloblastoma metastases (Fig. 2E).

In a study of mammalian brain development high levels of DAB2IP expression was found in the developing cerebellum, particularly in Purkinje cell precursors [49]. Although there is no evidence that medulloblastoma arises directly from Purkinje cells, these cells play an important part in the development of the normal cerebellum. Purkinje cells generate SHH that projects on granule neuron precursor cells and

stimulate their proliferation, before the granule neuron precursor cells migrate deeper into the forming cerebellum and differentiate further. A subgroup of medulloblastoma is believed to be derived form granule neuron precursor cells that fail to stop proliferating [3]. We showed that DAB2IP knock down in C17.2 neural precursor cells significantly reduced TNFα-induced caspase activation suggesting that DAB2IP has a pro-apoptotic function in stressed neural precursor cells. However since C17.2 cells are immortalized by overexpression of v-myc [31] the role of DAB2IP in altering apoptosis responses needs to be established in normal neural precursor cells.

We found a significant association between poor overall survival in medulloblastoma patients and reduced DAB2IP mRNA levels. Interestingly, no significant difference in DAB2IP expression was observed between the group of WNT associated medulloblastoma - which has the best prognosis - and Group 3 medulloblastoma - which has the worse prognosis [4]. This association was observed in metastatic as well as in non-metastatic medulloblastoma patients, albeit at near significant levels. These results demonstrate that DAB2IP expression is a prognostic marker for medulloblastoma outcome and suggest that patients with non-metastatic medulloblastoma with low DAB2IP expression may benefit from more aggressive treatment strategies. Recent studies have shown that medulloblastoma is a heterogeneous disease with diverse treatment outcome [23, 50]. Currently staging for treatment is based on clinical parameters such as age, extent of surgical resection, presence of metastases and histological classification [51, 52]. Various studies have suggested that this risk stratification could be improved by including molecular determinants [23, 50, 53-57]. However, it remains to be investigated to what extent DAB2IP could contribute to the sub-classification of medulloblastoma and whether it can aid as a prognostic factor in clinical practice.

In conclusion, we identified DAB2IP as a potential anti-apoptotic tumor suppressor in medulloblastoma. Further research in its use as a potentially important prognostic factor and/or therapeutic target may contribute to improvements in the future treatment of medulloblastoma patients.

MATERIALS AND METHODS

Detailed protocols are in the Supplementary Data.

Biologic samples. Original data on tumor samples from two retrospective studies [23, 26] were used for this study. Survival analysis was based on 108 cases for which expression and survival data was available. Patient and tumor characteristics are presented in Table 1A. In brief, all samples were snap frozen in the institutional pathology departments immediately upon arrival. All samples were reviewed by experienced neuropathologists and examined for tumor content. Total RNA was extracted using Trizol (Invitrogen). Gene expression profiles were obtained by Affymetrix HG-U133 Plus 2.0 arrays. Gene expression data were normalized using the GCRMA procedure. Informed consent and detailed methods are described elsewhere [23, 26].

Immunohistochemistry was performed on a largely independent medulloblastoma tissue micro array (TMA) cohort with tumors from 87 patients obtained from the files of the Department of Neuropathology of the Academic Medical Center (University of Amsterdam). Subgroup information was obtained by immunohistochemistry using antibodies for the subgroup-specific protein markers β-catenin (WNT), DKK1 (WNT), SFRP1 (SHH), NPR3 (Group 3), and KCNA1 (Group 4). Information on gender, age at diagnosis, histology, metastatic stage at diagnosis and survival are presented in Table 1B. The mean follow-up time of survivors in the TMA cohort was 6.2 years (range 0.1 - 19.4 years). Informed consent was obtained for the use of brain tissue and for access to medical records for research purposes. MB1 and MB2 primary human medulloblastoma tissues were obtained from surgical specimens after informed consent and approval by the Medical Ethical Committee of the VU University Medical Center.

Survival analysis. Overall survival was calculated from the time of diagnosis to the patient's last follow-up or death. Survival of patients was analyzed using Kaplan–Meier survival curves, and the log-rank test was used to examine the statistical significance. P-values <0.05 were considered significant. Prognostic impact of covariates on survival was evaluated on the basis of hazard ratios from Cox's proportional hazards regression model. Multivariate Cox's proportional hazards regression models were used to estimate effects of additional the covariates age, metastatic stage and histology.

Cells. Human D283-med, D556-med (Dr. Darrell Bigner, Duke University), Daoy (ATCC) and C17.2 murine cerebellar progenitor cells immortalized by v-myc [31] were cultured in DMEM containing 10% FBS and antibiotics.

Acumen proliferation assay. Cells were plated in 96-well plates (Greiner), fixed at 24, 48, 72 and 96 h after plating using formaldehyde, stained with DAPI and subsequently signal intensity was measured using an Acumen eX3 apparatus (TTP LabTech).

Apoptosis assay. Cells were plated in white opaque 96-well plates (Greiner) and treated with TNFα (Invitrogen). After 6 h of treatment, caspase activity was measured using the Caspase-Glo 3/7 assay (Promega) according to the manufacturer's instructions. Fluorescence and luminescence read-out was performed using a Tecan Infinite F200 Microplate Reader (Tecan Trading AG, Switzerland).

Clonogenic assay. Daoy cells were plated in six-well plates at a density of 500-1,000 cells per well depending on the used dose of irradiation or TNFα concentration. Subsequently cells were treated with increasing doses of irradiation or TNFα (10 ng/ml). After 10-14 days of culturing to allow colony formation, the colonies were fixed with 3.7% formaldehyde in PBS and stained with Giemsa solution. Groups consisting of 50 cells or more were defined as a colony. The colony counts using light microscopy were performed independently by at least two investigators.

ACKNOWLEDGEMENTS

We thank O. Delattre for providing patient survival data. We thank V.E. Marquez for providing DZNep. We also thank K. Cichowski for providing the DAB2IP overexpression construct, and J. T. Hsieh for providing a DAB2IP shRNA construct.

REFERENCES

1 Crawford JR, MacDonald TJ, Packer RJ. Medulloblastoma in childhood: new biological advances. *Lancet Neurol* 2007;6:1073-1085.

2 Smoll NR. Relative survival of childhood and adult medulloblastomas and primitive neuroectodermal tumors (PNETs). *Cancer* 2011.

3 Gilbertson RJ, Ellison DW. The origins of medulloblastoma subtypes. *Annu Rev Pathol* 2008;3:341-365.

4 Taylor MD, Northcott PA, Korshunov A, et al. Molecular subgroups of medulloblastoma: the current consensus. *Acta Neuropathol* 2011.

5 Srivastava VK, Nalbantoglu J. The cellular and developmental biology of medulloblastoma: current perspectives on experimental therapeutics. *Cancer Biol Ther* 2010;9:843-852.

6 Wang Z, Tseng CP, Pong RC, et al. The mechanism of growth-inhibitory effect of DOC-2/DAB2 in prostate cancer. Characterization of a novel GTPase-activating protein associated with N-terminal domain of DOC-2/DAB2. *J Biol Chem* 2002;277:12622-12631.

7 Chen H, Toyooka S, Gazdar AF, et al. Epigenetic regulation of a novel tumor suppressor gene (hDAB2IP) in prostate cancer cell lines. *J Biol Chem* 2003;278:3121-3130.

8 Dote H, Toyooka S, Tsukuda K, et al. Aberrant promoter methylation in human DAB2 interactive protein (hDAB2IP) gene in breast cancer. *Clin Cancer Res* 2004;10:2082-2089.

9 Yano M, Toyooka S, Tsukuda K, et al. Aberrant promoter methylation of human DAB2 interactive protein (hDAB2IP) gene in lung cancers. *Int J Cancer* 2005;113:59-66.

10 Dote H, Toyooka S, Tsukuda K, et al. Aberrant promoter methylation in human DAB2 interactive protein (hDAB2IP) gene in gastrointestinal tumour. *Br J Cancer* 2005;92:1117-1125.

11 Kong Z, Xie D, Boike T, et al. Downregulation of human DAB2IP gene expression in prostate cancer cells results in resistance to ionizing radiation. *Cancer Res* 2010;70:2829-2839.

12 Xie D, Gore C, Liu J, et al. Role of DAB2IP in modulating epithelial-to-mesenchymal transition and prostate cancer metastasis. *Proc Natl Acad Sci U S A* 2010;107:2485-2490.

13 Min J, Zaslavsky A, Fedele G, et al. An oncogene-tumor suppressor cascade drives metastatic prostate cancer by coordinately activating Ras and nuclear factor-kappaB. *Nat Med* 2010;16:286-294.

14 Xie D, Gore C, Zhou J, et al. DAB2IP coordinates both PI3K-Akt and ASK1 pathways for cell survival and apoptosis. *Proc Natl Acad Sci U S A* 2009;106:19878-19883.

15 Zhang R, He X, Liu W, et al. AIP1 mediates TNF-alpha-induced ASK1 activation by facilitating dissociation of ASK1 from its inhibitor 14-3-3. *J Clin Invest* 2003;111:1933-1943.

16 Sutter R, Shakhova O, Bhagat H, et al. Cerebellar stem cells act as medulloblastoma-initiating cells in a mouse model and a neural stem cell signature characterizes a subset of human medulloblastomas. *Oncogene* 2010;29:1845-1856.

17 Sherr CJ. Principles of tumor suppression. *Cell* 2004;116:235-246.

18 Mao J, Ligon KL, Rakhlin EY, et al. A novel somatic mouse model to survey tumorigenic potential applied to the Hedgehog pathway. *Cancer Res* 2006;66:10171-10178.

19 Oliver TG, Read TA, Kessler JD, et al. Loss of patched and disruption of granule cell development in a pre-neoplastic stage of medulloblastoma. *Development* 2005;132:2425-2439.

20 Sasai K, Romer JT, Kimura H, et al. Medulloblastomas derived from Cxcr6 mutant mice respond to treatment with a smoothened inhibitor. *Cancer Res* 2007;67:3871-3877.

21 Schuller U, Heine VM, Mao J, et al. Acquisition of granule neuron precursor identity is a critical determinant of progenitor cell competence to form Shh-induced medulloblastoma. *Cancer Cell* 2008;14:123-134.

22 Zindy F, Uziel T, Ayrault O, et al. Genetic alterations in mouse medulloblastomas and generation of tumors de novo from primary cerebellar granule neuron precursors. *Cancer Res* 2007;67:2676-2684.

23 Kool M, Koster J, Bunt J, et al. Integrated genomics identifies five medulloblastoma subtypes with distinct genetic profiles, pathway signatures and clinicopathological features. *PLoS One* 2008;3:e3088.

24 Roth RB, Hevezi P, Lee J, et al. Gene expression analyses reveal molecular relationships among 20 regions of the human CNS. *Neurogenetics* 2006;7:67-80.

25 Zhang H, Zhang H, Lin Y, et al. RIP1-mediated AIP1 phosphorylation at a 14-3-3-binding site is critical for tumor necrosis factor-induced ASK1-JNK/p38 activation. *J Biol Chem* 2007;282:14788-14796.

26 Fattet S, Haberler C, Legoix P, et al. Beta-catenin status in paediatric medulloblastomas: correlation of immunohistochemical expression with mutational status, genetic profiles, and clinical characteristics. *J Pathol* 2009;218:86-94.

27 Chen H, Tu SW, Hsieh JT. Down-regulation of human DAB2IP gene expression mediated by polycomb Ezh2 complex and histone deacetylase in prostate cancer. *J Biol Chem* 2005;280:22437-22444.

28 Glazer RI, Hartman KD, Knode MC, et al. 3-Deazaneplanocin: a new and potent inhibitor of S-adenosylhomocysteine hydrolase and its effects on human promyelocytic leukemia cell line HL-60. *Biochem Biophys Res Commun* 1986;135:688-694.

29 Smits M, Nilsson J, Mir SE, et al. miR-101 is down-regulated in glioblastoma resulting in EZH2-induced proliferation, migration, and angiogenesis. *Oncotarget* 2010;1:710-720.

30 Tan J, Yang X, Zhuang L, et al. Pharmacologic disruption of Polycomb-repressive complex 2-mediated gene repression selectively induces apoptosis in cancer cells. *Genes Dev* 2007;21:1050-1063.

31 Snyder EY, Deitcher DL, Walsh C, et al. Multipotent neural cell lines can engraft and participate in development of mouse cerebellum. *Cell* 1992;68:33-51.

32 Kawauchi D, Robinson G, Uziel T, et al. A mouse model of the most aggressive subgroup of human medulloblastoma. *Cancer Cell* 2012;21:168-180.

33 Pei Y, Moore CE, Wang J, et al. An animal model of MYC-driven medulloblastoma. *Cancer Cell* 2012;21:155-167.

34 Gibson P, Tong Y, Robinson G, et al. Subtypes of medulloblastoma have distinct developmental origins. *Nature* 2010;468:1095-1099.

35 Baeza N, Masuoka J, Kleihues P, et al. AXIN1 mutations but not deletions in cerebellar medulloblastomas. *Oncogene* 2003;22:632-636.

36 Huang H, Mahler-Araujo BM, Sankila A, et al. APC mutations in sporadic medulloblastomas. *Am J Pathol* 2000;156:433-437.

37 Huse JT, Holland EC. Targeting brain cancer: advances in the molecular pathology of malignant glioma and medulloblastoma. *Nat Rev Cancer* 2010;10:319-331.

38 Kasper M, Regl G, Frischauf AM, et al. GLI transcription factors: mediators of oncogenic Hedgehog signalling. *Eur J Cancer* 2006;42:437-445.

39 Koch A, Hrychyk A, Hartmann W, et al. Mutations of the Wnt antagonist AXIN2 (Conductin) result in TCF-dependent transcription in medulloblastomas. *Int J Cancer* 2007;121:284-291.

40 Raffel C, Jenkins RB, Frederick L, et al. Sporadic medulloblastomas contain PTCH mutations. *Cancer Res* 1997;57:842-845.

41 Taylor MD, Liu L, Raffel C, et al. Mutations in SUFU predispose to medulloblastoma. *Nat Genet* 2002;31:306-310.

42 von Bergh AR, Wijers PM, Groot AJ, et al. Identification of a novel RAS GTPase-activating protein (RASGAP) gene at 9q34 as an MLL fusion partner in a patient with de novo acute myeloid leukemia. *Genes Chromosomes Cancer* 2004;39:324-334.

43 Duggan D, Zheng SL, Knowlton M, et al. Two genome-wide association studies of aggressive prostate cancer implicate putative prostate tumor suppressor gene DAB2IP. *J Natl Cancer Inst* 2007;99:1836-1844.

44 Calvisi DF, Ladu S, Conner EA, et al. Inactivation of Ras GTPase-activating proteins promotes unrestrained activity of wild-type Ras in human liver cancer. *J Hepatol* 2011;54:311-319.

45 Gretarsdottir S, Baas AF, Thorleifsson G, et al. Genome-wide association study identifies a sequence variant within the DAB2IP gene conferring susceptibility to abdominal aortic aneurysm. *Nat Genet* 2010;42:692-697.

46 Yang L, Li Y, Ling X, et al. A common genetic variant (97906C>A) of DAB2IP/AIP1 is associated with an increased risk and early onset of lung cancer in Chinese males. *PLoS One* 2011;6:e26944.

47 Herranz N, Pasini D, Diaz VM, et al. Polycomb complex 2 is required for E-cadherin repression by the Snail1 transcription factor. *Mol Cell Biol* 2008;28:4772-4781.

48 Yokota N, Nishizawa S, Ohta S, et al. Role of Wnt pathway in medulloblastoma

oncogenesis. *Int J Cancer* 2002;101:198-201.

49 Homayouni R, Magdaleno S, Keshvara L, et al. Interaction of Disabled-1 and the GTPase activating protein Dab2IP in mouse brain. *Brain Res Mol Brain Res* 2003;115:121-129.

50 Ellison DW, Kocak M, Dalton J, et al. Definition of disease-risk stratification groups in childhood medulloblastoma using combined clinical, pathologic, and molecular variables. *J Clin Oncol* 2011;29:1400-1407.

51 Zeltzer PM, Boyett JM, Finlay JL, et al. Metastasis stage, adjuvant treatment, and residual tumor are prognostic factors for medulloblastoma in children: conclusions from the Children's Cancer Group 921 randomized phase III study. *J Clin Oncol* 1999;17:832-845.

52 Giangaspero F, Eberhart CG, Haaspalo H, Pietsch T, Wiestler OD, Ellison DW. Medulloblastoma. In: Louis DN, Ohgaki H, Wiestler OD, Cavenee WK, editors. WHO classification of tumours of the central nervous system. Lyon: IARC Press; 2007. p.132-40.

53 Cho YJ, Tsherniak A, Tamayo P, et al. Integrative genomic analysis of medulloblastoma identifies a molecular subgroup that drives poor clinical outcome. *J Clin Oncol* 2011;29:1424-1430.

54 Pfister S, Remke M, Benner A, et al. Outcome prediction in pediatric medulloblastoma based on DNA copy-number aberrations of chromosomes 6q and 17q and the MYC and MYCN loci. *J Clin Oncol* 2009;27:1627-1636.

55 Pomeroy SL, Tamayo P, Gaasenbeek M, et al. Prediction of central nervous system embryonal tumour outcome based on gene expression. *Nature* 2002;415:436-442.

56 Remke M, Hielscher T, Korshunov A, et al. FSTL5 Is a Marker of Poor Prognosis in Non-WNT/Non-SHH Medulloblastoma. *J Clin Oncol* 2011;29:3852-3861.

57 Poschl J, Lorenz A, Hartmann W, et al. Expression of BARHL1 in medulloblastoma is associated with prolonged survival in mice and humans. *Oncogene* 2011;30:4721-4730.

SUPPLEMENTARY MATERIALS AND METHODS

Meta-analysis of gene expression datasets

The NCBI Gene Expression Omnibus database (http://www.ncbi.nlm.nih.gov/geo/) was used to identify studies that compared gene expression in mouse medulloblastoma to normal mouse cerebellar precursor cells, yielding five different studies (1-5), and a total of seven independent tumor/normal datasets. All mouse-related studies employed models that mimic the SHH-subgroup medulloblastoma (Supplemental Table S1A). Each dataset was log2 transformed, median normalized, and the gene expression patterns of individual transcripts were subsequently examined across the individual datasets. Transcripts that showed at least a 2-fold down-regulation ($p<0.05$) in medulloblastoma as compared to control samples were selected. Since integrating the results of multiple screens can increase the specificity, we ranked the transcripts according to the number of datasets in which the particular transcripts was down-regulated. Further, using R2 algorithms that allow comparison of gene expression between individual datasets (R2: microarray analysis and visualization platform (http://r2.amc.nl)), the tumor suppressor candidates from the mouse datasets were compared to a human medulloblastoma gene expression dataset (GSE 10327) (6) and an independent gene expression dataset of normal human cerebellum (GSE 3526) (7). Finally, the list of down-regulated genes in mouse and human medulloblastoma was compared to a list of designated tumor suppressor genes. The list of tumor suppressor genes was established by interrogating the NCBI (http://www.ncbi.nlm.nih.gov/gene) and Amigo (8) Gene Ontology (GO) databases (Supplemental Table S1B). Genes that were present in both lists were regarded as putative tumor suppressor genes in medulloblastoma.

Lentiviral expression vectors

Lentiviral vectors were produced by co-transfecting subconfluent human embryonic kidney (HEK) 293T cells with a DAB2IP overexpression construct (kindly provided by Dr K. Cichowski, Harvard Medical School, Boston, MA, USA) or a DAB2IP shRNA construct (kindly provided by Dr J. T. Hsieh, University of Texas Southwestern Medical Center, Dallas, TX, USA) and lentiviral packaging agents (pMD2G, pMD2G pRRE, pRSV/REV), using Lipofectamin 2000 (Invitrogen) as a transfection reagent. Lentiviral vectors were collected 24 h after transfection. The supernatant was centrifuged to remove cell debris and stored at -80 °C.

Quantitative RT-PCR

Quantitative RT-PCR (qRT-PCR) analysis was used to determine the relative mRNA expression levels of DAB2IP, EZH2, and GAPDH mRNA. Total RNA was isolated using Trizol (Invitrogen), according to the manufacturer's protocol. Equal amounts of RNA were converted into cDNA using random primers (Invitrogen). Subsequently, quantitative PCR was performed using gene-specific primers (Applied Biosystems).

The Ct values were used to calculate the relative fold difference in mRNA levels. All experiments were performed using biological triplicates and experimental duplicates. The data were normalized to GAPDH expression levels.

Western blot analysis

Cell pellets were re-suspended in RIPA buffer including protease inhibitor. After 1 h the re-suspended pellets were centrifuged for 10 min at 10,000 rpm at 4°C. Supernatant was mixed with Laemmli buffer (Bio-RAD) including β- mercaptoethanol and heated at 97°C. A total of 30 µg of protein was loaded on a 10% SDS-polyacrylamide gel and separated for 1 h at 100V on an electrophoresis system (Bio-Rad). Next, proteins were transferred to PVDF membranes over night at 30V at 4°C by means of blot buffer (TRIS/glycine/methanol). After incubating the PVDF membranes with PBS for 15 min they were blocked with 5% milk in PBS-T for 1 h. Membranes were incubated for 1 h with mouse anti-EZH2 mAb (BD biosciences) at 1:1,000 dilution in blocking solution (1% milk in PBS-T), mouse anti-Actin (Millipore, MAB1501R) at 1:30,000 dilution, and overnight with rabbit anti-DAB2IP (1:1,000; Sigma). Membranes were washed with PBS-T four times for 15 min. Subsequently, membranes were incubated for 1 h with horseradish peroxidise (HRP) antimouse IgG (DAKO) at 1:3,000 dilution in 1% block buffer to detect primary anti- EZH2 antibody and anti-Actin antibody or HRP anti-rabbit IgG (DAKO) at 1:3,000 dilution to detect anti-DAB2IP antibody. Membranes were washed again with PBS-T four times for 15 min. ECL detection solution (GE Healthcare) was used to detect protein levels. Levels were visualized on X-ray film (GE Healthcare) and quantified using ImageJ software (NIH Image). Actin intensities were used to normalize DAB2IP and EZH2 levels. Normalized DAB2IP and EZH2 intensities were used to calculate the relative expression levels.

Immunohistochemical staining

Paraffin sections of human medulloblastoma tissue and human neocortex were stained with monoclonal mouse anti-EZH2 (BD biosciences) diluted 1:300 in antibody solution (Immunologic), or with monoclonal rabbit anit-DAB2IP (Sigma) diluted 1:50, for 1 h at room temperature. Sections were washed in PBS three times and incubated with secondary antibody (EnvisionHRP) for 30 min at room temperature. Following three times washing in PBS, positive reactions were visualized by incubating the sections with stable 3,3-diaminobenzidine for 10 min. After washing in distilled water, the sections were counterstained with hematoxylin for 1 min and analyzed using microscopy.

Reference List

1 1. Mao J, Ligon KL, Rakhlin EY, Thayer SP, Bronson RT, Rowitch D, et al. A novel somatic mouse model to survey tumorigenic potential applied to the Hedgehog pathway. Cancer Res 2006;66:10171-10178.

2 2. Oliver TG, Read TA, Kessler JD, Mehmeti A, Wells JF, Huynh TT, et al. Loss of patched and disruption of granule cell development in a preneoplastic stage of medulloblastoma. Development 2005;132:2425-2439.

3 3. Sasai K, Romer JT, Kimura H, Eberhart DE, Rice DS, Curran T. Medulloblastomas derived from Cxcr6 mutant mice respond to treatment with a smoothened inhibitor. Cancer Res 2007;67:3871-3877.

4 4. Schuller U, Heine VM, Mao J, Kho AT, Dillon AK, Han YG, et al. Acquisition of granule neuron precursor identity is a critical determinant of progenitor cell competence to form Shh-induced medulloblastoma. Cancer Cell 2008;14:123-134.

5 5. Zindy F, Uziel T, Ayrault O, Calabrese C, Valentine M, Rehg JE, et al. Genetic alterations in mouse medulloblastomas and generation of tumors de novo from primary cerebellar granule neuron precursors. Cancer Res 2007;67:2676-2684.

6 6. Kool M, Koster J, Bunt J, Hasselt NE, Lakeman A, van SP, et al. Integrated genomics identifies five medulloblastoma subtypes with distinct genetic profiles, pathway signatures and clinicopathological features. PLoS One 2008;3:e3088.

7 7. Roth RB, Hevezi P, Lee J, Willhite D, Lechner SM, Foster AC, et al. Gene expression analyses reveal molecular relationships among 20 regions of the human CNS. Neurogenetics 2006;7:67-80.

8 8. Carbon S, Ireland A, Mungall CJ, Shu S, Marshall B, Lewis S. AmiGO: online access to ontology and annotation data. Bioinformatics 2009;25:288-289.

Supplemental table S1. Microarray datasets characteristics

Title	Summary	Samples	Literature ref.	GEO ref.
Acquisition of granule neuron precursor identity and Hedgehog-induced medulloblastoma in mice.	Gene expression profiling of cerebellar tumors generated from various early and late stage CNS progenitor cells	27	(1)	GSE 11859
Medulloblastomas derived from Cxcr6 mutant mice respond to treatment with a Smoothened inhibitor	Study of mouse medulloblastoma in response to inhibitor of Smoothened	5	(2)	GSE 7212
Expression profiles of mouse medulloblastoma	Identification of distinct classes of up-regulated or down-regulated genes during Hh dependent tumorigenesis	10	(3)	GSE 9299 339 & 340
Genetic alterations in mouse medulloblastomas and generation of tumors from cerebellar granule neuron precursors	Identification of differently expressed genes among CGNPs and CGNPs transfected with retroviruses that express nmyc or cyclin-d1	10	(4)	GSE 6463 339 & 340
Patched heterozygous model of medulloblastoma	Analysis of granule cell precursors, pre-neoplastic cells, and tumor cells	14	(5)	GSE 2426 GDS1110

1. Schuller U, Heine VM, Mao J, Kho AT, Dillon AK, Han YG, et al. Acquisition of granule neuron precursor identity is a critical determinant of progenitor cell competence to form Shh-induced medulloblastoma. Cancer Cell 2008;14:123-134.
2. Sasai K, Romer JT, Kimura H, Eberhart DE, Rice DS, Curran T. Medulloblastomas derived from Cxcr6 mutant mice respond to treatment with a smoothened inhibitor. Cancer Res 2007;67:3871-3877.
3. Mao J, Ligon KL, Rakhlin EY, Thayer SP, Bronson RT, Rowitch D, et al. A novel somatic mouse model to survey tumorigenic potential applied to the Hedgehog pathway. Cancer Res 2006;66:10171-10178.
4. Zindy F, Uziel T, Ayrault O, Calabrese C, Valentine M, Rehg JE, et al. Genetic alterations in mouse medulloblastomas and generation of tumors de novo from primary cerebellar granule neuron precursors. Cancer Res 2007;67:2676-2684.
5. Oliver TG, Read TA, Kessler JD, Mehmeti A, Wells JF, Huynh TT, et al. Loss of patched and disruption of granule cell development in a pre-neoplastic stage of medulloblastoma. Development 2005;132:2425-2439.

Supplemental table S2. List of tumor suppressor genes, established by interrogating the Amigo and NCBI Gene Ontology (GO) databases

Gene	Database		Gene	Database	
Jun	AMIGO		LRRC3B		NCBI
Aatf	AMIGO		LSAMP		NCBI
Abl1	AMIGO		LTF		NCBI
Adcyap1	AMIGO		LZTS1		NCBI
ADPRH		NCBI	MAD1L1		NCBI
AFUA_2G11990		NCBI	Mad2l1	AMIGO	
AGTR2		NCBI	Mad2l1bp	AMIGO	
AHRR		NCBI	MADD	AMIGO	
Akt1		NCBI	MAL		NCBI
ALPL		NCBI	Map3k8		NCBI
An04g06500		NCBI	Mapk14	AMIGO	
Anapc10	AMIGO		MAPRE3		NCBI
ANXA1		NCBI	MBD2		NCBI
Apbb1	AMIGO		MCC		NCBI
Apbb2	AMIGO		Mcc_mapped		NCBI
Apc	AMIGO	NCBI	MCPH1		NCBI
APITD1		NCBI	Mdm2	AMIGO	
App	AMIGO		MGC108388		NCBI
ARHGAP29		NCBI	MIR21		NCBI
ARL11		NCBI	MIR34A		NCBI
ARL14		NCBI	MLL		NCBI
Atf5	AMIGO		Mnt	AMIGO	
Atm	AMIGO		Mov10l1	AMIGO	
Atr	AMIGO		MPP3		NCBI
Bak1	AMIGO		MRVI1		NCBI
BAP1		NCBI	Msh2	AMIGO	NCBI
BARD1		NCBI	MT1G		NCBI
Bax	AMIGO	NCBI	Mtap		NCBI
Bccip	AMIGO		Mtbp	AMIGO	
Bcl2	AMIGO		Mtor		NCBI
Bcr	AMIGO	NCBI	MTUS1		NCBI
Becn1		NCBI	MXD1		NCBI
BHD		NCBI	MXI1		NCBI
BLCAP		NCBI	Mycbp2	AMIGO	
Braf		NCBI	MYO18B		NCBI
brc-1		NCBI	N		NCBI
brc-2		NCBI	Nanog	AMIGO	
BRCA1		NCBI	NAP1L4		NCBI
Brca2	AMIGO	NCBI	Nbn	AMIGO	
brd-1		NCBI	NBR1		NCBI
Brsk1	AMIGO		NBR2		NCBI
Btc	AMIGO		NDRG2		NCBI
BTG2		NCBI	NDRG4		NCBI

Supplemental table S2. Continued

Gene	Database		Gene	Database	
Btg3	AMIGO		Neurog1	AMIGO	
Btg4	AMIGO	NCBI	NEWENTRY		NCBI
Btrc	AMIGO		NF1		NCBI
Bub1		NCBI	NF2		NCBI
Bub3	AMIGO		Nfatc1		NCBI
C2orf40		NCBI	Nfatc2		NCBI
C3orf51		NCBI	NFKB1		NCBI
Cables1	AMIGO		NME1		NCBI
Cables2	AMIGO		Notch1		NCBI
CADM1		NCBI	Npm1	AMIGO	
Calr	AMIGO		Nras	AMIGO	
CAPG		NCBI	NUDT2		NCBI
CARS		NCBI	Nup214	AMIGO	
Casp3	AMIGO		NUP98		NCBI
CASP8		NCBI	Nusap1	AMIGO	
Cat		NCBI	OPCML		NCBI
CAV1		NCBI	Osm	AMIGO	
CBFA2T3		NCBI	PALB2		NCBI
CCDC136		NCBI	PANX2		NCBI
CCNC		NCBI	PARK2		NCBI
Ccnd1	AMIGO	NCBI	PAWR		NCBI
Ccnd2	AMIGO		PDCD4		NCBI
Ccnd3	AMIGO		Pde3a	AMIGO	
Ccne1	AMIGO		PF4		NCBI
Ccne2	AMIGO		PHB2		NCBI
Ccng2	AMIGO		PHLDA2		NCBI
Ccni	AMIGO		PIG8		NCBI
CD36_72340		NCBI	PINX1		NCBI
CD81		NCBI	PITX1		NCBI
Cdc23	AMIGO		Pkia	AMIGO	
Cdc42	AMIGO		PLAGL1		NCBI
CDH1		NCBI	PLCE1		NCBI
Cdh11		NCBI	Pml	AMIGO	NCBI
CDH4		NCBI	PPM1A		NCBI
Cdk1	AMIGO		Ppp2ca	AMIGO	
Cdk11b	AMIGO		PPP2R1B		NCBI
Cdk2ap2		NCBI	PRDM1		NCBI
Cdk4	AMIGO		PRDM2		NCBI
Cdk5	AMIGO		PRKAR1A		NCBI
Cdkn1a	AMIGO	NCBI	PRKCDBP		NCBI
Cdkn1b	AMIGO	NCBI	Prox1	AMIGO	NCBI
Cdkn2a	AMIGO	NCBI	PRR5		NCBI
CDKN2B		NCBI	Psmg2	AMIGO	

Supplemental table S2. Continued

Gene	Database		Gene	Database	
Cdkn2c		NCBI	Pten	AMIGO	NCBI
Cdt1	AMIGO		Ptpn11	AMIGO	
CEBPA		NCBI	Ptprc	AMIGO	
CEBPD		NCBI	PTPRD		NCBI
Cenpe	AMIGO		PTPRG		NCBI
Cenpf	AMIGO		PTPRJ		NCBI
Cep192	AMIGO		PTPRK		NCBI
CHD5		NCBI	Ptprv	AMIGO	
Chek1	AMIGO		Pura	AMIGO	
CHEK2		NCBI	Rad9	AMIGO	
Cited2	AMIGO		RAF1		NCBI
CLCA2		NCBI	RALA		NCBI
CLDN23		NCBI	Ranbp1	AMIGO	
Clspn	AMIGO		RAP1GAP		NCBI
CNOT7		NCBI	RARB		NCBI
Cops5	AMIGO		RASAL1		NCBI
CREBL2		NCBI	RASSF1		NCBI
Csk		NCBI	RASSF2		NCBI
Csnk2a2	AMIGO		RASSF5		NCBI
CST5		NCBI	Rb1	AMIGO	NCBI
CST6		NCBI	RB1CC1		NCBI
CTNNB1		NCBI	RBBP7		NCBI
Cul7	AMIGO		Rbf		NCBI
Cul9	AMIGO		Recql4	AMIGO	
CYGB		NCBI	Rhob	AMIGO	NCBI
CYLD		NCBI	RND3		NCBI
CYP27B1		NCBI	Robo1		NCBI
DAB2IP		NCBI	Rock2	AMIGO	
Dazl	AMIGO		RPL10		NCBI
Dbf4	AMIGO		Rpl24	AMIGO	
DCC		NCBI	Rprm	AMIGO	
Dcn		NCBI	Rps6	AMIGO	
DEC1		NCBI	RPS6KA6		NCBI
DEHA0B05984g		NCBI	RRM1		NCBI
DFNA5		NCBI	RUNX1		NCBI
Dicer1		NCBI	Runx3	AMIGO	NCBI
DIRAS3		NCBI	S100A11		NCBI
DKK1		NCBI	SASH1		NCBI
DKK3		NCBI	sbb		NCBI
DLC1		NCBI	SEC14L2		NCBI
DLEC1		NCBI	SEMA3B		NCBI
DUSP6		NCBI	SEPT9		NCBI
E2f1	AMIGO		SERPINB5		NCBI

Supplemental table S2. Continued

Gene	Database		Gene	Database	
E2f2	AMIGO		Sfn	AMIGO	NCBI
E2f4	AMIGO		SFRP1		NCBI
E2f5	AMIGO		SFRP5		NCBI
E4f1	AMIGO		SHPRH		NCBI
Egfr		NCBI	SIAH1		NCBI
EGR1		NCBI	Sik1	AMIGO	
EHI_049820		NCBI	Sipa1	AMIGO	
EHI_098430		NCBI	Sirt1		NCBI
EHI_143090		NCBI	Skp2	AMIGO	
EHI_187800		NCBI	SLC22A18		NCBI
Epb4.1l3		NCBI	SLC39A1		NCBI
Epgn	AMIGO		SLC5A8		NCBI
EPHB4		NCBI	SLC9A3R1		NCBI
Ereg	AMIGO		SLIT2		NCBI
ERRFI1		NCBI	SMAD2		NCBI
Esr1	AMIGO	NCBI	SMAD3		NCBI
ETS2		NCBI	SMAD4		NCBI
EXT1		NCBI	SMAD5		NCBI
EXT2		NCBI	SMARCA2		NCBI
EZH2		NCBI	SMARCB1		NCBI
FABP3		NCBI	SNORD50A		NCBI
Fas		NCBI	SOCS1		NCBI
Fat2		NCBI	SOD2		NCBI
Fat3		NCBI	Sparc		NCBI
FAT4		NCBI	Spdya	AMIGO	
Fbxo5	AMIGO		Spdye4	AMIGO	
Fgf8	AMIGO		SPINT2		NCBI
FHIT		NCBI	SRPX		NCBI
FLCN		NCBI	ST13		NCBI
Foxg1	AMIGO		ST7L		NCBI
Foxo4	AMIGO		STAT3		NCBI
FOXP1		NCBI	Stat5a	AMIGO	
ft		NCBI	Stat5b	AMIGO	
Fzr1	AMIGO		STIM1		NCBI
Gadd45a	AMIGO		Stra8	AMIGO	
Gadd45b	AMIGO		SYNPO2		NCBI
Gadd45g	AMIGO		SYT13		NCBI
GAK		NCBI	SYVN1		NCBI
GALR1		NCBI	Tacc3	AMIGO	
Gas1	AMIGO			NCBI	NCBI
GAS8		NCBI	TCEAL7		NCBI
GJB2		NCBI	TCF3		NCBI
Gmnn	AMIGO		TCF4		NCBI

Supplemental table S2. Continued

Gene	Database		Gene	Database	
GNMT		NCBI	TCL1A		NCBI
GPC3		NCBI	TEP1		NCBI
Gpr3	AMIGO		TES		NCBI
GPX3		NCBI	TFAP2A		NCBI
GRP		NCBI	Tgfb2	AMIGO	NCBI
GSTP1		NCBI	Tgfbr2		NCBI
H2afx	AMIGO		Thrb		NCBI
HACE1		NCBI	THSD1		NCBI
Hdac3	AMIGO	NCBI	THY1		NCBI
Hectd3	AMIGO		TIMP3		NCBI
Herc2	AMIGO		Tipin	AMIGO	
HIC1		NCBI	TMEFF1		NCBI
HIF1A		NCBI	TMEFF2		NCBI
Hivep3		NCBI	TMEM158		NCBI
Hmgb1	AMIGO		TMPRSS11A		NCBI
HOPX		NCBI	TNFAIP3		NCBI
Hoxa13	AMIGO		TP53		NCBI
Hspa8	AMIGO		TP73		NCBI
Hus1	AMIGO		TRIM3		NCBI
ID4		NCBI	Trp53	AMIGO	NCBI
Ifnz	AMIGO		Trrap	AMIGO	
Igf2r		NCBI	TSC1		NCBI
IGFBP3		NCBI	TSC2		NCBI
Ikzf1		NCBI	Tsc22d1		NCBI
ING1		NCBI	TSG11		NCBI
ING3		NCBI	TSPAN32		NCBI
ING4		NCBI	TSSC1		NCBI
INTS6		NCBI	TSSC4		NCBI
IRF1		NCBI	Tubg1	AMIGO	
ISOC2		NCBI	TUSC3		NCBI
Itgb1	AMIGO		TUSC4		NCBI
ITS		NCBI	Uba3	AMIGO	
JDP2		NCBI	Uba7		NCBI
JST		NCBI	Ube2b	AMIGO	
Junb	AMIGO		UBE4B		NCBI
KCNRG		NCBI	UCHL1		NCBI
KDM3B		NCBI	UPP1		NCBI
KIF1B		NCBI	VHL		NCBI
KLF10		NCBI	VPS53		NCBI
KLF5		NCBI	Vwa5a		NCBI
KLF6		NCBI	WDR11		NCBI
Kras		NCBI	WFDC1		NCBI
Krtap16-7	AMIGO		Wfdc15a		NCBI

Supplemental table S2. Continued

Gene	Database		Gene	Database	
l(2)gl		NCBI	WIF1		NCBI
LDOC1		NCBI	WISP3		NCBI
Lif	AMIGO		WIT1		NCBI
LIMD1		NCBI	WT1		NCBI
LOC100015738		NCBI	wt1-B		NCBI
LOC100049824		NCBI	WTAP		NCBI
LOC100089976		NCBI	XAF1		NCBI
LOC100156810		NCBI	Xpc	AMIGO	
LOC464013		NCBI	Xpo1	AMIGO	
LOC472922		NCBI	YAP1		NCBI
LOC534968		NCBI	Ywhah	AMIGO	
LOC683581		NCBI	ZBTB33		NCBI
LOC706725		NCBI	Zfp369	AMIGO	
LOX		NCBI	ZIC1		NCBI
LRIG3		NCBI	ZMYND10		NCBI
LRP12		NCBI	ZNF224		NCBI
LRP1B		NCBI	Zzef1	AMIGO	

Supplemental table S3A. Putative tumor suppressor genes highly down regulated in medulloblastoma versus normal cerebellum datasets

Gene
Atxn7l1
Gad1
Gucy1a3
Aqp4
Kcnd3
Grid2
Tcfap2b
Cacnb2
Calb1
Camk2d
Car8
Elmo1
Elovl7
Gdf10
Gja1
Map2k7
Neurod2
Sema4f
Snrpn
Syt1
Chchd7
Frmd5
Ednrb
Cpeb2
Sema5a
Als2
Slc8a1
Mtch2
Slc1a3
ZNF521
Zfhx4
Unc5c
Limch1
Runx1t1
SPTBN1
Rad23a
Pax3

Supplemental table S3B. Established (GO) tumor suppressor genes down regulated in medulloblastoma (MB) versus normal cerebellum datasets

Gene	Reported tumor suppressor in a.o.	Reported tumor suppressor in MB (Y/N)
Cables1	Colorectal (1), Ovarian (2)	N
Cygb	Lung and Breast (3)	N
Hopx	Endometrial (4), Gastric (5)	N
Ptprj	Colorectal (6), Meningioma(7)	N
Dab2ip	Prostate (8), Breast (9), Lung (10)	N
Errfi1	Glioblastoma (11)	N
Fat2	Squamous Carcinoma (12)	N
Gas8	Breast (13)	N
Lrp1b	Lung (14), Urothelial (15), Thyroid (16)	N
Lrrc3b	Gastric (17), Colorectal (18)	N
Madd	Ovarian (19)	N
Mal	Lung (20), Colorectal (21), Breast (22)	N
Mapre3	HNSCC (23)	N
Ndrg4	Colorectal (24)	N
Opcml	Ovarian(25), Glioma & Medulloblastoma (26)	Y (26)
Slc9a3r1	Liver (27), Breast (28)	N
Spint2	Renal (29), Gastric (30), Medulloblastoma (31)	Y (31)
Dlc1	Hepatocellular (32), Breast and Colon and Prostate (33), Supratentorial Primitive Neuro -Ectoderrmal Tumor (34)	N
Lsamp	Osteosarcoma(35)	N
Sash1	Breast(36), Colorectal(37)	N
Id4	Colorectal (38), Leukemia(39), Breast (40), Prostate (41)	N
Fabp3	Breast(42)	N
Clca2	Breast (43), Colorectal (44)	N
Stat5b	Hepatocellular(45)	N
Runx1	Leukemia (46)	N
Cdh1	Gastric	

&breast (47), Colorectal (48), Ovarian (49), Medulloblastoma (50) Y (50)

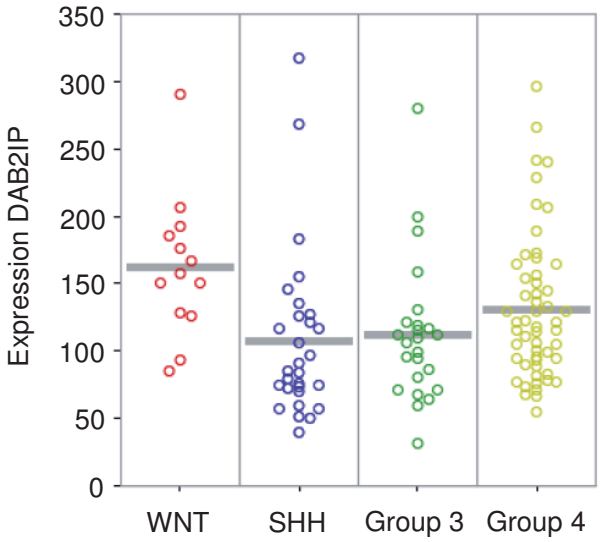

Supplementary figure 1.

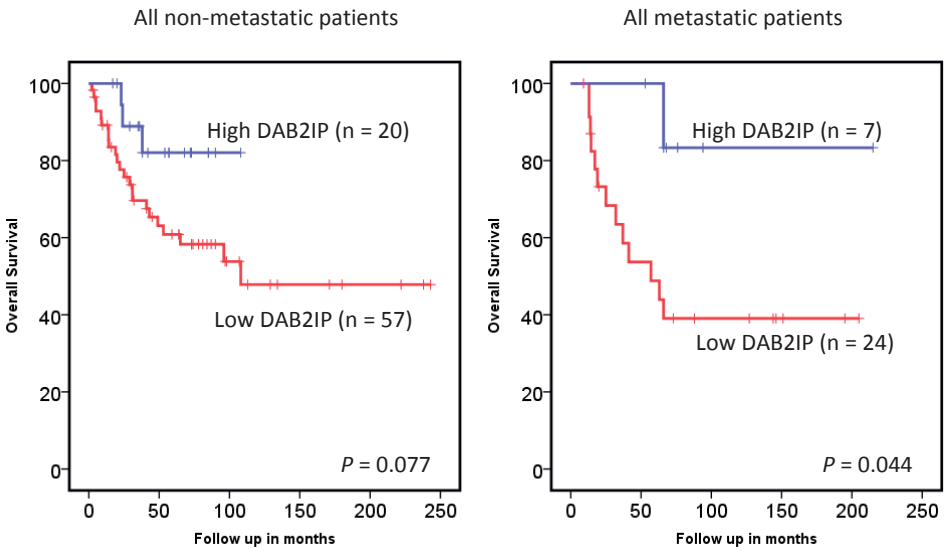

Supplementary figure 2.

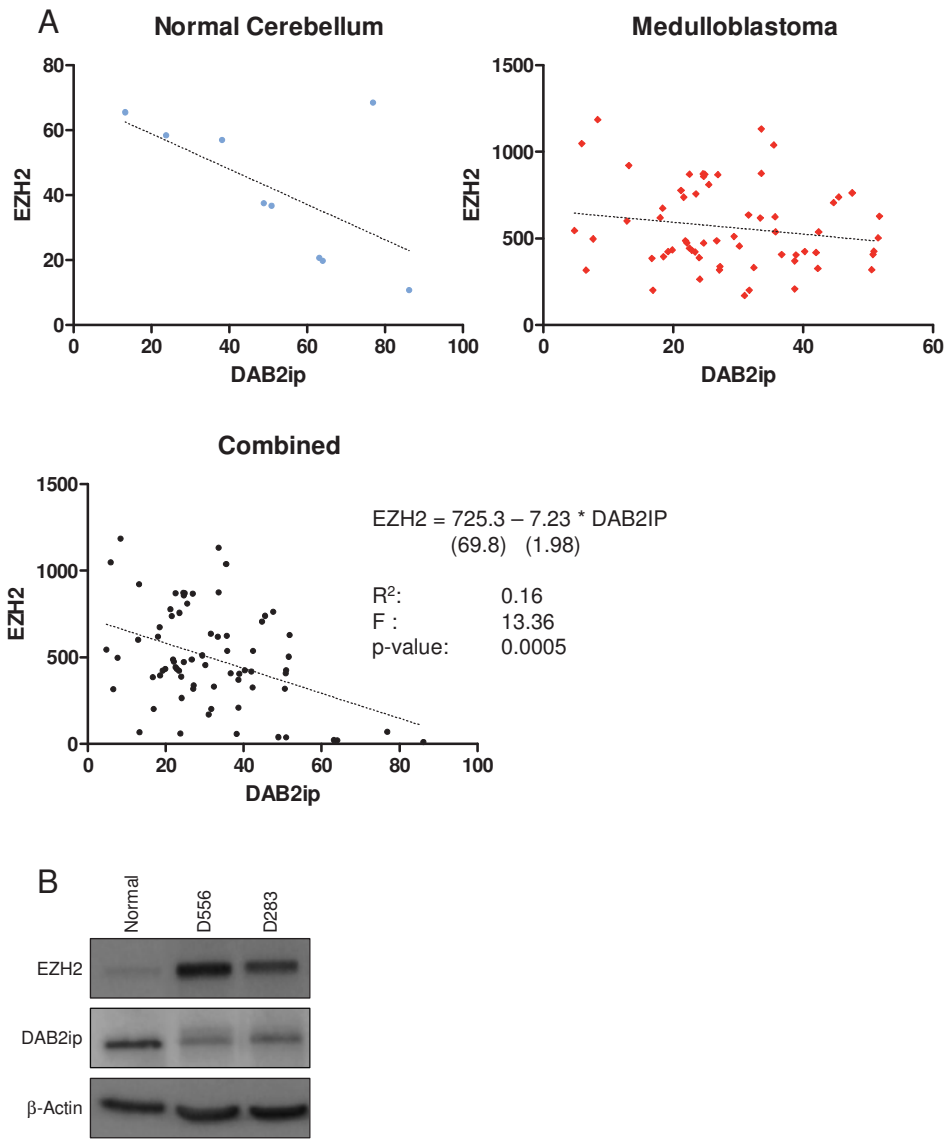

Supplementary figure 3.

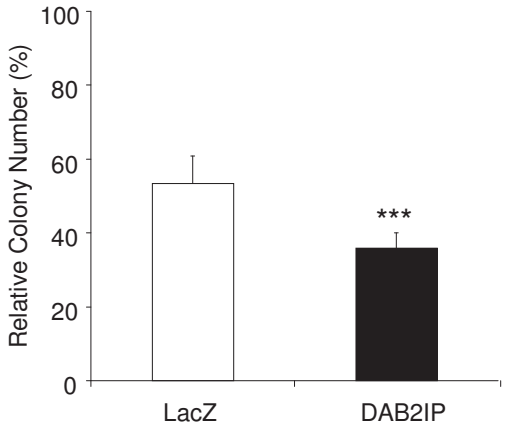

Supplementary figure 4

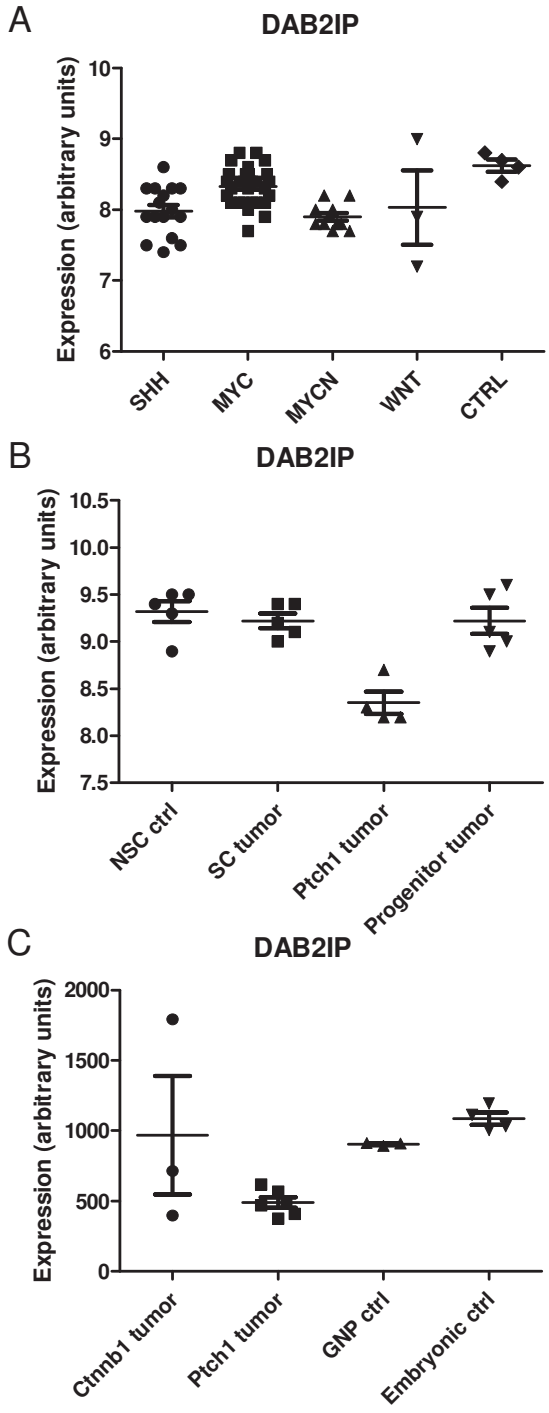

Supplementary figure 5

5

RASAL1 IS A PUTATIVE TUMOR SUPPRESSOR IN NEURAL PROGENITOR CELLS

Sjoerd van Rijn, Michiel Smits, Dirk Geerts, Jonas Nilsson
David P. Noske, W. Peter Vandertop, and Thomas Wurdinger

Manuscript in preparation

ABSTRACT

Glioblastoma (GBM) cells are proposed to arise from neural progenitor cells (NPCs) after substantial loss of tumor suppressor gene (TSG) regulation. Mutations of TP53, PTEN and NF1 are often correlated with GBM and loss of these genes in NPCs results in malignant glioma formation. Our research aimed at identifying novel TSGs that could drive oncogenesis in NPCs. We performed an *in silico* analysis of GBM gene expression data and identified 23 genes that were significantly downregulated as putative tumor suppressor genes. We investigated the potential oncogenic function of the five most significantly deregulated TSGs and TP53 in NPCs, using our epitope-tagged multiplex Gaussia luciferase reporter assay. Upon shRNA-mediated knockdown of the tumor suppressor candidates in NPCs, we observed a significant growth advantage *in vitro* for RASAL1, YWHAH, SYT13 and CHD5. Intracranial injection in mice of pooled NPCs, expressing luciferase reporter enzymes and with confirmed knockdown of the tumor suppressor candidates, resulted in tumor formation *in vivo* in two of 12 mice as measured by bioluminescence imaging, whereas mice injected with wild-type NPCs (n=12) did not result in detectable tumor growth. Immunohistological analysis of the formed tumors revealed that RASAL1, a member of the GAP1 GTPase-activating proteins, was responsible for driving the tumor formation in NPCs. Our proof-of-concept results suggest that RASAL1 is a tumor suppressor gene that participates in the transformation of NPCs.

Key words: Glioma, glioblastoma, brain cancer, transformation, oncogenesis, neural progenitor cells, NPCs, tumor suppressor, multiplex luciferase assay, gaussia luciferase, TP53, p53, NF1, PTEN, RASAL1

INTRODUCTION

Gliomas are the most common primary tumors in the brain. The most malignant form, glioblastoma, is one of the most lethal forms of cancer (Maher et al., 2001)(Zhu and Parada, 2002). Gliomas are highly infiltrative tumors and resistant to conventional radiation and chemotherapy, resulting in poor survival, with a median survival of approximately 18 months for glioblastoma (Stupp et al., 2005).

Although the cell of origin remains controversial, gliomas have been considered to arise from differentiated glia that undergo a process of dedifferentiation and from undifferentiated neural progenitor cells (NPCs) (Sanai et al., 2005)(Sauvageot et al., 2007)(Alcantara Llaguno et al., 2009)(Friedmann-Morvinski et al., 2012). Analysis of early tumor development in mouse models suggests that glioblastomas arise in the subventricular zone (SVZ), the residential area of NPCs (Zhu et al., 2005)(Kwon et al., 2008)(Alcantara Llaguno et al., 2009)(Friedmann-Morvinski et al., 2012). The SVZ is an extensive germinal layer that contains NPCs on the walls of the lateral ventricles of adult mammals (Alvarez-Buylla and Lim, 2004). Neurogenesis also occurs in the subgranular zone (SGZ) of the dentate gyrus, which produces local neurons that incorporate into the granular cell layer (Gage, 2000; Zhao et al.). In humans, the SVZ and SGZ have both been shown to harbor neural stem cells (Eriksson et al., 1998)(Sanai et al., 2004).

Llaguno et al. (Alcantara Llaguno et al., 2009) demonstrated that in NPCs mutations or deletions of tumor suppressor (TS) genes that frequently occur in glioblastoma, including in the TS genes TP53, NF1, and PTEN, give rise to malignant gliomas in mice. Friedmann-Morvinski et al. (Friedmann-Morvinski et al., 2012) demonstrated that combinatorial knockdown of NF1 and TP53 in differentiated mouse astrocytes and neurons could also result in the formation of malignant gliomas, by causing dedifferentiation of astrocytes and neurons towards the neural progenitor state. Mice with mutations in the TS genes TP53, NF1, and PTEN develop high-grade gliomas with complete penetrance (Alcantara Llaguno et al., 2009)(Kwon et al., 2008; Zhu et al., 2005). Moreover, TP53 and PTEN mutations are among the most frequent mutations reported in gliomas (Furnari et al., 2007)(Maher et al., 2001). Neurofibromatosis type 1 patients, with germline mutations in NF1, have increased susceptibility to gliomas (Gutmann et al., 2002). The TCGA consortium reported that NF1, TP53, and PTEN are among the top-5 most mutated genes in human glioblastoma (McLendon, 2008). Moreover, mice with heterozygous germline or conditional somatic TP53 mutations in their NPCs, combined with conditional somatic NF1 heterozygosity, develop gliomas (Zhu et al., 2005), which is enhanced by additional loss of PTEN (Kwon et al., 2008). The tumors formed in these models highly resemble their human equivalents.

RAS proteins are molecular switches for signaling cascades that modulate many aspects of cell biology (Wennerberg et al., 2005), which are regulated by RAS guanine nucleotide exchange factors (GEFs) and RAS GTPase-activating proteins (GAPs) (Bourne et al., 1990; Cherfils and Zeghouf, 2013; Feig, 1994). Interestingly, NF1 belongs to the class of RAS-GAPs, that also includes DAB2IP, which we recently identified as a novel TS in medulloblastoma (Smits et al., 2012).

Here we aimed at the identification of novel glioblastoma TS genes in NPCs. We performed expression analysis of 243 glioblastoma and non-neoplastic brain tissue samples and identified 23 TS genes significantly downregulated in glioblastoma. We functionally analyzed the top-5 of the TS candidates in mouse NPCs *in vitro* and *in vivo*, using our $Gluc_{tag}$ multiplex multi-culture system (van Rijn et al., 2013, 2014). We identified the RAS-GAP gene RASAL1 as a novel putative tumor-driving suppressor gene in murine NPCs.

RESULTS

Identification of tumor suppressor candidates in glioblastoma

We performed an analysis of TCGA expression data (Dong et al., 2010) to identify candidate tumor suppressor genes that are downregulated in glioblastoma. The mRNA expression data of 243 glioblastoma samples were compared with 11 healthy control samples. After statistical analysis 1236 genes were considered significantly deregulated, 347 genes were upregulated (28.1%) and 889 genes (71.9%) were downregulated (Fig. 1a). We then compared the list of significantly downregulated genes with a previously compiled list of tumor suppressor (TS) genes (Smits et al., 2012), revealing 23 TS candidates downregulated in glioblastoma (Fig. 1b-c and Table 1). We compared the 23 downregulated TS genes in glioblastoma with expression data (unpublished data) of other brain tumor types (Fig. 1d). This analysis revealed that all 23 glioblastoma TS candidates are also downregulated in medulloblastoma or in pediatric high-grade glioma. In addition, we confirmed the TS down-regulation in eight independent glioblastoma datasets (Fig. 1e, table 4). Next, we evaluated the protein expression of the TS candidates in glioblastoma and non-neoplastic brain, demonstrating that also the protein levels of nine TS candidates are clearly downregulated in large proportions of glioma tissues, in particular four of the top-5 significantly downregulated TS candidates MAPRE3, RASAL1, YWHAH, SYT13 (Fig. 1f). Next, we analyzed the expression of the tumor suppressor candidates in the four subtypes of GBM and found that there is a clear distinction of the expression of these genes in the mesenchymal, classical, proneural and neural subtypes (Fig. 1g).

Functional analysis of tumor suppressor candidates in NPCs *in vitro*

We decided to take the five most significantly downregulated tumor suppressor candidates (Fig. 2a-b) for functional knockdown analysis and we choose TP53 as a control gene. To analyze the role of these TS candidates in glioblastoma oncogenesis we used NPCs obtained from the SVZ of mice on embryonic day 13.5 (E13.5) after fertilisation and stably expressing Firefly luciferase (Fluc) and mCherry (red). These cells were transduced with six different reporters, each consisting of cerulean fluorescent protein (blue) and the Gaussia luciferase enzyme fused to a unique epitope tag ($Gluc_{tag}$), resulting in six

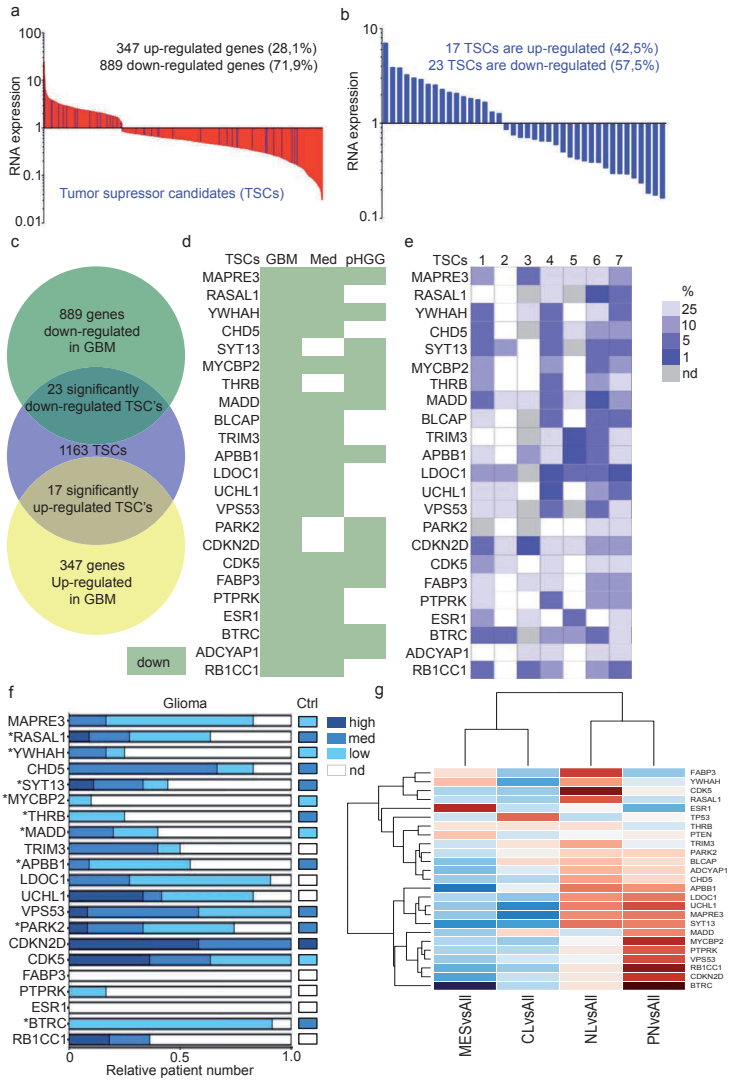

Figure 1. *Identification of tumor suppressor candidates in GBM* (a) RNA gene expression analysis in GBM. RNA of 1236 genes was significantly up- or downregulated in 243 GBM tumor samples. Blue lines represent the 40 significantly deregulated putative tumor suppressor genes. (b) 23 of the 40 significantly deregulated genes were downregulated. (c) Venn diagram shows the up- and downregulated genes and overlap with the putative tumor suppressor genes. (d) RNA of the 23 significantly downregulated putative tumor suppressor genes in GBM are also frequently found to be downregulated in other types of brain tumors such as medulloblastoma (Med) and pediatric high-grade glioma (pHGG). (e) When we analyzed other GBM datasets, the 23 putative tumor suppressors were often found to be downregulated. Blue colors and numbers represent % of normal expression, nd = not determined. (f) Nine putative tumor suppressors show a clear decrease (depicted with an *) in protein expression. Blue colors represent low, medium or high expression, nd = not determined. (g) RNA expression analysis of the 23 putative tumor suppressor genes between the four subtypes of GBM compared to average expression of all subtypes together. MES = mesenchymal, CL = classical, NL = neural, PN = proneural and All = all subtypes.

Table 1. *Significantly downregulated tumor suppressor candidates in GBM.* The 23 hits from the *in silico* analysis to identify putative GBM tumor suppressor genes. Gene names and description.

gene	description
MAPRE3	microtubule-associated protein, RP/EB family, member 3
RASAL1	RAS protein activator like 1 (GAP1 like)
YWHAH	tyrosine 3-monooxygenase/tryptophan 5-monooxygenase activation protein, eta
CHD5	chromodomain helicase DNA binding protein 5
SYT13	synaptotagmin XIII
MYCBP2	MYC binding protein 2, E3 ubiquitin protein ligase
THRB	thyroid hormone receptor, beta
MADD	MAP-kinase activating death domain
BLCAP	bladder cancer associated protein
TRIM3	tripartite motif containing 3
APBB1	amyloid beta (A4) precursor protein-binding, family B, member 1 (Fe65)
LDOC1	leucine zipper, down-regulated in cancer 1
UCHL1	ubiquitin carboxyl-terminal esterase L1 (ubiquitin thiolesterase)
VPS53	vacuolar protein sorting 53 homolog (S. cerevisiae)
PARK2	parkin RBR E3 ubiquitin protein ligase
CDKN2D	cyclin-dependent kinase inhibitor 2D (p19, inhibits CDK4)
CDK5	cyclin-dependent kinase 5
FABP3	fatty acid binding protein 3, muscle and heart (mammary-derived growth inhibitor)
PTPRK	protein tyrosine phosphatase, receptor type, K
ESR1	estrogen receptor 1
BTRC	beta-transducin repeat containing E3 ubiquitin protein ligase
ADCYAP1	adenylate cyclase activating polypeptide 1 (pituitary)
RB1CC1	RB1-inducible coiled-coil 1

murine NPC reporter cell lines (NPC-Fluc-Gluc$_{tag1-5}$) (Fig. 2c). Next, we selected the top-5 TS candidates, i.e. MAPRE3, RASAL1, YWHAH, SYT13 and CHD5, and TP53 and stably transduced the six NPC-Fluc-Gluc$_{tag}$ cell lines with individual shRNAs directed against these TSs (Table 2). We confirmed TS knockdown by qRT-PCR in the five NPC-Fluc-Gluc$_{tag}$ reporter cell lines by direct comparison to their parental control cell lines (Fig. 2d). The analysis of NPC-Fluc-Gluc$_{HA}$ cells, transduced with a shRNA directed against MAPRE3, revealed a knockdown of <25% and was omitted from further analysis; all other TS shRNAs resulted in a knockdown of >90% (Fig. 2d). Subsequently, we functionally compared the proliferation rates of NPC-Fluc-Gluc$_{tag}$ cell lines expressing the shRNAs against the four remaining TS candidates (RASAL1, YWHAH, SYT13 and CHD5) with their parental NPC-Fluc-Gluc$_{tag}$ cell lines. We used the NPC-Fluc-Gluc$_{tag}$ reporter cell lines in a previously developed multiplex bioluminescence-based proliferation assay (Van Rijn et al. 2013, 2014), in order to determine the potential proliferative advantage as a result of the knockdown of the TSs. Briefly, cells express Gaussia luciferase (Gluc) that is fused to an epitope tag (Gluc$_{tag}$) that can bind to an epitope tag-specific antibody. Each cell line expresses a specific Gluc$_{tag}$ and therefore it is possible to identify the

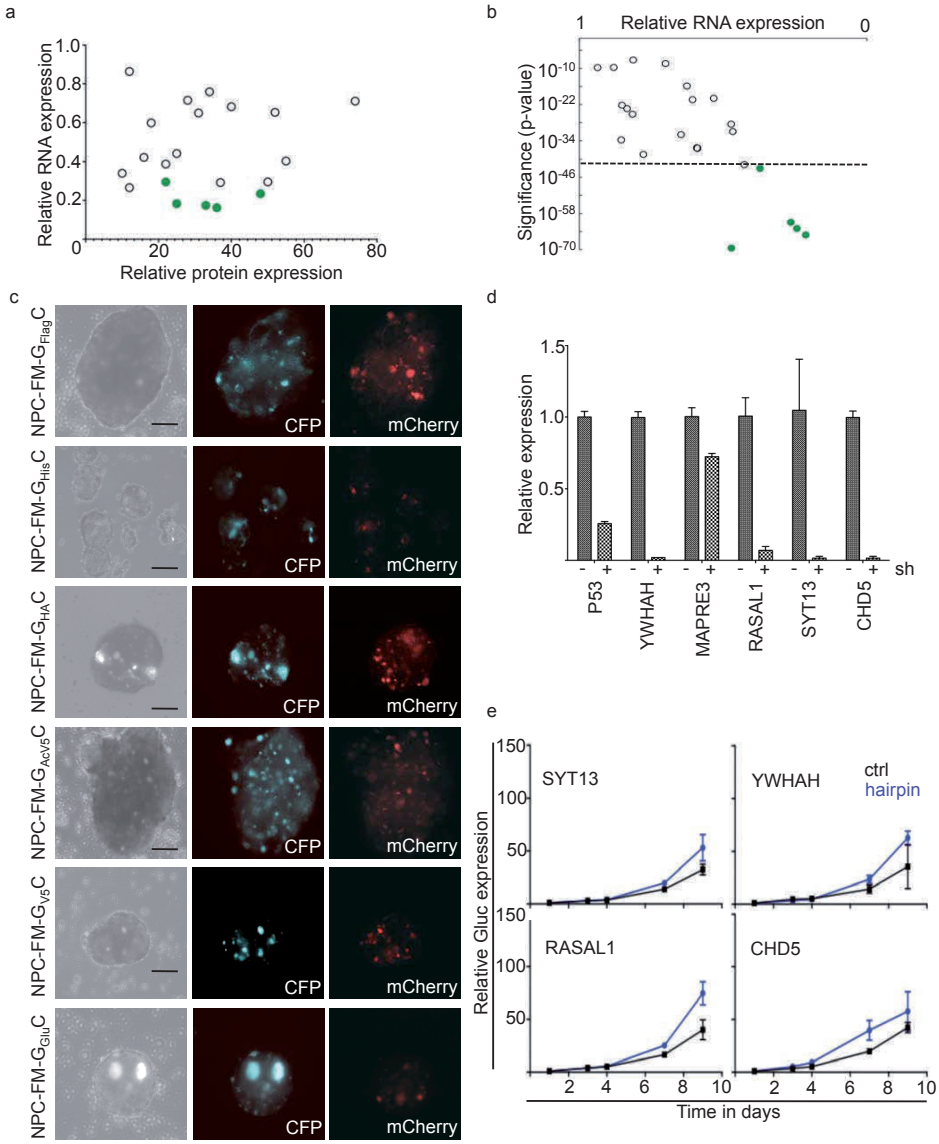

Figure 2. *Functional analysis of tumor suppressor candidates in NPCs in vitro.* (a) Selection of putative tumor suppressor genes for *in vitro* analysis. There is no correlation between RNA expression and protein expression. (b) We therefore selected the five most significantly downregulated tumor suppressor candidates for functional analysis. As a control we also analysed TP53. (c) Lentiviral transduction of Fluc-mCherry (red) and Gluc$_{Tag}$-CFP (blue) to construct six cell lines. Each cell line is then lentivirally transduced to express a short hairpin against the six tumor suppressor candidates. (d) QRT-PCR of short hairpin knockdown of tumor suppressor candidates in NPCs. (e) *In vitro* growth assay using Gluc as a read-out for proliferation of NPC lines. Blue lines represent NPC with tumor suppressor knock down, black lines are control NPCs.

relative expression of each cell line within a co-culture of all the cell lines. Using the $Gluc_{tag}$ multiplex assay, cell proliferation was monitored of all NPC cell lines within a single co-culture over a period of nine days. Of note, knockdown of RASAL1, YWHAH, SYT13 and CHD5 resulted in a modest but significant proliferative advantage of the NPCs, as compared to the control cell lines (Fig. 2e).

Functional analysis of TS candidates in NPCs *in vivo*

Next, we mixed the four RASAL1, YWHAH, SYT13 and CHD5 NPC knockdown cell lines and, in parallel, the parental control NPC cells in equal amounts (5×10^4 cells per cell line), prior to stereotactic injection of the pooled cells into the mouse striatum (n=12). We used Fluc bioluminescence imaging to monitor potential tumor growth *in vivo* (Fig. 3a). None of the injections with wild-type control NPC cells (n=12) resulted in a Fluc signal, as measured over a period of 120 days, and confirming the incapacity of wild-type NPCs to form tumors after injection of these cells into the striatum of mice. Of note, two out of the twelve mice injected with NPCs subjected to TS knockdown did give a Fluc signal, indicative of tumor growth by transformation of NPC cells due to TS knockdown. We sacrificed the mice and isolated the brains to perform IHC using tag-specific antibodies (Fig. 3b). Staining with the AcV5 antibody (for RASAL1 identification) showed a positive staining of the formed tumor mass, in contrast to the other antibodies used and staining of the NPC control brains with the AcV5 antibody. We also stained with H&E for histological identification of the tumor (Fig. 3c). These results indicate that knockdown of RASAL1 in the NPC-Fluc-$Gluc_{AcV5}$ cells caused the observed tumor growth in the striatum of mice, suggesting that RASAL1 is a putative tumor suppressor in NPCs. When we analyzed RASAL1 gene expression, we found that low RASAL1 expression provides a slight but significant survival advantage in GBM (Fig. 3d, 3 months $p<0.05$), but not in gliomas in general (Fig. 3e). Protein expression analysis in the Human Protein Atlas reveals high RASAL1-expression in the hippocampus and the lateral ventricle of normal brains, but low or no RASAL1 expression in 73% of gliomas.

Table 2. *NPC cell lines for in vitro and in vivo functional analysis.* Mouse neuronal precurs cells were lentivirally transduced with Firefly luciferase, co-expressed with mCherry (Fluc-mCherry). Then, each cell line was lentivirally transduced with Gaussia luciferase fused to a specific epitope tag and co-expressed with Cerulean fluorescent protein ($Gluc_{tag}$-CFP). Finally, short hairpins against putative tumor suppressors were transduced.

NPC cell line	TSG short hairpin	abbreviation
mNPC-Fluc-mCherry-$Gluc_{Flag}$-CFP	YWHAH	NPC-FM-G_{Flag}C
mNPC-Fluc-mCherry-$Gluc_{His}$-CFP	P53	NPC-FM-G_{His}C
mNPC-Fluc-mCherry-$Gluc_{HA}$-CFP	MAPRE3	NPC-FM-G_{HA}C
mNPC-Fluc-mCherry-$Gluc_{AcV5}$-CFP	RASAL1	NPC-FM-G_{AcV5}C
mNPC-Fluc-mCherry-$Gluc_{V5}$-CFP	SYT13	NPC-FM-G_{V5}C
mNPC-Fluc-mCherry-$Gluc_{Glu}$-CFP	CHD5	NPC-FM-G_{Glu}C

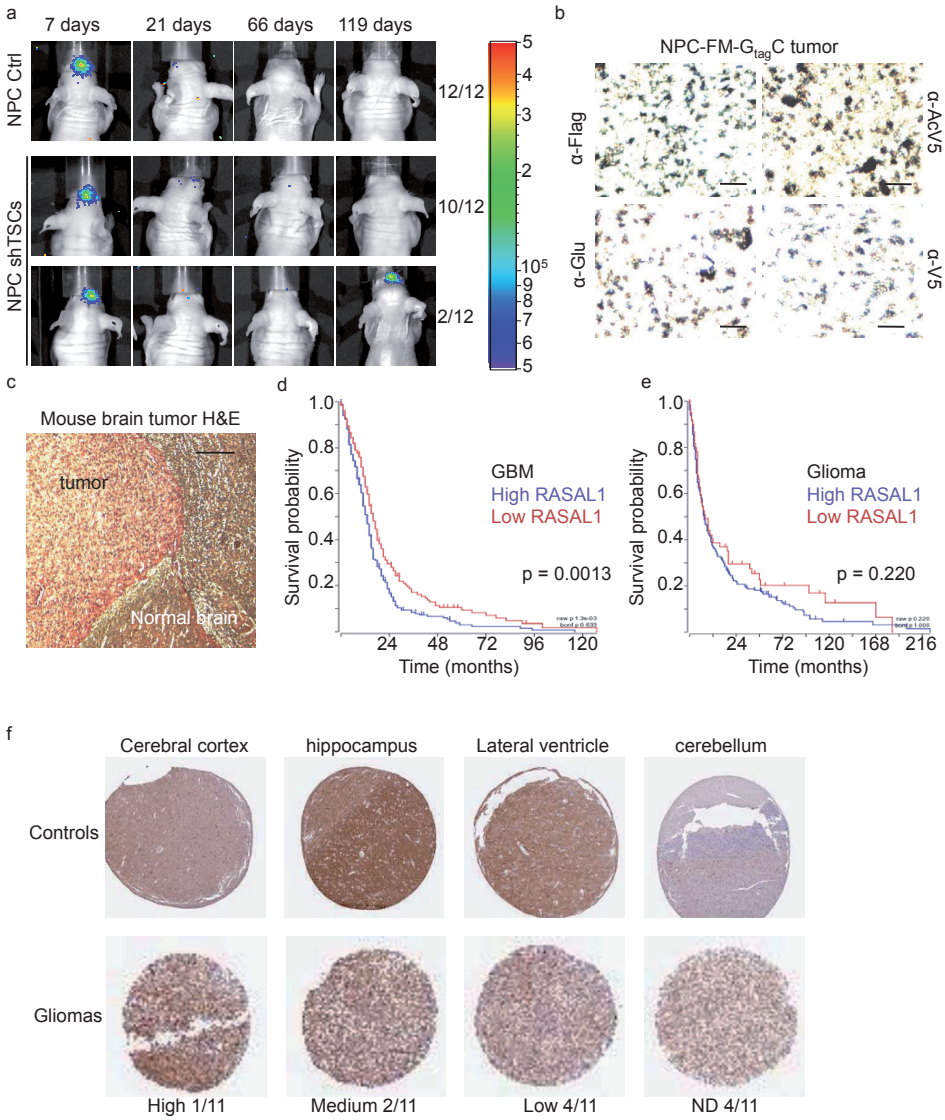

Figure 3. *Functional analysis of tumor suppressor candidates in NPCs in vivo.* (a) Intracranial injection of the six NPCs with tumor suppressor gene knockdown and control NPCs. Mice were followed for 119 days post injection. (b) After sacrifice of the mice, brains were isolated and sliced for immunohistochemistry using antibodies against the Gluc$_{Tag}$. RASAL1 knockdown cells show modest staining. (c) H&E staining of the mouse brain tumor formed after injection of NPCs with tumor suppressors knockdown. Bar is 200 µm. (d) Survival data of RASAL1 downregulation in GBM. (e) Survival data of RASAL1 downregulation in glioma. (f) RASAL1 staining in GBM tumor tissue and in control brain tissues. Nd = not detected.

DISCUSSION

Here we identified a novel TS candidate in NPCs, RASAL1. Knockdown of RASAL1 in NPCs resulted in a proliferative advantage of NPCs in vitro. After intracranial injection of NPCs with knockdown of RASAL1 resulted in tumor growth in two out of twelve mice.

RASAL1, like NF1 and DAB2IP, is a member of the RAS-GAP proteins, tightly regulating RAS activity. RASAL1 is downregulated in several solid tumors (Seto et al., 2011) and loss of RASAL1 activity has been correlated with hyperactive RAS (Calvisi et al., 2011; Liu et al., 2013; Ohta et al., 2009). RASAL1 can be downregulated via transcriptional regulation by PITX (Kolfschoten et al., 2005), or via epigenetic silencing by DNA methylation and histone acetylation - restored by treatment with 5'-AZA and TSA, respectively. We investigated whether PITX1 was also downregulated in glioblastoma tissues but we did not find any evidence in the TCGA glioblastoma dataset (data not shown). Hence, it is not unlikely that the downregulation of RASAL1 is caused by epigenetic mechanisms. In future studies it would be of interest to determine whether RASAL1 downregulation in glioblastoma cells can be restored by 5'-AZA and/or TSA, inhibitors of DNA methylation and histone acetylation, respectively, although genetic deletion or mutation of the RASAL1 gene may provide an alternative explanation. The effect of RASAL1 downregulation on RAS-signaling and the cell cycle has been extensively reported by others (Calvisi et al., 2011; Chen et al., 2013; Kolfschoten et al., 2005; Liu et al., 2013; Ohta et al., 2009), and may at least partly explain the highly proliferative nature of glioblastoma cells.

In this study we compared the expression of the TS candidates in glioblastoma, medulloblastoma and pediatric high grade glioma (pHGG) tissues (Fig. 1d). A total of nine out of 23 TS genes were downregulated in all three brain tumor types, suggesting a more pivotal role of these genes in brain tumors or in tumors in general in comparison to genes that are more exclusively deregulated in specific brain tumors. For example, 10 genes are more exclusively downregulated in glioblastoma and medulloblastoma, including RASAL1, and four genes are more exclusively downregulated in glioblastoma and pHGG. It is striking to observe that all TS candidates that are significantly downregulated in glioblastoma are also downregulated in either medulloblastoma or pHGG. It may be of interest to also further explore these TS genes in medulloblastoma and/or pHGG.

Glioblastomas, as well as other tumor types, may propagate themselves via a subset of cancer stem-like cells (Reya et al., 2001)(Dalerba and Clarke, 2007; Scadden, 2014; Singh et al., 2004), which have characteristics in common with NPCs. Future analysis of tumors formed by RASAL1-knockdown should therefore include further characterization of the tumor subtype and potential glioblastoma stem-like cells. Future experiments may also indicate whether downregulation or deletion of RASAL1, solely or in combination with combinatorial deletion of TP53, NF1, or PTEN, can also result in transformation of differentiated astrocytes and/or neurons, giving rise to glioblastomas.

Llagunoi et al. (Alcantara Llaguno et al., 2009) demonstrate that in contrast to normal adult neural stem cells that are strictly confined to the SVZ or SGZ, tumors arising from tumor

suppressor-deficient neural stem cells or their progeny are not restricted to these niches and actually migrate away from their normal locations, thus accounting for the presence of tumors elsewhere in the forebrain, including the cortex, striatum, hippocampus, and thalamus. The tumors that formed after injection of neural progenitor cells with knockdown of RASAL1 into the striatum of mice showed solid growth, although single infiltrating cells were observed as well. However, it remains to be investigated whether RASAL1-knockdown or deletion in NPCs using endogenous tumor suppressor-based mouse models will also result in highly invasive gliomas. Therefore, further characterization of the tumors formed after RASAL1-knockdown in NPCs is warranted.

METHODS

Mouse neuronal precursor cell isolation and culture. Primary mouse neuronal precursors were isolated as described previously (Rietze and Reynolds, 2006). Briefly, Primary NPCs were isolated from the brain subventricular zone (SVZ) of E13.5 embryos. NPCs were maintained in Neurobasal medium (Life Technologies) supplemented with 0.5 mM stable glutamine (Life Technologies) 1x N2 supplement (Life Technologies), 1x Stempro neural supplement (Life Technologies), 20 ng/mL EGF (Sigma) and 10ng/mL bFGF (Sigma). For passaging, neurospheres were collected and spun down with 150 x G for 5 minutes and dissociated with Accutase (Life Technologies), diluted to the desired concentration and resuspended in Neurobasal medium as described previously. For cell culturing and experiments we used ultra low attachment cell culture containers (Corning) and cells were kept at 37˚C and 5% CO_2.

Lentivirus transduction. The mouse NPCs were first lentivirally transduced with Firefly luciferase (Fluc) reporter for *in vivo* bioluminescent imaging to detect cell proliferation. Then the Gaussia luciferase reporter, fused to an epitope tag, was lentivirally transduced for *ex vivo* bioluminescent blood monitoring of the cells. Finally, a short hairpin was expressed against the tumor suppressor gene of interest, using lentiviral transduction. To produce the virus, the bioluminescent reporter constructs or the short hairpin was co-transfected with a third generation lentiviral packaging mix (pMDLg/pRRE, pRSV-Rev and pMD2.G, Addgene) in HEK293T cells using Lipofectamine 2000 (Life Technologies). Virus was harvested two and three days after transfection and cell debris was spun down for five minutes at 1,000 × g. U87 cells were transduced overnight with lentivirus using a multiplicity of infection of 100 transducing units per cell in the presence of 8 µg/ml polybrene in standard culture conditions.

Fluorescence microscopy. Successful transduction was verified by visualizing CFP (co-expressed with the $Gluc_{tag}$ construct) and mCherry fluorescent protein (co-expressed with Fluc) using fluorescent microscopy (Leica).

Immunostaining and antibodies. For mouse tissue staining, tumors were removed and embedded in paraffin. Microtome sections of 5 µm on glass slides were deparaffinized

in xylene and rehydrated in ethanol series of 100%, 96%, and 70% ethanol. Endogenous peroxide was blocked with 0.3% H_2O_2 in methanol for 30 minutes. After rinsing with water, antigens were retrieved with citrate buffer (pH 6) with 0.05% Tween 20 using a microwave (Bosch, five minutes 900 watt, 10 minutes 360 watt). After slowly cooling, tissues were washed three times with PBS and incubated with primary antibody (10 µg/ml), for one hour at room temperature. After washing three times again, tissues were incubated with REAL Envision Rabbit anti-mouse (Dako and REAL DAB+ stained (Dako). Nuclei were counterstained with haematoxylin. Tissue sections were dehydrated with ethanol series as before and fixed in xylene. Cells and sections were imaged and photographed by light microscopy (Leica).

In vivo experiments. All *in vivo* experiments were subject to ethical committee approval and are in accordance with VU University Medical Center and Dutch law on animal experimentation (Wet op de dierproeven, WOD). For intracranial tumor implantation, a stereotactic frame (Harvard Biosciences) was used to inject cells vertically into the right hemisphere. General anesthesia was induced by subcutaneous injection of buprenorphine hydrochloride (0.1 mg/kg). The mice were further anesthetized with oxygen containing 2.5% isofluorane. After skin incision, lidocaine drops (5 mg/ml in PBS) were administered topically. A small drill was used to drill a hole into the skull. Coordinates used for injection were X = 0.5 mm, Y = 2 mm, Z = -2 mm from the bregma. A mix of 6 x 10^5 NPCs (1 x 10^5 NPCs per tumor suppressor short hairpin knockdown) in 5 µl of Neurobasal medium was injected vertically. On indicated days after injection, we performed Fluc bioluminescence activity *in vivo* by injecting $_D$-luciferin (100 mg/kg) intraperitoneally. Imaging was performed with an IVIS CCD camera and analyzed with Living Image software (Caliper Life Sciences). We collected 100 µl mouse blood aliquots from the tail vein in Microvette CB300 EDTA capillary tubes (Sarstedt) for *ex vivo* whole Gluc.

RT-PCR. NPC RNA was isolated using mirVana (Life Technologies) according to manufacturer's guidelines. cDNA was generated using Omniscript RT kit (Qiagen) and PCR was performed in triplo using FastStart SYBR Green Master (Rox) mix (Roche). Real time PCR was performed in the ABI 7500 thermal cycler (Life Technologies). Primers for tumor suppressor gene amplification are shown in table 3.

Table 3. *Primers for gene knockdown RT-qPCR.* After transduction with putative tumor suppressor gene short hairpin, knockdown was verified using RT-qPCR.

Gene	Gene ID	Forward primer 5′-3′	Reverse primer 5′-3′	Product bp.
MAPRE3	100732	ATGGCTGTCAATGTGTACTCCA	TCATGGCGACTCAGATTCTCA	56
RASAL1	19415	GGAAGCAGTGACCCCTATTGT	AAGGTGAACGGTGTACTCCTC	114
YWHAH	22629	CTTGGCTCTGCTTGACAAGTT	GCGGTAGTAATCGCCCTTCAT	97
CHD5	269610	AGCCCGTGAGTCTTCCCAA	TGTCTGACATCTCGTCATTGC	105
SYT13	80976	CGGCCCAACAGTTCAACATTA	GCCGGGGACCATAGATGTC	87
TP53	22059	CACAGCACATGACGGAGGTC	TCCTTCCACCCGGATAAGATG	101

In silico analysis. TCGA gene expression data was obtained from (Dong et al., 2010). We compared the TS candidates with GBM RNA expression data (table 4) in Oncomine (www.oncomine.org) and protein expression data in The Human Protein Atlas (www.proteinatlas.org). We then compared TS candidate expression between the GBM classical, mesenchymal, proneural and neural subtypes using R and gene expression data from (Verhaak et al., 2010). Survival data for RASAL1 in glioma and GBM was obtained from R2: Genomics analysis and visualization platform (r2.amc.nl), using the data set Tumor Glioblastoma TCGA 540.

Table 4. *Oncomine gene expression datasets.* The datasets used for oncomine GBM gene expression analysis, number of samples used and references.

Number	Data set type	Data set		# Samples	reference
1	Glioblastoma vs. Normal	Bredel Brain 2	mRNA	54	Cancer Res, 2005
2	Glioblastoma vs. Normal	Lee Brain	mRNA	101	Cancer Cell, 2006
3	Glioblastoma vs. Normal	Liang Brain	mRNA	38	Proc Natl Acad Sci U S A, 2005
4	Glioblastoma vs. Normal	Murat Brain	mRNA	84	J Clin Oncol, 2008
5	Glioblastoma vs. Normal	Shai Brain	mRNA	42	Oncogene, 2003
6	Glioblastoma vs. Normal	Sun Brain	mRNA	180	Cancer Cell, 2006
7	Brain Glioblastoma vs. Normal	TCGA Brain 1	mRNA	557	No Associated Paper, 2013

ACKNOWLEDGEMENTS

We are grateful to Dimphna Meijer who kindly provided mouse neuronal precursor cells. This research was funded by CCA-VICI fellowships.

REFERENCES

1 Alcantara Llaguno, S., Chen, J., Kwon, C.-H., Jackson, E.L., Li, Y., Burns, D.K., Alvarez-Buylla, A., and Parada, L.F. (2009). Malignant astrocytomas originate from neural stem/progenitor cells in a somatic tumor suppressor mouse model. Cancer Cell *15*, 45–56.

2 Alvarez-Buylla, A., and Lim, D.A. (2004). For the long run: maintaining germinal niches in the adult brain. Neuron *41*, 683–686.

3 Bourne, H.R., Sanders, D.A., and McCormick, F. (1990). The GTPase superfamily: a conserved switch for diverse cell functions. Nature *348*, 125–132.

4 Calvisi, D.F., Ladu, S., Conner, E.A., Seo, D., Hsieh, J.-T., Factor, V.M., and Thorgeirsson, S.S. (2011). Inactivation of Ras GTPase-activating proteins promotes unrestrained activity of wild-type Ras in human liver cancer. J. Hepatol. *54*, 311–319.

5 Chen, H., Pan, Y., Cheng, Z.-Y., Wang, Z., Liu, Y., Zhao, Z.-J., and Fan, H. (2013). Hypermethylation and clinicopathological significance of RASAL1 gene in gastric cancer. Asian Pac. J. Cancer Prev. *14*, 6261–6265.

6 Cherfils, J., and Zeghouf, M. (2013). Regulation of small GTPases by GEFs, GAPs, and GDIs. Physiol. Rev. *93*, 269–309.

7 Dalerba, P., and Clarke, M.F. (2007). Cancer stem cells and tumor metastasis: first steps into uncharted territory. Cell Stem Cell *1*, 241–242.

8 Dong, H., Siu, H., Luo, L., Fang, X., Jin, L., and Xiong, M. (2010). Investigation gene and microRNA expression in glioblastoma. BMC Genomics *11 Suppl 3*, S16.

9 Eriksson, P.S., Perfilieva, E., Björk-Eriksson, T., Alborn, A.M., Nordborg, C., Peterson, D.A., and Gage, F.H. (1998). Neurogenesis in the adult human hippocampus. Nat. Med. *4*, 1313–1317.

10 Feig, L.A. (1994). Guanine-nucleotide exchange factors: a family of positive regulators of Ras and related GTPases. Curr. Opin. Cell Biol. *6*, 204–211.

11 Friedmann-Morvinski, D., Bushong, E.A., Ke, E., Soda, Y., Marumoto, T., Singer, O., Ellisman, M.H., and Verma, I.M. (2012). Dedifferentiation of neurons and astrocytes by oncogenes can induce gliomas in mice. Science *338*, 1080–1084.

12 Furnari, F.B., Fenton, T., Bachoo, R.M., Mukasa, A., Stommel, J.M., Stegh, A., Hahn, W.C., Ligon, K.L., Louis, D.N., Brennan, C., et al. (2007). Malignant astrocytic glioma: genetics, biology, and paths to treatment. Genes Dev. *21*, 2683–2710.

13 Gage, F.H. (2000). Mammalian neural stem cells. Science *287*, 1433–1438.

14 Gutmann, D.H., Rasmussen, S.A., Wolkenstein, P., MacCollin, M.M., Guha, A., Inskip, P.D., North, K.N., Poyhonen, M., Birch, P.H., and Friedman, J.M. (2002). Gliomas presenting after age 10 in individuals with neurofibromatosis type 1 (NF1). Neurology *59*, 759–761.

15 Kolfschoten, I.G.M., van Leeuwen, B., Berns, K., Mullenders, J., Beijersbergen, R.L., Bernards, R., Voorhoeve, P.M., and Agami, R. (2005). A genetic screen identifies PITX1 as a suppressor of RAS activity and tumorigenicity. Cell *121*, 849–858.

16 Kwon, C.-H., Zhao, D., Chen, J., Alcantara, S., Li, Y., Burns, D.K., Mason, R.P., Lee, E.Y.-H.P., Wu, H., and Parada, L.F. (2008). Pten haploinsufficiency accelerates formation of high-grade astrocytomas. Cancer Res. *68*, 3286–3294.

17 Liu, D., Yang, C., Bojdani, E., Murugan, A.K., and Xing, M. (2013). Identification of RASAL1 as a major tumor suppressor gene in thyroid cancer. J. Natl. Cancer Inst. *105*, 1617–1627.

18 Ma, B.B.Y., Sung, F., Tao, Q., Poon, F.F., Lui, V.W., Yeo, W., Chan, S.L., and Chan, A.T.C. (2010). The preclinical activity of the histone deacetylase inhibitor PXD101 (belinostat) in hepatocellular carcinoma cell lines. Invest. New Drugs *28*, 107–114.

19 Maher, E.A., Furnari, F.B., Bachoo, R.M., Rowitch, D.H., Louis, D.N., Cavenee, W.K., and DePinho, R.A. (2001). Malignant glioma: genetics and biology of a grave matter. Genes Dev. *15*, 1311–1333.

20 McLendon (2008). Comprehensive genomic characterization defines human glioblastoma genes and core pathways. Nature *455*, 1061–1068.

21 Ohta, M., Seto, M., Ijichi, H., Miyabayashi, K., Kudo, Y., Mohri, D., Asaoka, Y., Tada, M., Tanaka, Y., Ikenoue, T., et al. (2009). Decreased expression of the RAS-GTPase activating protein RASAL1 is associated with colorectal tumor progression. Gastroenterology *136*, 206–216.

22 Reya, T., Morrison, S.J., Clarke, M.F., and Weissman, I.L. (2001). Stem cells, cancer, and cancer stem cells. Nature *414*, 105–111.

23 Rietze, R.L., and Reynolds, B.A. (2006). Neural stem cell isolation and characterization. Methods Enzymol. *419*, 3–23.

24 Van Rijn, S., Nilsson, J., Noske, D.P., Vandertop, W.P., Tannous, B.A., and Würdinger, T. (2013). Functional multiplex reporter assay using tagged Gaussia luciferase. Sci. Rep. *3*, 1046.

25 Van Rijn, S., Würdinger, T., and Nilsson, J. (2014). Multiplex functional bioluminescent reporters using Gaussia luciferase fused to epitope tags in an immunobinding assay. Methods Mol. Biol. *1098*, 231–247.

26 Sanai, N., Tramontin, A.D., Quiñones-Hinojosa, A., Barbaro, N.M., Gupta, N., Kunwar, S., Lawton, M.T., McDermott, M.W., Parsa, A.T., Manuel-García Verdugo, J., et al. (2004). Unique astrocyte ribbon in adult human brain contains neural stem cells but lacks chain migration. Nature *427*, 740–744.

27 Sanai, N., Alvarez-Buylla, A., and Berger, M.S. (2005). Neural stem cells and the origin of gliomas. N. Engl. J. Med. *353*, 811–822.

28 Sauvageot, C.M., Kesari, S., and Stiles, C.D. (2007). Molecular pathogenesis of adult brain tumors and the role of stem cells. Neurol. Clin. *25*, 891–924, vii.

29 Scadden, D.T. (2014). Nice neighborhood: emerging concepts of the stem cell niche. Cell *157*, 41–50.

30 Seto, M., Ohta, M., Ikenoue, T., Sugimoto, T., Asaoka, Y., Tada, M., Mohri, D., Kudo, Y., Ijichi, H., Tateishi, K., et al. (2011). Reduced expression of RAS protein activator like-1 in gastric cancer. Int. J. Cancer *128*, 1293–1302.

31 Singh, S.K., Hawkins, C., Clarke, I.D., Squire, J.A., Bayani, J., Hide, T., Henkelman, R.M., Cusimano, M.D., and Dirks, P.B. (2004). Identification of human brain tumour initiating cells. Nature *432*, 396–401.

32 Smits, M., van Rijn, S., Hulleman, E., Biesmans, D., van Vuurden, D.G., Kool, M., Haberler, C., Aronica, E., Vandertop, W.P., Noske, D.P., et al. (2012). EZH2-regulated DAB2IP is a medulloblastoma tumor suppressor and a positive marker for survival. Clin. Cancer Res. *18*, 4048–4058.

33 Stupp, R., Mason, W.P., van den Bent, M.J., Weller, M., Fisher, B., Taphoorn, M.J.B., Belanger, K., Brandes, A.A., Marosi, C., Bogdahn, U., et al. (2005). Radiotherapy plus concomitant and adjuvant temozolomide for glioblastoma. N. Engl. J. Med. *352*, 987–996.

34 Verhaak, R.G.W., Hoadley, K. a, Purdom, E., Wang, V., Qi, Y., Wilkerson, M.D., Miller, C.R., Ding, L., Golub, T., Mesirov, J.P., et al. (2010). Integrated genomic analysis identifies clinically relevant subtypes of glioblastoma characterized by abnormalities in PDGFRA, IDH1, EGFR, and NF1. Cancer Cell *17*, 98–110.

35 Wennerberg, K., Rossman, K.L., and Der, C.J. (2005). The Ras superfamily at a glance. J. Cell Sci. *118*, 843–846.

36 Zhao, Y., Huang, Q., Zhang, T., Dong, J., Wang, A., Lan, Q., Gu, X., and Qin, Z. Ultrastructural studies of glioma stem cells/progenitor cells. Ultrastruct. Pathol. *32*, 241–245.

37 Zhu, Y., and Parada, L.F. (2002). The molecular and genetic basis of neurological tumours. Nat. Rev. Cancer *2*, 616–626.

38 Zhu, Y., Guignard, F., Zhao, D., Liu, L., Burns, D.K., Mason, R.P., Messing, A., and Parada, L.F. (2005). Early inactivation of p53 tumor suppressor gene cooperating with NF1 loss induces malignant astrocytoma. Cancer Cell *8*, 119–130.

39 Oncomine: www.oncomine.org The Human Protein Atlas: www.proteinatlas.org R2: Genomics analysis and visualization platform: r2.amc.nl

6

BIOLUMINESCENCE-MEDIATED LONGITUDINAL MONITORING OF ADIPOSE-DERIVED STEM CELLS IN A LARGE MAMMAL *EX VIVO* ORGAN CULTURE

Mirte Peeters, Sjoerd van Rijn, Pieter-Paul A. Vergroesen, Cornelis P. L. Paul, David P. Noske, W. Peter Vandertop, Thomas Wurdinger, Marco N. Helder

Scientific Reports 5, 13960 (2015)

ABSTRACT

Recently, *ex vivo* three-dimensional organ culture systems have emerged to study the physiology and pathophysiology of human organs. These systems also have potential as a translational tool in tissue engineering; however, this potential is limited by our ability to longitudinally monitor the fate and action of cells used in regenerative therapies Therefore, we investigated luciferase-mediated bioluminescence imaging (BLI) as a non-invasive technique to continuously monitor cellular behavior in *ex vivo* whole organ culture.

Goat adipose-derived stem cells (gADSCs) were transduced with either Firefly luciferase (Fluc) or *Gaussia* luciferase (Gluc) reporter genes and injected in isolated goat intervertebral discs (IVD). Luciferase activity was monitored by BLI for at least seven days of culture. Additionally, possible confounders specific to avascular organ culture were investigated. Gluc imaging proved to be more suitable compared to Fluc in monitoring gADSCs in goat IVDs.

We conclude that BLI is a promising tool to monitor spatial and temporal cellular behavior in *ex vivo* organ culture. Hence, *ex vivo* organ culture systems allow pre-screening and pre-validation of novel therapeutic concepts prior to *in vivo* large animal experimentation. Thereby, organ culture systems can reduce animal use, and improve the speed of innovation by overcoming technological, ethical and financial challenges.

Key words: Adipose derived stem cells, *ex vivo* organ cultures, intervertebral discs, bioluminescent imaging, loaded disc culture system, *Gaussia* luciferase, Firefly luciferase

INTRODUCTION

Recently, *ex vivo* three-dimensional (3D) whole organ culture systems have emerged as means with which to study the physiology and pathophysiology of human organs and tissues. Pluripotent human stem cells and their self-organizing capacities have been used to develop bowel, kidney, brain, retina and liver-bud organoids[1,2]. Additionally, animal and human tissue explants are used in long-term *ex vivo* culture. Intestines, intervertebral discs, pancreas and skin explants have been cultured to study biological and pathological processes[2–6]. Subsequently, these 3D culture systems are increasingly used to study therapies, for instance in prostate cancer[7].

In addition to traditional drug-based approaches, tissue engineering aims to regenerate damaged or degenerated tissue and organs using cells or regeneration inducting factors. However, the fate and action of these cells after implantation are often hard to determine, and research will therefore benefit from longitudinal monitoring of cellular behavior. Luciferase-mediated bioluminescence imaging (BLI) is a non-invasive imaging technique which allows real-time *in vivo* monitoring of location and proliferation of luciferase-expressing cells[8,9]. BLI is based on the emission of photons produced during substrate conversion by luciferase enzymes. These photons can be detected by a cooled charged coupled device (CCD) through several millimeters of tissue. The considerable penetration depth, including cartilage and bone, and the higher signal-to-noise ratio of the BLI technique are marked advantages compared to conventional fluorescent cell viability assays which require laser excitation for cell visualization. Different dye methods used to determine cell viability require lysis or fixation of cells or tissue. This results in termination of the experiment, and therefore impedes longitudinal monitoring of cell viability within a single sample. Finally, BLI has been shown to be highly correlated to the above mentioned cell viability assays (for both Fluc and Gluc) and is therefore a well-established method for cell viability monitoring[10,11]. These advantages highlight the potential of BLI for longitudinal evaluation of cellular therapies in *ex vivo* tissue culture[12].

In vivo, bioluminescent imaging is only performed in small animal models[13–17]. Results found in small animals are often difficult to extrapolate to the human situation since they do not properly reflect the human physiology and/or dimensional conditions[18]. On the other hand, the size of large mammals impedes *in vivo* bioluminescent imaging due to the current penetration depth of BLI. The use of BLI in *ex vivo* organ culture systems offers a potent solution to overcome this problem.

Recently, we developed an *ex vivo* loaded disc organ culture system (LDCS), to study the physiology of intervertebral discs (IVD) and their response to mechanical loads[4,19]. This system allows us to investigate the process of intervertebral disc degeneration, identified as an important etiological factor of low back pain[20,21]. In the LDCS goat IVDs are used as they are a representative model for the human IVD[22]. In addition, the LDCS allows for preclinical *ex vivo* evaluation of therapies aimed at tissue regeneration prior to actual *in vivo* animal experimentation[23], without the problems related with the translation of small animal research to humans.

Mesenchymal stem cells (MSCs) are excellent candidates for regenerative therapies because of their relatively young age and multi-differentiation potential. Furthermore, studies directly comparing young and adult chondrocytes with age-matched MSCs showed that - based on aggrecan ultrastructure, ECM composition, and cellular proliferation - MSCs produce a superior cartilage-like neo-tissue compared to either young or adult chondrocytes[24,25]. Previous research showed successful luciferase reporter transductions of MSCs obtained from humans and animals[13,26–28]. *In vivo*, MSCs show promising results when transplanted into rat and rabbit IVDs, and these cells survive, differentiate, and increase the production of functional extracellular matrix, thereby arresting the degeneration process[29–31]. Furthermore, MSCs are easy to harvest in large quantities from adipose tissue and are therefore often used for tissue engineering purposes[32].

The aim of the current study has been to evaluate the use of luciferase-mediated bioluminescence imaging for longitudinal monitoring of adipose derived mesenchymal stem cells injected in large mammal IVDs, cultured in an *ex vivo* organ culture system. We investigated the feasibility of commonly used luciferases: the intracellular Firefly luciferase (Fluc) and the naturally secreted *Gaussia* luciferase (Gluc) which can be detected in the cell as well as in the extracellular environment [33]. Additionally, possible confounders specific to avascular organ culture were investigated.

MATERIAL AND METHODS

Cell Culture. Mesenchymal stem cells were isolated from subcutaneous adipose tissue, collected from skeletally mature Dutch female milk goats (age 3-5 years). Isolation of the stem cells was performed as described by Zuk *et al*[34]. The research protocol was approved by the Scientific Board and the Animal Ethics Committee of the VU University, and is in accordance with national guidelines and regulations. In brief, between 50 and 100 grams of tissue was harvested subcutaneously from the para-vertebral area. Adipose tissue was minced, washed in phosphate buffered saline (PBS, Life Technologies), and digested using 1 U Liberase TM (Roche) per gram of tissue in PBS for 60 minutes at 37°C under gentle shaking conditions. The digested tissue was filtered through a 100 µm mesh filter to remove residual extracellular matrix and to obtain a single cell suspension. The resulting single cell suspension, containing adipose stem cells, was diluted in Dulbecco's modified Eagle's medium (DMEM, Life technologies) containing 10% Hyclone fetal bovine serum (FBS, Thermo Scientific), Penicillin (10,000 units/ml), streptomycin (10 mg/ml) and amphotericin B (25 µg/ml) (1% PSF; Sigma Aldrich) and plated at 1-4 x 10^6 nucleated cells/cm^2. Twenty-four hours after seeding, culture medium was refreshed and goat adipose derived stem cells (gADSCs) were obtained by expanding the plastic adherent cells. As a positive control, U87 glioblastoma cells were cultured in DMEM complemented with 10% FBS and 1% PSF. All cells were grown in a humidified incubator at 37°C and 5% CO_2. Medium was refreshed twice a week and upon reaching near-confluence cells were detached using 0.25% trypsin / 0.1%

EDTA (Life Technologies) and diluted for further culture. For all experiments involving gADSCs, we used early passage gADSCs (≤ passage 4).

Isolation of intervertebral discs. Spines of skeletally mature 3-to-5-year-old Dutch female milk goats were obtained from a local abattoir. Lumbar IVDs were dissected within 24 hours after sacrifice, as described by Paul *et al*[4]. Briefly, we dissected the intervertebral discs (T13-L1 to L5-L6) including the adjacent cartilaginous endplates under sterile conditions using an oscillating surgical saw. Excess ligaments and posterior elements were removed, and IVDs were cleaned to remove blood, and washed in PBS supplemented with 1% PSF. Using these IVDs, we bypassed the technological, ethical and financial challenges that are involved with laboratory animal experimentation.

Lentivirus production and transduction. The Gluc and Fluc lentivirus vector reporters co-encode the fluorescent genes Cyan Fluorescent Protein (CFP) and mCherry, respectively, as described elsewhere (Fig 1a)[10,35]. To produce lentivirus particles, the lentivirus reporters were co-transfected with a third generation lentiviral packaging plasmid mix (pMDLg/pRRE, pRSV-Rev and pMD2.G, Addgene) in HEK293T cells using Lipofectamine 2000 (Life Technologies), according to manufacturer's guidelines. Lentivirus particles were harvested two and three days after transfection and cell debris was spun down for five minutes at 1000 x G. We plated low passage gADSCs and U87 cells in 25 cm^2 culture flasks and when the cultures reached ~60% confluence we transduced them with the Gluc-CFP or the Fluc-mCherry bioluminescent reporter gene with a multiplicity of infection 10-20. Transfection was achieved by washing the cells with PBS and subsequently adding 3 ml of lentivirus-conditioned medium. After an incubation period of four hours for the gADSCs, or overnight for the U87 cells we removed the lentivirus conditioned medium and washed the cells with PBS. Finally, we added fresh culture medium. We verified transduction efficiency by fluorescence microscopy (Leica) of the co-expressed fluorescent reporters. gADSCs expressing Gluc and CFP are further mentioned as gADSC-GC. gADSCs expressing Fluc and mCherry are referred to as gADSC-FM. For the U87 cells the same terminology is used: U87-GC and U87-FM cells.

In vitro bioluminescent activity measurements of Gluc and Fluc. To measure Fluc activity, we lysed the gADSC-FM with 100 µl Reporter Lysis Buffer (Promega) and three freeze-thaw cycles. Aliquots of 10 µl lysate were mixed with 40 µl of Luciferase Assay Reagent (Promega). Luciferase activity was measured immediately after mixing for two seconds using a tube luminometer (Berthold Technologies) and expressed as Relative Light Units (RLU). For Gluc activity, the Gluc substrate coelenterazine was prepared freshly by diluting the coelenterazine stock (Nanolight, 5 mg/ml in methanol) 1:1000 in PBS + 0.1% Triton X-100, to a final concentration of 5 µg/ml. A total of 10 µl of Gluc conditioned medium was collected from the cell culture of gADSC-GC cells, 40 µl coelentrazine was added and activity was measured as described above. To determine luciferase activity over time, 100, 1000 or 10,000 gADSCs were plated in a 24 wells plate (n=3 per condition) and luciferase activity was measured 1, 4 and 7 days after initial plating.

Ex vivo bioluminescent imaging. A total of 0.5 x 10^6 gADSC-FM, gADSC-GC, U87-FM or U87-GC cells was suspended in 50 µl DMEM. Cells were injected in the nucleus pulposus (NP) via the left lateral side, through the annulus fibrosus of the IVD using a 29G needle of 1 cm length (Fig. 1c). Pilot experiments to image Gluc and Fluc expressing cells in the IVD were performed to determine suitable substrate concentration and imaging conditions. We imaged Fluc activity by injecting 50 µl of 30 mg/ml d-luciferin (Goldbio Technology) dissolved in PBS into the NP prior to each BLI measurement. Gluc activity was measured by injecting 50 µl of 1 mg/ml coelenterazine substrate in PBS + 0.1% Triton X100 prior to each BLI measurement. For both groups, luciferase activity was measured directly after substrate administration using the IVIS CCD camera (Perkin Elmer). Exposure times were 10 minutes for IVDs injected with Fluc reporter cells, and 30 seconds for IVDs injected with Gluc reporter cells. As a negative control we imaged IVDs injected with Fluc or Gluc substrate and as a positive control the high Fluc/Gluc expressing U87 glioma tumor cells are run alongside in parallel experiments for *ex vivo* imaging of cells in IVDs. We analyzed the images with Living Image software (Perkin Elmer) and activity was defined as the sum of all photons/second (p/s) detected within a defined region of interest (ROI).

Repetitive substrate addition to reporter expressing cells. We conducted the following experiments to determine the possible toxic effect of repetitive addition of the luciferase substrates on gADSC (*i.e.* d-luciferin for gADSC-FM and coelenterazine for gADSC-GC). gADSC-FM were seeded at 5000 cells/cm^2 in complete culture medium, and bioluminescence activity was assessed after 1 and 4 days. Fluc substrate, d-luciferin, was diluted in complete pre-warmed (37°C) culture medium (to a concentration of 150, 250, 500 and 1000 µg/ml d-luciferin). The concentrations were selected based on the by Xenogen[36] advised concentration for *in vitro* use of d-luciferin (150 µg/ml) and the amount of d-luciferin we injected in the IVD during the *ex vivo* experiments (1000 µg/ml). Directly before imaging, culture medium was aspirated from the cells, and the d-luciferin-containing medium was added to the cells. Fluc activity was measured by determining photon count using a CCD camera for 30 seconds. Signal intensities were defined as the sum of all photons/second detected within a single well and values were normalized to the total amount of DNA per well. DNA content was quantified using the CyQuant GR (LifeTechnologies) assay according to manufacturer's protocol. Cells were washed with PBS and lysed with 200 µl sterile Milli-Q and a freeze-thaw cycle. For the cells receiving the substrate repetitively, medium containing d-luciferin was not refreshed after imaging at day 1. This way, we mimicked the *ex vivo* situation where d-luciferin is contained in the avascular IVD and is only partially eliminated through diffusion, which is a similar process to the slow nutrient exchange.

To determine the effect of repeated coelenterazine substrate administration on gADSCs, we cultured gADSC-GC at 5000 cells/cm^2 and measured Gluc activity for 4 consecutive days. We added either coelenterazine (1 mg/ml or 5 µg/ml, *i.e. ex vivo* and *in vitro* concentrations), or methanol (equivalent amount to coelenterazine 1

mg/ml), dissolved in complete culture medium. As a negative control we added only complete culture medium to the cells. Similar to the Fluc imaging, culture medium was aspirated from the cells, coelenterazine-containing medium was added and Gluc activity was measured immediately for 30 seconds using CCD imaging. Culture medium containing coelenterazine or methanol was left on the cells after imaging. Gluc activity was normalized for the total DNA amount of the well, similar to the Fluc reporter cells as described above.

Stability of secreted Gluc. Because the highly charged extracellular matrix and avascular nature of the IVD might limit excretion or degradation of secreted Gluc, the stability of Gluc in our *ex vivo* IVD organ was assessed. First, the stability and potential binding of secreted Gluc to the negatively charged proteoglycans of the NP matrix was determined using isolated NP explants that were obtained from goat IVDs. NP explants were isolated by the removal of one IVD endplate and subsequent NP resection. The explants were incubated in either 1 ml PBS or 1 ml PBS containing 0.25 U/ml Chondroitinase ABC (CABC) for 18 hours. CABC is an enzyme that degrades the proteoglycans (an extracellular matrix component of the nucleus), thereby mimicking the early changes in IVD degeneration[37]. After three washing steps of 2 hours in PBS, NP explants were incubated in complete culture medium. Thereafter, we injected NP explants with 50 µl of Gluc-conditioned medium, obtained from 5 x 10^6 U87-GC cells. The initial Gluc activity of the conditioned medium was 6.5 x 10^6 RLU, measured in 50 µl medium. Gluc activity in the NP explants was measured by adding 50 µl coelenterazine substrate (1 mg/ml) at various time points for a period of two weeks. Culture medium of the NP explants was refreshed at the days of imaging.

In order to test the possible confinement of secreted Gluc within the complete IVD (including the annulus fibrosus and endplates), we injected IVDs either with 50 µl of Gluc conditioned medium or 0.5 x 10^6 U87-GC cells. We cultured the discs in the LDCS using the same conditions as described in the section below. Bioluminescence activity was measured at 1, 3, 5 and 7 days post Gluc injection, using the same imaging protocol as described in the section "*ex vivo* bioluminescence imaging". Culture medium of the IVDs was refreshed at the days of imaging.

Imaging of gADSCs and U87 control cells in the IVD over time. We injected 0.5 x 10^6 U87-GC, U87-FM cells, gADSC-GC or gADSC-FM in the IVDs (n=4 for U87, n=8 for gADSC) and assessed BLI at day 1, 3, 5 and 7 after cell injection, as described in the section "*ex vivo* bioluminescence imaging" above. All discs were cultured in individual culture chambers in the LDCS (Fig. 1b) in DMEM supplemented with, 10% FBS, 1% PFS, 3.5 g/L glucose (Merck, final concentration 4.5 g/L), 25 mMol HEPES buffer (Life Technologies) and 50 µg/ml ascorbate-2-phosphate (Sigma Aldrich). Because IVD cell viability depends on loading, a simulated physiological loading (SPL) condition, consisting of a diurnal dynamical loading (1 Hz sinusoidal) regime as described by Paul *et al.* was applied to each IVD[4]. Culture medium of IVDs injected with gADSCs-GC

and U87-GC was collected and secreted Gluc was measured using the luminometer as described in the "*in vitro* bioluminescence imaging" section above.

Histological analysis of IVDs. After the *ex vivo* experiment, we fixed the IVDs in 4% formalin for two weeks and decalcified them in Kristensen's fluid for another two weeks. Midsagittal slices (3-5 mm) were cut from the midline of the IVD using a scalpel, processed for dehydration and embedded in paraffin. With a microtome, 3 micrometer thin sections were cut starting from the midsagittal line, stained with haematoxylin and eosin (H&E) and analyzed using light microscopy.

Statistical analysis. Where applicable, data are presented as mean ± standard deviation for each experiment. Different experimental groups were compared and analyzed by a one-way analysis of variance (ANOVA) using SPSS Statistics software version 22 or Graphpad Prism version 6. A p-value <0.05 was considered statistically significant.

RESULTS

Transduction and characterization of gADSCs

We estimated the lentivirus vector transduction efficiency for both reporters (Fig. 1a) by fluorescence microscopy of CFP or mCherry expression to be ~60% for the gADSCs and ~90% for the U87 cells (Fig. 2a). Expression of the fluorescent proteins in the U87 cells was increased compared to the gADSCs; therefore longer exposure times were needed for a clear visualization of CFP and mCherry in the gADSCs. In different *in vitro* experiments we characterized the expression of Firefly and *Gaussia* luciferase by the transduced gADSCs. Luciferase activity was found to be proportional to the amount of cells (Fig. 2b). In addition, an increase of luciferase activity over time was measured for both gADSC-FM and gADSC-GC (Fig. 2c), indicating cell growth. We confirmed this by counting cells. Fluc half-life is relatively short (about 4 hours[38]) compared to the *in vitro* Gluc half-life (about six days[39]). Since Gluc is also secreted from the cells into the culture medium, it can easily accumulate over time (Fig. 2c). Taken together, this results in a cumulative effect for Gluc and a subsequent steeper slope for Gluc activity compared to Fluc activity.

Microscopic analysis showed no significant effect of the lentivirus transduction on the morphology of the gADSCs. When we expanded the gADSCs for more than four passages, both the transduced and non-transduced cells started to spread out and showed increased stress fiber content. Therefore we decided to use only low passage gADSCs ($P < 4$) , not showing any stress fibers, for all experiments.

Finally, the lentivirus vector transduction did not negatively influence the proliferation rate of the gADSCs over time (Fig. 2d), since the proliferation rate of the gADSC-FM and gADSC-GC showed a similar increase to non-transduced cells (gADSC-ctrl). Comparable results with U87 cells were described earlier[40]. We conclude that lentivirus vector transduction does not alter gADSC morphology or growth properties and we can therefore use both Fluc and Gluc as reporters to monitor gADSC viability and proliferation.

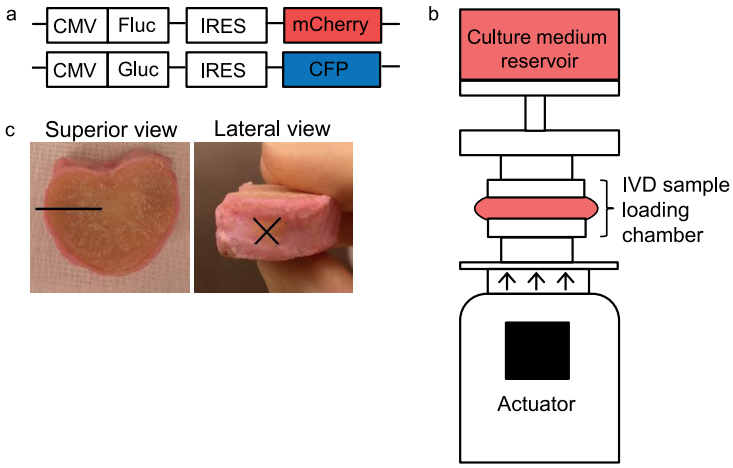

Figure 1. Methods for goat adipose derived stem cell imaging *ex vivo*. **(A)** Schematic depiction of the Firefly luciferase (Fluc) reporter co-expressing mCherry and of the *Gaussia* luciferase reporter co-expressing Cerulean fluorescent protein (CFP). **(B)** Schematic overview of the loaded disc culture system (LDCS) that we use to simulate the normal physiological conditions of the intervertebral disc (IVD). For details see Paul *et al*. 2012[4]. **(C)** Superior and lateral view of the goat IVD. Location of cell injection is depicted by "X" and needle track is shown by the black line.

Imaging U87 and gADSC cells in IVDs

First, we determined if the bioluminescent signal of the cells could be detected by the CCD camera through the IVD endplate. We started by injecting $0.5x10^6$ U87-FM or U87-GC reporter cells in IVDs. U87 cells have a high lentivirus vector transduction efficiency and explicit expression of the reporters. We therefore expected these cells to be easily detectable using BLI. Cell injection was directly followed by injection of the respective substrates and bioluminescent signals of both reporter cell lines could be detected in intact IVDs (Fig. 2e). BLI activity for Fluc and Gluc signals differed greatly, with Fluc activity in the order of 10^7 photons per second (p/s) and Gluc activity in the order of $5x10^9$ p/s.

When we injected $0.5x10^6$ gADSCs, we were also able to detect a bioluminescent signal in the IVDs (Fig. 2e). The activity of gADSCs was comparable to the U87 cells signals, with measured activity in the order of 10^7 p/s for Fluc and $5x10^9$ p/s for Gluc. This experiment demonstrated that it is indeed possible to capture the emitted photons externally after passing through the cartilaginous endplate and small part of the vertebral body (~3.5mm of tissue).

Cell viability and Fluc and Gluc activity after repetitive substrate addition to reporter expressing cells

Because the IVD is avascular, excess substrate and reaction products are not readily eliminated from the IVD. We therefore tested the effect of repetitive addition of the luciferase substrates on gADSCs. For the gADSC-FM no significant differences in

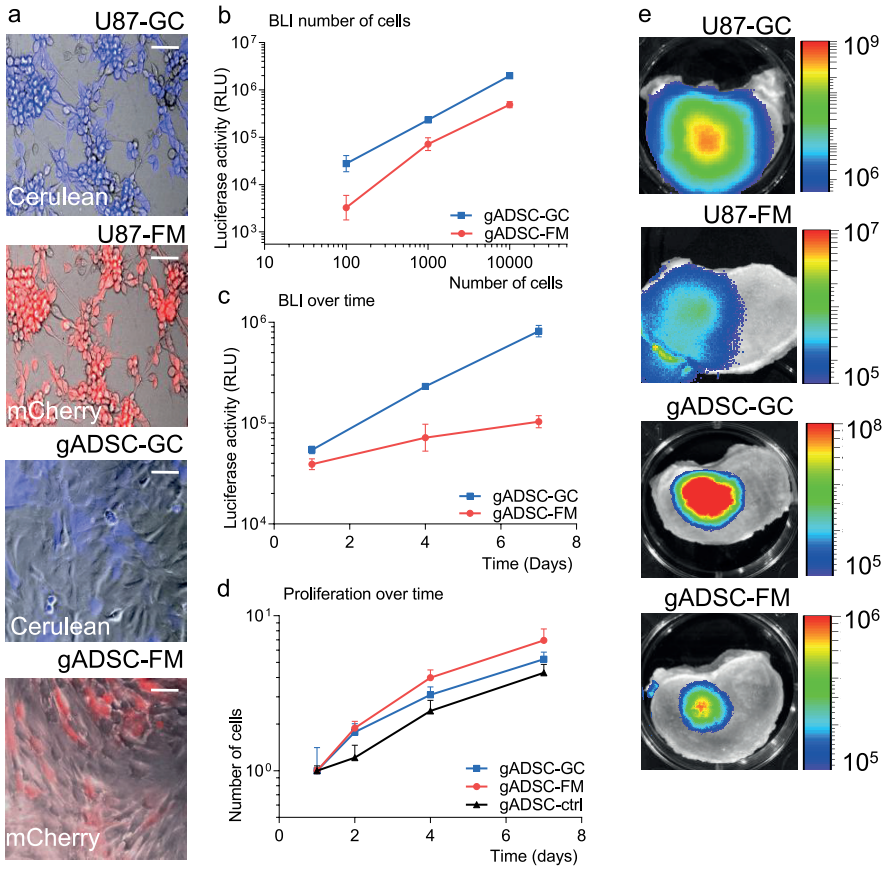

Figure 2. Characterization of goat adipose derived stem cell and U87 reporter cells. **(A)** Fluorescent microscopy overlay images of U87 cells and gADSCs expressing Fluc-mCherry (FM) or Gluc-CFP (GC). Bars represent 100 µm. **(B, C, D)** Fluc reporter and Gluc reporter measurements of gADSC cells *in vitro*. Measurements are in triplicate and error bars represent SD. **(B)** Different amount of cells were plated and one day later, Fluc and Gluc activity was measured. **(C)** Gluc and Fluc activity was measured over the time of seven days. **(D)** gADSC cells were plated and counted over the time of seven days to analyze growth rates. **(E)** Bioluminescence imaging with a CCD camera of an IVD injected with U87-GC, U87-FM, gADSC-GC and gADSC-FM**.** Imaging was performed directly after injection of the reporter cells. Scale bar represent bioluminescence in relative light units (RLU).

amount of DNA for all groups were found both on day one and day four (p=0.166 and p=0.185 respectively), indicating there is no adverse or toxic effect as a result of repetitive addition of the substrate to the cells (data not shown). However, we did observe a decrease in Fluc activity per cell when the gADSC-FM received the substrate repetitively (Fig. 3a). This decrease in activity was also shown to be dependent on the dose substrate cells received previously. Cells that received 500 or 1000 µg/ml substrate on day one showed a significant decrease in Fluc activity on day four (p=0.007, p=0.003, respectively, Fig. 3a). We conclude that, while there is a

decrease in Fluc activity after repetitive substrate addition to the Fluc reporter cells, this decrease in activity cannot be explained by substrate toxicity to the cells.

For the Gluc substrate coelenterazine, we observed a significant decrease in DNA content after repeated addition of the high concentration substrate (1 mg/ml) to gADSC-GC (p=0.001, Fig. 3b). DNA content of the gADSC-GC that repetitively received a low concentration substrate (5 µg/ml) increased over time, although total DNA content was lower compared to the cells that only received a single dose of substrate on day 4. The decrease in DNA content cannot be due to the dissolvent (methanol), since cells receiving an equal amount of methanol but without coelenterazine did not show a decrease in DNA content (Fig. 3b). The total Gluc activity per cell remained constant (data not shown). These results indicate a dose-dependent toxic effect of the Gluc substrate coelenterazine, mainly due to coelenterazine rather than the methanol dissolvent.

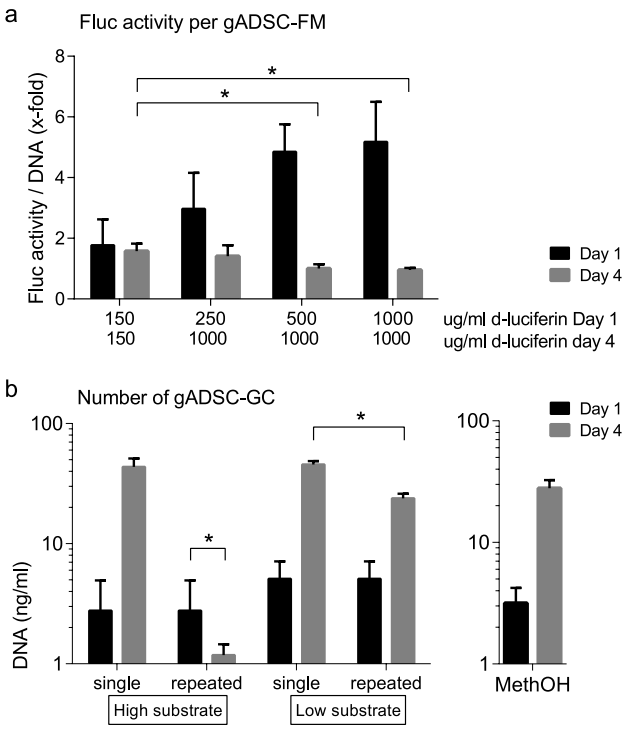

Figure 3. Repeated Fluc and Gluc substrate addition to goat adipose derived stem cell. **(A)** Fluc substrate was repeatedly added to gADSC-FM cells and bioluminescent activity was measured 1 and 4 days after initial plating, with different concentrations of Fluc substrate on day 1 and the same concentration on day 4. Measured activity was normalized for the amount of DNA per well. **(B)** Gluc substrate in two different concentrations (high substrate: coelenterazine 1 mg/ml and low substrate: coelenterazine 5 µg/ml) or methanol was added to gADSC-GC cells. Bioluminescent activity was measured 1 and 4 days after initial plating. DNA contents of all groups were measured. **(A, B)** Experiments were performed in triplicate, data are represented as mean ± SD, * statistically significant different (p<0.05), ** (p<0.01).

Gluc does not bind to the extracellular matrix of the NP and is not confined within the IVD

Because secreted Gluc is not removed by circulation in the avascular IVD and is only eliminated by diffusion, knowledge of its stability in our *ex vivo* IVD organ is necessary to correlate Gluc expression to cell viability. To study potential binding of Gluc to the negatively charged proteoglycans in the NP matrix, we injected medium containing secreted Gluc to NP explants and followed Gluc activity for 15 days. When measuring Gluc activity over time, we could not observe a significant difference between the CABC degenerated NPs and the control NPs (Fig. 4a). During the first three days, there was a trend towards higher Gluc activity in the control NPs over the CABC treated NPs, but this non-significant difference was diminished after day three. Therefore we conclude that the possible binding of Gluc to the negatively charged proteoglycans of the nucleus pulposus forms no significant problem in Gluc imaging in IVDs.

To investigate if secreted Gluc is stable and confined within the intact IVDs, we compared IVDs injected with a single dose of medium containing secreted Gluc with IVDs injected with Gluc secreting U87-GC cells. Near background Gluc activity could be observed in the IVDs injected with Gluc conditioned medium for at least seven days (Fig. 4b, c) whereas in the isolated NP explants, activity could be monitored for barely three days (observed on BLI images, data not shown). The Gluc activity of IVDs injected with U87-GC cells clearly remained higher compared to the IVDs injected with medium containing secreted Gluc for the first seven days post-injection (Fig. 4b, c). Gluc expressing cells in IVDs displayed a detectable and quantifiable dynamic range of Gluc activity while the Gluc activity of conditioned medium remained stable but low over time. This result suggests that changes in Gluc activity can be monitored over time and is not significantly hampered by residual Gluc stability.

Imaging of gADSCs and U87 cells in the IVD over time

For longitudinal monitoring of luciferase expressing cells injected in the IVD, we initially imaged the U87 reporter cells. The U87-GC cells injected in IVDs and cultured in the LDCS showed a strong bioluminescent signal that could be monitored up to the seventh day after cell injection (Fig. 5a). The U87-FM cells injected in the IVD showed a very low (near background) signal that was scattered over the entire disc (Fig. 5a). As with the U87 cells, a strong bioluminescent signal was found for the gADSC-GC whereas the gADSC-FM showed a low background signal (Fig. 5a). The initial signal of the gADSC-GC was lower compared to the U87-GC, however, it was more stable over time (Fig. 5a, b). Gluc could not be detected in the 50 ml culture medium obtained from the individual culture chambers of the LDCS, either for U87-GC cells nor for gADSC-GC injected IVDs. This might be due to the relative large volume of the culture medium compared to the amount of Gluc produced by the luciferase positive cells.

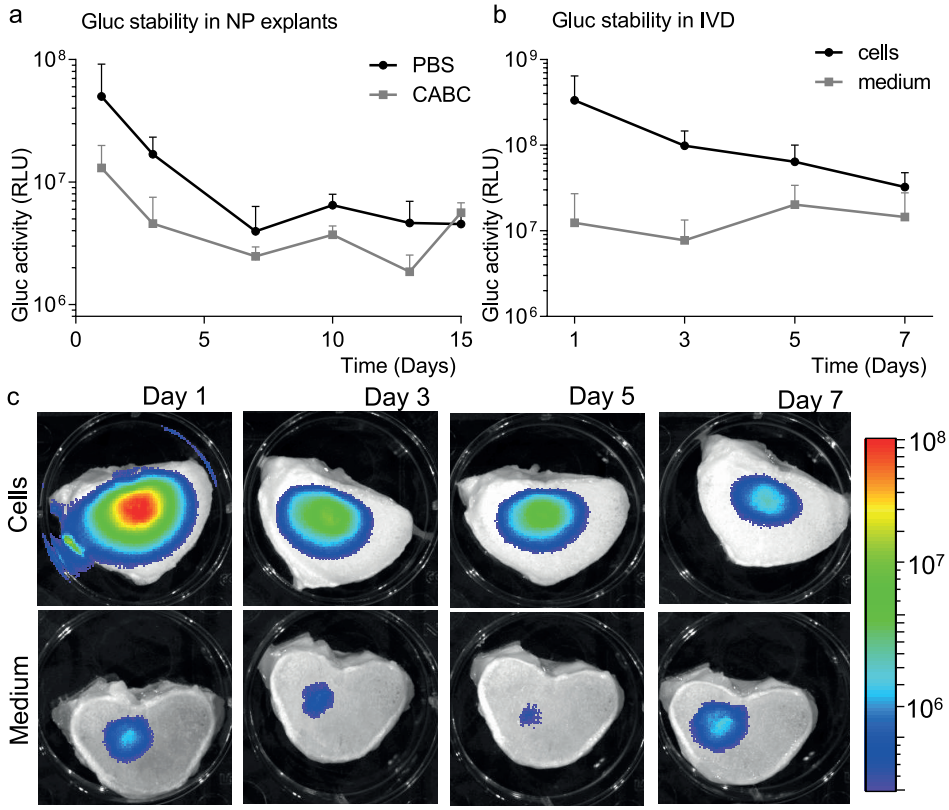

Figure 4. Stability of Gluc in the IVD **(A)** Gluc containing medium was injected and imaged in NP explants with or without pre-treatment with proteoglycan degrading Chondroitinase ABC. **(B)** IVD injection of medium containing secreted Gluc or Gluc expressing U87-GC cells. Gluc activity was determined on specified time points. **(C)** Representative BLI pictures of Gluc activity over time. Scale bars represent bioluminescence (RLU). Experiments were performed in triplicate, data are represented as mean ± SD.

Clusters of cells can be observed in IVDs injected with gADSC-GC, gADSC-FM, U87-GC and U87-FM cells

We processed the IVDs injected with gADSC-GC, gADSC-FM, U87-GC and U87-FM cells for histological viewing after a culture period of seven days and bioluminescent imaging. We could clearly observe a void within the nucleus pulposus of injected IVDs. No such voids were observed in sections of control discs. Therefore, we consider these voids to be due to injections of cells and substrate in the NP. Inside these voids we could clearly identify clusters of cells that were not found in control IVDs (Fig. 5c, d). Moreover, the gADSCs showed a more organized pattern and intact morphology compared to the scattered distribution for U87 cells, suggesting an increased cell loss within the clusters in the U87 cells (Fig. 5c, d). This corresponds to the reduction of BLI signal for the U87-GC cells.

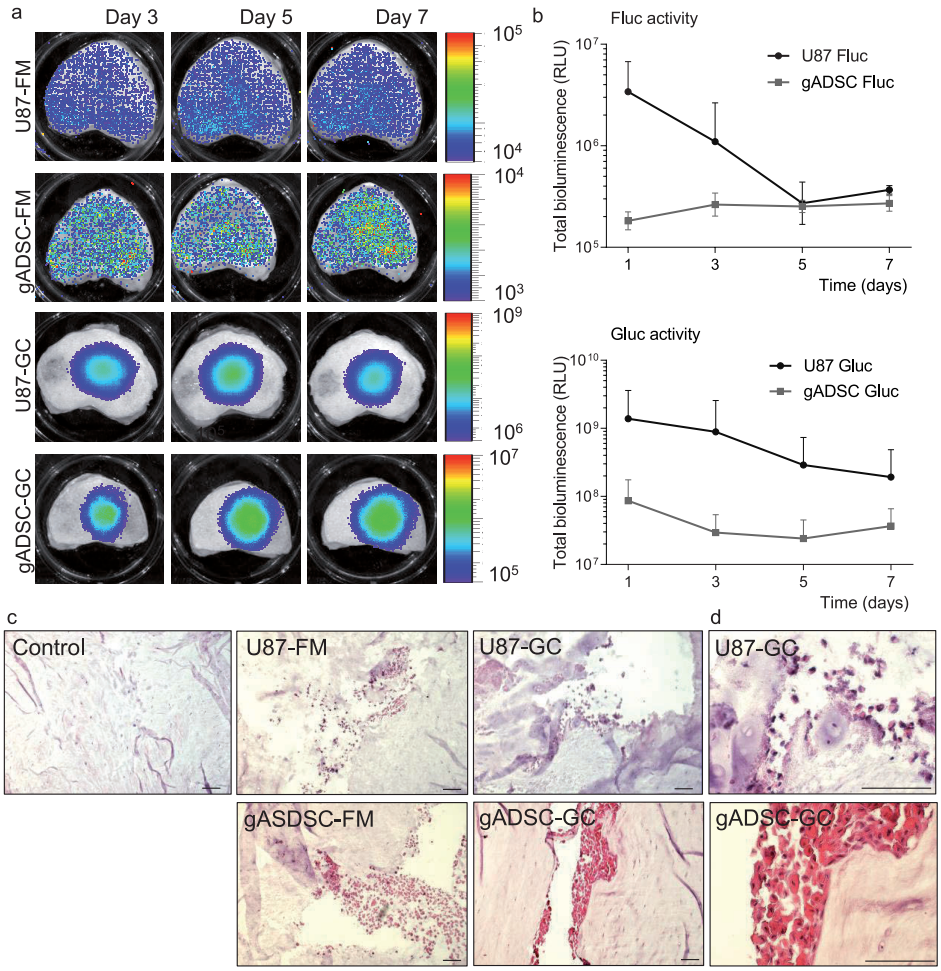

Figure 5. Injection of U87-FM, U87-GC, gADSC-FM and Gluc-GC reporter cells in intervertebral discs *ex vivo*. **(A)** Representative BLI images of luciferase activity of IVDs injected with U87-GC, U87-FM, gADSC-GC or gADSC-FM**.** Imaging was performed 3, 5 and 7 days after injection of the reporter cells. Scale bars represent bioluminescence (RLU). **(B)** Quantification of bioluminescent signals. Data are represented as mean ± SD, n=4 for U87 cells and n=8 for gADSCs. **(C)** Bright field microscopy of H&E staining of IVDs injected with U87-GC, U87-FM, gADSC-GC and gADSC-FM reporter cells. Controls are IVDs without injected cells. Bars represent 100 µm. **(D)** Magnification of selected images from **(C)** showing a more organized pattern and healthy appearance for the gADSCs. Bars represent 100 µm.

DISCUSSION

In this manuscript we aimed to determine the feasibility of using bioluminescent imaging of adipose derived stem cells to monitor and evaluate cell fate and distribution in *ex vivo* culture. In this study the IVD serves as an example of an *ex vivo* organ culture. We evaluated the use of two different luciferases - the intracellular sequestered Firefly luciferase (Fluc)

and the naturally secreted *Gaussia* luciferase (Gluc) - for longitudinal cellular imaging within a single sample. We conclude that the Gluc reporter is more suitable for imaging gADSCs in the IVD, as it shows a stable signal for up to seven days. After at least seven days of culture, histological analysis verified the presence of intact cells inside the IVD.

On the cellular level, we observed a lower bioluminescent signal in gADSCs compared to the U87 cell line. This can be expected since tumor cells have a much higher metabolism and activity compared to gADSCs. Also the higher transduction efficiency of U87 cells compared to gADSCs is reflected in the increased BLI signal.

On the reporter level, we found lower BLI signals for the Fluc than for the Gluc reporter in our *in vitro* assays. This could possibly be explained by the differences in gene sensitivity as the *Gaussia* luciferase produces a 2,000-fold higher bioluminescent signal compared to the Fluc reporter[39]. Moreover, the long half-life of Gluc in culture medium results in a cumulative effect[39] (Fig 2c).

A striking observation was the finding that luciferase activity of Fluc-expressing gADSCs decreased significantly after repeated administration of substrate *in vitro*. This decrease in activity could not be explained by a toxic effect of the substrate on the cells. We can only speculate about the exact mechanism that causes this decrease, although a change in cell membrane permeability for d-luciferin after initial contact could be a possible cause. Another hypothesis is a negative effect due to a possible accumulation of the residual oxyluciferin after the luciferase oxidation reaction. In contrast to Fluc, a dose-dependent toxic effect was observed for the Gluc substrate coelenterazine *in vitro*.

The *in vitro* experiments, nevertheless, appear to be an aggravated simulation of the *ex vivo* IVD culture. Diffusion in the NP upon injection will lower the local substrate concentration over time, enhanced by mechanical loading of the IVD. The limited effect of Gluc substrate toxicity is supported particularly by the healthy appearance of the gADSCs cells in the IVD (Fig. 5c, d). The decreased viable appearance and morphology of the U87 tumor cells, which have a much higher metabolism and anabolic activity compared to gADSCs, may be the result of a "transition shock" after injection in the hostile environment of low nutrition and oxygenation within the IVD. These harsh conditions may also explain the observed lower BLI signals for the Fluc reporter compared to the Gluc reporter *ex vivo* (Fig 5a). Both the Fluc and Gluc reporters need O_2 for substrate conversion, but Fluc is also dependent on ATP and Mg^{2+}, elements likely scarce in the avascular IVD due to the minimal exchange of nutrients and other substances[41,42]. Furthermore, the intracellular localization of Fluc might also impair photon conversion. For *in vitro* assays, cells are usually lysed before Fluc activity is determined, thus interaction of the enzyme with the substrate may be considered optimal, while in the case of intact cells, either *in vitro* or in the IVD, the substrate-Fluc interaction may be hampered. In contrast, when Gluc is synthesized, it is also secreted into the external milieu, and thus likely enhancing substrate conversion and higher BLI signals.

Possible confounders in our study could be the containment of secreted Gluc in the IVD through binding to the extracellular matrix or entrapment within the intact

IVD. We were able to show that Gluc is not efficiently bound in the nucleus pulposus (NP) by the proteoglycans (Fig. 4a). When comparing Gluc expressing cells with Gluc conditioned medium, an increase in BLI signal is observed for the U87-GC cells injected in the IVD (Fig 4b). Although a direct comparison between Gluc expressing cells and Gluc conditioned medium is difficult, a stable Gluc production by the injected cells is indicated by two results: First, only intracellular Gluc could be present in the cells at the moment of injection, while a clear and high BLI signal could be observed after one day in situ, indicating Gluc production by the cells. Secondly, even though the injected Gluc expressing cells represent a relatively larger volume of cells compared to injected amount of Gluc conditioned medium this could not explain the whole 150-fold increase in BLI signal. While the BLI signal of the injected Gluc-conditioned medium remains essentially unchanged and low over time (Fig. 4d), the BLI signal of the Gluc expressing cells decreases. This decrease indicates that dynamic Gluc activity can readily be detected in the IVD and can be the result of a reduction in cell viability. Reduction of BLI signal is predominantly observed in U87 cells, gADSCs showed a far more stable albeit lower Gluc signal (Fig. 5b). This is in line with the decreased cell quality observed in the histological evaluations (Fig 5c, d). Together, these data indicate that that gADSCs are more able to cope with the hostile IVD environment, and that Gluc can be used as a reporter for stem cell imaging in large animal IVDs.

Although the described method in the current study shows great potential and many alternative applications, some limitations have to be considered concerning the current set-up of this system. The adipose derived stem cells receive the luciferase reporters via transduction by a lentivirus vector. The use of lentivirus vector is an unspecific approach with viral integration in multiple genomic loci and could therefore result in unpredictable genetic modifications and subsequent off-target genetic aberrations and phenotypes of the host cells. However, in multiple lentivirus vector transductions we did not find any signs of differences in cell viability, proliferative capacity or differences in experimental outcomes, implying that this undesired genetic modification is unlikely to occur. Nevertheless, only a complete genomic analysis will provide certainty. Also, the loaded disc culture system is a model system for the intervertebral disc, and although demonstrated to maintain the IVD native properties for over three weeks, it is limited in experimental duration and immune competency compared to the *in vivo* situation. The complexity of the assembly of the loaded disc culture system entails the risk of bacterial contamination after consecutive measurements. Despite these limitations we suggest that the use of an *ex vivo* organ culture allows longitudinal non-invasive real-time monitoring of (stem) cells in organs and complex tissues located in the deeper areas of the body.

Two previous studies reported on the use of bioluminescence imaging for cellular therapies for the intervertebral disc. Omlor *et al*.[43] used Fluc to monitor cellular activity of autologous mesenchymal stem cells injected in the porcine IVD. Three days after cell injection, Fluc activity was measured by pulverizing the NP and subsequent lysis of the

cells. Fluc activity was largely reduced, as shown similarly in the current study. In contrast to our study, lysis of the cells in the study of *Omlor et al*. did not allow further monitoring of cell activity within a single sample. Francisco *et al*.[17] transduced porcine NP cells with Fluc. These labeled porcine cells were injected in rat IVD explants and Fluc activity was monitored for 14 days. After *in vivo* injection of Fluc expressing porcine cells in the rat IVD, BLI signal was only assessed after 15 hours, without longitudinal follow-up. Not only is a different cell type used (NP cells versus gADSCs in the present study), but the rat IVD used in the study by Francisco *et al.* is also not comparable to the human IVD. The small size of the rat IVD favors nutrient diffusion and BLI signal detection. Furthermore, murine IVDs have different biomechanical properties and also retain their notochordal cells in adult life[44]. These cells are considered stem cell-like NP precursor cells and could therefore create a more suitable microenvironment for the injected reporter cells. Thus, although *ex vivo* BLI imaging in the IVD is not new, the current study is the first to show longitudinal monitoring of gADSCs in large animal IVDs.

The application of *ex vivo* imaging of cells, in particular ADSCs and tumor cells, is of interest for the all organ culture models, as it gives insight in the physiology, pathophysiology and therapeutic response. However, the demonstrated cell imaging in intervertebral discs can be interpreted as a worst-case scenario compared to other tissues because of the a-vascularity and subsequent physiological scarcity of nutrients. Therefore, extrapolation of feasibility to highly vascularized organs such as bowel wall, prostate and liver seems highly plausible. However, use of BLI *ex vivo* is influenced by containment of luciferase and toxicity of substrate that should be investigated and considered for every specific tissue.

CONCLUSION

In this manuscript we propose live stem cell bioluminescent imaging as a promising tool for the understanding of cellular behavior of large animal organs, studied in 3D organ cultures. We were able to image luciferase-expressing U87 glioma cells and primary gADSCs transplanted in an *ex vivo* organ culture *i.e.* the goat IVD. The Gluc expressing gADSCs show a stable BLI signal over time after injection in the IVD. Furthermore, we investigated a range of possible confounders that could interfere with the bioluminescent imaging of gADSCs in IVDs. Table 1 gives a comprehensive overview of the advantages and disadvantages of Gluc and Fluc bioluminescent reporters. We aim to use this imaging method for longitudinal investigation of the fate and behavior of gADSCs in the IVD, in order to gain a better understanding of their behavior in, and interactions with the native cells and matrix in the IVD and ultimately optimize their regenerative capacities. Also, using this setup one is able to circumvent the technological, ethical and financial challenges that are involved with life animal experimentation and imaging.

Table 1. Overview of the advantages and disadvantages of Firefly and Gaussia luciferase

Advantages	Disadvantages
Gaussia luciferase	
Luciferase oxidation reaction does not require ATP or Mg^{2+}	Luciferase oxidation reaction requires O_2
Requires short photon measure time	Long stability of secreted Gluc *in vitro*
Photons emitted have a shorter wavelength = more energy and longer penetration depth	Coelenterazine substrate toxicity
Advantages	**Disadvantages**
Firefly luciferase	
Contained within the cells	Substrate needs to enter the cells
d-luciferin substrate not toxic	Luciferase oxidation reaction requires O_2, ATP and Mg^{2+}
Short half-life	Requires long photon measure time
	Photons emitted have a larger wavelength = less energy and penetration depth

ACKNOWLEDGEMENTS

We like to thank Willem de Jong for preparation and processing of tissue sections, Klaas Walter Meyer and Paul Sinnige for assistance in the preparation of the experiments and Alan Brind for proofreading the manuscript. Funding for this study was provided by the European Commission (FP7 project ''NPmimetic''; Grant number #246351) (MP), CCA/VICI Fellowships (SvR) and NWO-VIDI grants (TW).

AUTHOR CONTRIBUTIONS

TW, CPLP and MH conceived this study and MP, SVR, and PPAV designed the experimental setup, with help of TW and MH. MP, SVR and PPAV performed the experiments. MP and SVR wrote the manuscript, which was edited and reviewed by all the authors (MP, SVR, PPAV, CPLP, DPN, WPT, TW and MNH).

DISCLOSURE OF POTENTIAL CONFLICTS OF INTEREST

None of the authors have any conflict of interest to declare relating to the content of this work.

REFERENCES

1 Lancaster, M. a. & Knoblich, J. a. Organogenesis in a dish: Modeling development and disease using organoid technologies. *Science (80-.).* **345,** 1247125–9 (2014).

2 Sato, T. & Clevers, H. Growing self-organizing mini-guts from a single intestinal stem cell: mechanism and applications. *Science* **340,** 1190–1194 (2013).

3 Shih, H. P. & Sander, M. in *Stem cells tissue repair* 229–223 (2010).

4 Paul, C. P. L. *et al.* Simulated-physiological loading conditions preserve biological and mechanical properties of caprine lumbar intervertebral discs in ex vivo culture. *PLoS One* **7,** e33147 (2012).

5 Wilson, S. S., Tocchi, A., Holly, M. K., Parks, W. C. & Smith, J. G. A small intestinal organoid model of non-invasive enteric pathogen-epithelial cell interactions. *Mucosal Immunol.* **8,** 352–361 (2014).

6 Steinstraesser, L. *et al.* A human full-skin culture system for interventional studies. *Eplasty* **9,** 27–40 (2009).

7 Gao, D. *et al.* Organoid Cultures Derived from Patients with Advanced Prostate Cancer. *Cell* **159,** 176–187 (2014).

8 Aguilar, E. *et al.* In Vivo Bioluminescence Imaging of Cell Differentiation in Biomaterials A Platform for Scaffold Development. *Tissue Eng. Part A* **19,** 593–603 (2013).

9 De Boer, J., van Blitterswijk, C. & Löwik, C. Bioluminescent imaging: emerging technology for non-invasive imaging of bone tissue engineering. *Biomaterials* **27,** 1851–1858 (2006).

10 Wurdinger, T. *et al.* A secreted luciferase for ex vivo monitoring of in vivo processes. *Nat. Methods* **5,** 171–173 (2009).

11 Tannous, B. a, Kim, D.-E., Fernandez, J. L., Weissleder, R. & Breakefield, X. O. Codon-optimized Gaussia luciferase cDNA for mammalian gene expression in culture and in vivo. *Mol. Ther.* **11,** 435–43 (2005).

12 Nam, S. Y., Ricles, L. M., Suggs, L. J. & Emelianov, S. Y. Imaging Strategies for Tissue Engineering Applications. *Tissue Eng. part B* **21,** 88–102 (2015).

13 Geuze, R. E. *et al.* Luciferase Labeling for Multipotent Stromal Cell Tracking in Spinal Fusion Versus Ectopic Bone. *Tissue Eng. Part A* **16,** 3343–3351 (2010).

14 Preda, M. B. *et al.* Remote transplantation of mesenchymal stem cells protects the heart against ischemia-reperfusion injury. *Stem Cells* **32,** 2123–34 (2014).

15 Di Rocco, G. *et al.* Analysis of biodistribution and engraftment into the liver of genetically modified mesenchymal stromal cells derived from adipose tissue. *Cell Transplant.* **21,** 1997–2008 (2012).

16 Leo, B. M., Li, X., Balian, G. & Anderson, D. G. In vivo bioluminescent imaging of virus-mediated gene transfer and transduced cell transplantation in the intervertebral disc. *Spine (Phila. Pa. 1976).* **29,** 838–844 (2004).

17 Francisco, A. T. *et al.* Injectable Laminin-Functionalized Hydrogel for Nucleus Pulposus Regeneration. *Biomaterials* **34,** 7381–7388 (2013).

18 Alini, M. *et al.* Are animal models useful for studying human disc disorders/ degeneration? *Eur. spine J.* **17,** 2–19 (2008).

19 Paul, C. P. L. *et al.* Dynamic and static overloading induce early degenerative processes in caprine lumbar intervertebral discs. *PLoS One* **8,** e62411 (2013).

20 Luoma, K. *et al.* Low back pain in relation to lumbar disc degeneration. *Spine (Phila. Pa. 1976).* **25,** 487–492 (2000).

21 Cheung, K. M. C. *et al.* Prevalence and pattern of lumbar magnetic resonance imaging changes in a population study of one thousand forty-three individuals. *Spine (Phila. Pa. 1976).* **34,** 934–940 (2009).

22 Smit, T. H. The use of a quadruped as an in vivo model for the study of the spine - biomechanical considerations. *Eur. Spine J.* **11,** 137–144 (2002).

23 Vergroesen, P.-P. a. *et al.* A Biodegradable Glue For Annulus Closure. *Spine (Phila. Pa. 1976).* **40,** 622–628 (2015).

24 Kopesky, P., Lee, H. & Vanderploeg, E. Adult equine bone marrow stromal cells produce a cartilage-like ECM mechanically superior to animal-matched adult chondrocytes. *Matrix Biol.* **29,** 427–438 (2010).

25 Lee, H., Kopesky, P. & Plaas, A. Adult bone marrow stromal cell-based tissue-engineered aggrecan exhibits ultrastructure and nanomechanical properties superior to native cartilage. *Osteoarthr. Cartil.* **18,** 1477–1486 (2010).

26 Prins, H., Fernandes, H., Rozemuller, H., Blitterswijk, C. Van & Boer, J. De. Spatial distribution and survival of human and goat mesenchymal stromal cells on hydroxyapatite and b-tricalcium phosphate. *J. Tissue Eng. Regen. Med.* (2012). doi:10.1002/term

27 Roncali, E. *et al*. New device for real-time bioluminescence imaging in moving rodents. *J. Biomed. Opt.* **13,** 054035 (2008).

28 Bagó, J. R. *et al*. In vivo bioluminescence imaging of cell differentiation in biomaterials: a platform for scaffold development. *Tissue Eng. Part A* **19,** 593–603 (2013).

29 Chen, W.-H. *et al.* Intervertebral disc regeneration in an ex vivo culture system using mesenchymal stem cells and platelet-rich plasma. *Biomaterials* **30,** 5523–5533 (2009).

30 Yang, X. & Li, X. Nucleus pulposus tissue engineering: a brief review. *Eur. spine J.* **18,** 1564–1572 (2009).

31 Sakai, D. *et al.* Differentiation of mesenchymal stem cells transplanted to a rabbit degenerative disc model: potential and limitations for stem cell therapy in disc regeneration. *Spine (Phila. Pa. 1976).* **30,** 2379–2387 (2005).

32 Helder, M. N., Knippenberg, M., Klein-Nulend, J. & Wuisman, P. I. J. M. Stem cells from adipose tissue allow challenging new concepts for regenerative medicine. *Tissue Eng.* **13,** 1799–1808 (2007).

33 Badr, C. E. & Tannous, B. a. Bioluminescence imaging: progress and applications. *Trends Biotechnol.* **29,** 624–633 (2011).

34 Zuk, P. A. *et al.* Human Adipose Tissue Is a Source of Multipotent Stem Cells? *Mol. Biol. Cell* **13,** 4279–4295 (2002).

35 Dull, T. *et al.* A third-generation lentivirus vector with a conditional packaging system. *J. Virol.* **72,** 8463–8471 (1998).

36 Xenogen. Reconstitution and use of D-Luciferin Firefly Potassium Salt (cat # XR-1001) Preparation of Luciferin for In Vitro Bioluminescent Assays Preparation of Luciferin for In Vivo Bioluminescent Assays. *Protoc. XP-1a1* 1001

37 Hoogendoorn, R. J. W., Wuisman, P. I., Smit, T. H., Everts, V. E. & Helder, M. N. Experimental intervertebral disc degeneration induced by chondroitinase ABC in the goat. *Spine (Phila. Pa. 1976).* **32,** 1816–1825 (2007).

38 Auld, D. S., Thorne, N., Maguire, W. F. & Inglese, J. Mechanism of PTC124 activity in cell-based luciferase assays of nonsense codon suppression. *Proc. Natl. Acad. Sci. U. S. A.* **106,** 3585–3590 (2009).

39 Tannous, B. Gaussia luciferase reporter assay for monitoring of biological processes in culture and in vivo. *Nat. Protoc.* **4,** 582–591 (2009).

40 Van Rijn, S. *et al.* Functional multiplex reporter assay using tagged Gaussia luciferase. *Sci. Rep.* **3,** 1046–1 – 1046–5 (2013).

41 Urban, J. P. G., Smith, S. & Fairbank, J. C. T. Nutrition of the intervertebral disc. *Spine (Phila. Pa. 1976).* **29,** 2700–2709 (2004).

42 Wuertz, K., Godburn, K., Neidlinger-Wilke, C., Urban, J. & Iatridis, J. Behavior of Mesenchymal Stem Cells in the Chemical Microenvironment of the Intervertebral Disc. *Spine (Phila. Pa. 1976).* **33,** 1843–1849 (2008).

43 Omlor, G. W. *et al.* Methods to monitor distribution and metabolic activity of mesenchymal stem cells following in vivo injection into nucleotomized porcine intervertebral discs. *Eur. Spine J.* **19,** 601–12 (2010).

44 Hoogendoorn, R. J. W., Helder, M. N., Smit, T. H. & Wuisman, P. I. J. M. Notochordal Cells in Mature Caprine Intervertebral Discs. *Eur. Cells Mater.* **10 Suppl.,** 59 (2005).

7 DISCUSSION

In this thesis we aimed to develop and apply functional bioluminescent reporter systems in order to study complex pathologies and therapeutic modalities of the nervous system. Patients harboring brain tumors suffer not only on a physiological level but also on a cognitive level, and this poses a tremendous burden on not only their own well-being, but also on that of their relatives. Brain tumors are thought to arise from aberrant neural stem cells and while stem cells can be the origin of pathologies, they can also play a role in regaining health. Spinal pathologies, such as disc herniation and chronic lower back pain, occur frequently and affect many people, with a high economic and social impact as a consequence. More insight into the molecular mechanisms of these diseases could provide us with novel treatment opportunities, while a better understanding of current and emerging therapeutic strategies could improve the clinical outcome of these patients, reducing the burden of both patients and society.

Brain tumors

Brain tumors are complex diseases requiring complex therapeutic options, which are often still limited. With almost 1,000 new glioma patients (of which 60% is a WHO grade IV glioblastoma multiforme) in The Netherlands every year, it forms the most prevalent brain tumor in adults. The current treatment of surgical resection, irradiation and temozolomide chemotherapy results in a modest survival benefit of 18 months (*1*). GBMs are derived from cells with astrocytic origin and may have risen from, or give rise to, neural stem cells (*3*, *4*). Despite their reciprocal origin and features, recent studies have shown the existence of four subtypes of GBM (classical, mesenchymal, pro-neural and neural) with variable genetic background (*5*). In addition, all four subtypes have been shown to be present within a single tumor (*6*).

While GBMs mostly arise in adults, medulloblastoma is the most common brain tumor in children, with about 50-60 new cases per year in The Netherlands (IKNL, 0-14 years, www.cijfersoverkanker.nl). While 70-80% survive for more than five years, all treatment options carry an inherent risk for neurological deficits and cognitive impairment in a majority of patients (*2*). In medulloblastoma, also four subgroups (Wnt, Shh, group 3 and 4) can be distinguished and these correlate with differential outcome of patients (*7*). This makes the genetic profile of brain tumors significantly complex, whereas the therapeutic strategy of brain tumors is more or less equal for all subtypes. Current therapeutic strategies for brain tumors are therefore, quite insufficient and thus eligible for extensive research.

The complexity and sensitivity of the brain makes treatment of brain tumors a formidable challenge. On one side, surgery and irradiation may result in brain damage, which has large implications for the patients' functioning. A conservative approach on the other hand, with limited surgical resection and irradiation, may lead to residual disease and rapid recurrent tumor growth. Chemotherapy, and other therapeutic approaches, are usually very limited since most compounds fail to cross the blood-brain-barrier (BBB) (*8*). To improve, and especially personalize, brain tumor treatment, novel and targeted therapeutic approaches are required. In order to be able to obtain the most advantage of

these targeted treatment modalities, a functional molecular profile of individual tumors is needed to complement the current histological and radiological imaging approaches (*9*).

Low back pain and tissue regeneration

While low back pain in itself is not life-threatening, it poses a major social and economic burden in developed countries (*10*). In The Netherlands, prevalence is around 58-84%, meaning that many people suffer from low back pain resulting in work and social disability. When chronic low back pain is caused by intervertebral disc (IVD) degeneration, and conservative therapies and standard surgical approaches fail, it might be beneficial to induce disc regeneration by implantation of mesenchymal stem cells (*11*). The use of adipose tissue-derived mesenchymal stem cells may provide a good choice, since these cells are easy to obtain. This is in contrast with bone marrow-derived mesenchymal stem cells, which are also often studied for their regenerative capacities (*12*, *13*). Currently, preclinical models of intervertebral disc degeneration and regeneration are insufficient. Most studies use rodent models, which differ significantly in physiology and IVD cellular content compared to human IVDs (*14*). Also, these models require live animals to inflict IVD degeneration and to inject stem cells for tissue regeneration studies (*15*)(*13*). For our research we set up an *ex vivo* IVD culture system based on caprine IVDs, since they show the best resemblance to human discs when comparing size, vascularization and chondrocyte content (*16*). These surplus IVDs were derived from consumption goats and therefore, did not require experimental animals, greatly reducing economical as well as ethical impact.

Functional molecular imaging

To study brain tumor biology and stem cell tissue regeneration biology, molecular imaging tools can provide more functional and molecular insight. A multiplex approach for functional molecular imaging might make large-scale functional screening strategies available to the scientific community, greatly boosting functional biology output. Bioluminescent imaging using luciferases has several advantages over alternative imaging, such as a high signal-to-background ratio, deeper tissue penetration and low cost reagents and equipment. Despite earlier efforts to combine multiple luciferases in a multiplex assay (*17*), a real multiplex approach was not yet available and in this light our work filled in a gap in the toolbox. Gaussia luciferase (Gluc) is naturally secreted from cells and this makes *ex vivo* detection possible. Secretion of the reporter makes it available outside of the cell and we used this property to fuse Gluc with an epitope tag to be able to use tag-specific antibodies to specifically isolate Gluc-tag. The epitope tag is a viral, or bacterial, peptide and the sequence of epitope tags is virtually infinite. This allowed us to construct a virtually infinite number of Gluc-tag reporters, allowing large-scale screening and quantification of functional bioluminescent reporters. The multiplex functional reporter assay heavily depends on tag-antibody binding efficiency. Every tag requires an appropriate antibody with high affinity for the tag in order to be

able to effectively bind Gluc-tag from animal blood or cell culture medium. Currently, the amount of efficient tag-antibody binding is still fairly limited, reducing the large-scale capacities of our assay, but optimization and tag-antibody affinity might overcome this issue. Another drawback of this assay is the need to genetically modify cells in order to make them express the desired reporters, which requires lentiviral, or retroviral, transduction of cells with possibly undesired genetic aberrations as a consequence. The genetic hazards of current gene editing techniques make it inappropriate for clinical imaging in patients, and the benefits still remain in the preclinical research setting. Recent developments in gene editing methods such as CRISPR-Cas9 (*18*) might prove to be much more specific, with reduced off-target effects, paving the way for gene editing in patients. Despite these emerging technologies, large-scale functional screening in patients is still far away since introduction of a large amount of reporters in cells requires major gene editing in patients' cells.

Stem cells and tumor heterogeneity

We developed the Gluc-tag assay as a quantitative method to study tumor heterogeneity or cellular interactions. The Gluc-tag assay makes it possible to equip different cells with a cell-specific functional bioluminescent reporter. In complex tissues or heterogeneous tumors, different cells have different origins, or have a variety of genetic modifications. The Gluc-tag assay allows us to study gene functions, or to study other cellular modifications such as exposure to compounds, irradiation and environmental challenges. Other applications would be to study cancer and healthy cell interactions, or to study stem cells in complex, mixed tissues and follow their fate and differentiation. Since stem cell progeny differentiate and change cellular shape, it could be beneficial to identify progeny cells in complex mixtures of cells. When the different cells are mixed in culture, it would be possible to determine the functional read-out of every cell in the cell culture mixture. In this way it might be possible to determine specific cell viability, gene promoter activity or any other functional bioluminescent application. Currently, fluorescence is often used to study different cells in co-culture, but the method is limited due to overlap of emission spectra and it also requires complex optics and detection equipment (*19*, *20*). The benefit of functional fluorescent reporters is the ability to actually identify the different cells under a fluorescent microscope, whereas functional multiplex bioluminescence is based on enzyme activity and light production. While different luciferases can produce light of different wavelengths, it requires sophisticated equipment to separate multiple light wavelengths. By using epitope tags, fused to luciferases enzyme, and tag antibody immunobinding assays there is a potentially large amount of reporters and no need for special equipment. Cell identification and spatial resolution can be performed by immunohistochemical staining for epitope tags of tissues. In live cell functional molecular imaging, a trade-off has to be made between the large amount of multiplex bioluminescent reporters without spatial resolution or a limited amount of fluorescent reporters with spatial resolution.

In silico gene expression analysis of tumor suppressors

Currently, the online depository of gene expression data is rapidly increasing, making large amounts of data of various origins available to the scientific community. While this enables scientists to compare their own tumor data with data from others, or with data from other tumors, it is often challenging to compare data between gene expression experiments since all experiments are essentially comparable but in details very different. This interexperimental variation might result in false positive or false negative hits. DNA/RNA sequencing or other gene expression methods should be primarily used for screening purposes and hits should be validated in more detail to provide detailed information about gene expression and function. In our effort to determine driving tumor suppressors in medulloblastoma and glioblastoma we analyzed gene expression data to identify down-regulated putative tumor suppressor genes. We identified putative tumor suppressor genes using the publicly available Amigo gene ontology database (*21*) and decided that putative tumor suppressor genes are genes that have been associated with tumor suppression in the literature. Unfortunately, the current database does not support the GO term "tumor suppressor" anymore since it considers this term no longer a normal cell feature but more a pathological phenomenon and refers to regulation of cell cycle as an alternative. While this choice makes sense, it makes it hard to update our current list of tumor suppressors. The database Genecards (*22*) provides a search function that allows a search for tumor suppressor in the genes function, or in the publications, but we recommend verification of putative tumor suppressor hits with the database and literature for confirmation.

Tumor suppressors in the RAS pathway

The RAS oncogene is considered to be one of the most powerful cancer drivers (*23*) and is often affected in many types of tumor (*24*)(*25*). While the RAS gene can be mutated itself, the RAS pathway may also be affected by aberrations in RAS-interacting genes and thereby, enhance tumor growth and apoptosis evasion. In malignant brain tumors, mutations in the RAS gene are not frequently observed although the RAS pathway is activated in 88% of GBMs (*26*). Frequently inactivated genes in GBM are the RAS-inactivating NF1 and the PI(3)K-inactivating PTEN, resulting in activation of the RAS-pathway. In this light, it is not very surprising that we identified RAS-interacting genes to be involved in brain tumors. RAS GTPases are a class of proteins that inactivate RAS and loss of these genes may have substantial effects on tumor progression. The loss of DAB2IP-activity has been associated with the activity of EZH2, a methylation enhancer that is also associated with other cancer-related genes. EZH2 can methylate genes, in order to decrease their expression, and therefore, it is considered a promising target in cancer treatment (*27*). While targeting EZH2 opens treatment possibilities, reactivation of DAB2IP is less likely to be achieved but we did show that it has prognostic value in medulloblastoma patients.

RASAL1 is a GTPase that we associated with GBM oncogenesis. The gene is significantly down-regulated in GBM and it caught our interest since it is the second RAS

GTPase that popped up in our research, underlining the importance of RAS GTPases and the RAS-pathway in brain cancers. Moreover, RASAL1 has also been associated with other tumors (*28*, *29*). The expression of RASAL1 is, as with DAB2IP, also found to be epigenetically silenced (*30*) but a relation with EZH2 has yet to be determined. When knocked down, the gene might have a role in GBM formation from neural stem cells. We tested this using mouse neural precursor cells injected into mouse brains. While our results cannot be extrapolated to human cells in the human brain, it still poses a significant indication for human oncogenesis. Past research attempted to interfere with the RAS oncogene itself but since RAS is not easily susceptible to small molecule inhibitors, it has not led to any significant treatment modalities that improve patient outcome. While the interest in RAS-interference has diminished after these disappointing results, recent advances and improvements in drug design methods and interaction analysis methods has led to a RAS renaissance (*23*). While RAS has gained interest as a drugable target again, it remains a huge challenge and therefore, there might be opportunities in interfering with RAS-interacting genes and other genes involved in the RAS-pathway. This approach could open up RAS-associated treatment modalities.

Future directions

The functional multiplex bioluminescence assay we described in chapters two and three was a proof-of-principle to determine the feasibility of multiplexing Gluc reporters fused to epitope tags. In our study we initially created 14 Gluc-tag reporters, but we had to discard four Gluc-tag reporters after *in vitro* validation of the Gluc-tag immunobinding assay since we were not able to obtain tag-specific antibodies that efficiently bind these reporters. Of the 10 remaining reporters, we were able to detect only six Gluc-tag reporters efficiently after immunobinding experiments *in vitro*, as well as *in vivo*. Future optimization and development of the assay could increase the number of tag-antibody combinations. This can be done by assay optimization, antibody development or tag development.

Another limiting factor of the multiplex bioluminescence approach is the current need for a relatively large volume of cell culture medium, or animal liquid such as blood, to use in the immunobinding assay. Currently, the assay is developed at 96-well format, requiring at least 30 microliter of sample per immunobinding assay. In order to improve multiplex capacities of the assay, it is necessary to downscale the immunobinding assay to antibody chip array format on glass slides, or within a small chamber. This might be done by development of array printing to print tag-specific antibodies on a chip (*31*) and to perform the immunobinding assay on this printed chip. The use of antibody arrays requires considerably less samples for a significantly larger amount of reporters, greatly improving multiplex capacities of the assay.

Another application for the Gluc-tag assay would be the development of a Gluc-tag-based recombination-induced tag exchange (RITE) (*32*). This would allow the conditional expression of a gene of interest in target reporter cells, in combination with expression of a recombinase gene. Using a recombinase-expressing lentiviral vector, we would be able

to activate a gene of interest and combine this event with the exchange of the epitope tag fused to the Gluc-reporter. This would allow for temporal bioluminescent imaging of cells that successfully express the gene of interest, since these cells would obtain a different Gluc-tag than the original cell line. This approach could enhance tissue- and tumor heterogeneity studies by providing multiculture bioluminescent imaging.

In chapter four we conducted a meta-analysis of medulloblastoma and glioblastoma gene expression using publicly available, online gene expression databases. We identified DAB2IP as a RAS GTPase tumor suppressor gene that is repressed in medulloblastoma and thereby inhibits apoptosis of cancer cells. Also, we found that DAB2IP-expression is repressed epigenetically by EZH2-trimethylation (*33*). While we were able to use DAB2IP-expression as a diagnostic marker for medulloblastoma survival, it might be more challenging to regain DAB2IP-activity in cancer cells in order to normalize them. Gene therapy is an option for DAB2IP-normalization, however, this approach is currently considered too risky. A therapeutic approach where EZH2 is inhibited to prevent DAB2IP down-regulation might prove to be more realistic. Efforts to silence EZH2 are ongoing since this gene is more frequently associated with other tumors. EZH2 activity can be silenced by miRNAs (*34*) or drug compounds (*35*)(*27*). It would be interesting to specifically study EZH2- and DAB2IP-modulation in medulloblastoma by compound screen, and also to develop a special bioluminescent EZH2-methylation reporter, since read-out is cheap and easy to perform. Another option would be to develop a DAB2IP-promoter activity reporter to study EZH2- and DAB2IP-activity.

In chapter five we identified 23 significantly down-regulated genes as putative tumor suppressors in GBM. When we decreased the expression of five of the most significantly down-regulated genes in mouse neural stem cells, and injected cell mixtures into the mouse brain, we detected cell growth in two mice. We used the Gluc-tag system to identify each cell line but were unable to detect any Gluc after immunobinding. IHC revealed that the tumors might have been positive for the reporter correlating with RASAL1 down-regulation. We will use CRISPR/Cas9 (*36*) to knock out putative tumor suppressor gene expression in neural stem cells in an effort to validate our previous results and to determine putative tumor suppressor pathways involved in GBM-oncogenesis. When we identify GBM-oncogenesis pathways to therapeutically interact on, we could then perform drug screens on these cells to specifically target GBM subsets that depend on tumor suppressor inactivity.

In chapter six we set up an *ex vivo* system to image adipose-derived mesenchymal stem cells in large animal IVDs. We showed that the use of secreted Gluc is more effective than the use of Fluc. We might be able to use our system to study stem cell regeneration in IVD degeneration. Questions such as stem cell fate and their mode of action still need to be addressed in order to understand IVD regeneration. Insight into regenerative stem cell biology possibly allows for optimization and stimulation of stem cell transplantation in order to increase regenerative efficacy for intervertebral disc degenerative diseases and/or to improve current treatment strategies for patients.

REFERENCES

1 R. Stupp *et al.*, Radiotherapy plus concomitant and adjuvant temozolomide for glioblastoma. *N. Engl. J. Med.* **352**, 987–96 (2005).

2 N. R. Smoll, Relative survival of childhood and adult medulloblastomas and primitive neuroectodermal tumors (PNETs). *Cancer.* **118**, 1313–22 (2012).

3 H. Zheng *et al.*, p53 and Pten control neural and glioma stem/progenitor cell renewal and differentiation. *Nature.* **455**, 1129–33 (2008).

4 D. Friedmann-Morvinski *et al.*, Dedifferentiation of neurons and astrocytes by oncogenes can induce gliomas in mice. *Science.* **338**, 1080–4 (2012).

5 R. G. W. Verhaak *et al.*, Integrated genomic analysis identifies clinically relevant subtypes of glioblastoma characterized by abnormalities in PDGFRA, IDH1, EGFR, and NF1. *Cancer Cell.* **17**, 98–110 (2010).

6 C. W. Brennan *et al.*, The somatic genomic landscape of glioblastoma. *Cell.* **155**, 462–77 (2013).

7 M. D. Taylor *et al.*, Molecular subgroups of medulloblastoma: the current consensus. *Acta Neuropathol.* **123**, 465–72 (2012).

8 D. Groothuis, The blood-brain and blood-tumor barriers: A review of strategies for increasing drug delivery. **2**, 45–59 (2000).

9 D. N. Louis *et al.*, The 2007 WHO classification of tumours of the central nervous system. *Acta Neuropathol.* **114**, 97–109 (2007).

10 A. D. Woolf, B. Pfleger, Burden of major musculoskeletal conditions. *Bull. World Health Organ.* **81**, 646–56 (2003).

11 H. Tapp, E. N. Hanley, J. C. Patt, H. E. Gruber, Adipose-Derived Stem Cells: Characterization and Current Application in Orthopaedic Tissue Repair. *Exp. Biol. Med.* **234**, 1–9 (2009).

12 K. E. A. van der Bogt *et al.*, Comparison of transplantation of adipose tissue- and bone marrow-derived mesenchymal stem cells in the infarcted heart. *Transplantation.* **87**, 642–52 (2009).

13 D. Sakai *et al.*, Regenerative effects of transplanting mesenchymal stem cells embedded in atelocollagen to the degenerated intervertebral disc. *Biomaterials.* **27**, 335–45 (2006).

14 M. Alini *et al.*, Are animal models useful for studying human disc disorders/degeneration? *Eur. spine J.* **17**, 2–19 (2008).

15 N. Kimelman *et al.*, 455. Genetically Engineered Adult Stem Cells and Hybrid Scaffolds as a Platform for Intervertebral Disc Regeneration. *Mol. Ther.* **13**, S175–S176 (2006).

16 C. P. L. Paul *et al.*, Simulated-physiological loading conditions preserve biological and mechanical properties of caprine lumbar intervertebral discs in ex vivo culture. *PLoS One.* **7**, e33147 (2012).

17 B. Sherf, S. Navarro, R. Hannah, K. Wood, Dual-Luciferase® reporter assay: An advanced co-reporter technology integrating firefly and Renilla luciferase assays. *Promega Notes* (1996) (available at http://dibernardo.tigem.it/internal-site/files/website/luc_assay.pdf).

18 P. Mali *et al.*, RNA-guided human genome engineering via Cas9. *Science.* **339**, 823–6 (2013).

19 E. Betzig, G. H. Patterson, R. Sougrat, Imaging intracellular fluorescent proteins at nanometer resolution. **313**, 1642–1645 (2006).

20 N. C. Shaner, P. A. Steinbach, R. Y. Tsien, A guide to choosing fluorescent proteins. *Nat. Methods.* **2**, 905–9 (2005).

21 M. Ashburner *et al.*, Gene ontology: tool for the unification of biology. The Gene Ontology Consortium. *Nat. Genet.* **25**, 25–9 (2000).

22 M. Rebhan, V. Chalifa-Caspi, J. Prilusky, D. Lancet, GeneCards: integrating information about genes, proteins and diseases. *Trends Genet.* **13**, 163 (1997).

23 H. Ledford, Cancer: The Ras renaissance. *Nature.* **520**, 278–280 (2015).

24 A. T. Baines, D. Xu, C. J. Der, Inhibition of Ras for cancer treatment: the search continues. *Future Med. Chem.* **3**, 1787–808 (2011).

25 J. BOS, RAS ONCOGENES IN HUMAN CANCER - A REVIEW. **49**, 4682–4689 (1989).

26 McLendon, Comprehensive genomic characterization defines human glioblastoma genes and core pathways. *Nature.* **455**, 1061–8 (2008).

27 C. H. Li, Y. Chen, Targeting EZH2 for Cancer Therapy: Progress and Perspective. *Curr. Protein Pept. Sci.* (2015) (available at http://www.ncbi.nlm.nih.gov/pubmed/25854924).

28 D. Liu, C. Yang, E. Bojdani, A. K. Murugan, M. Xing, Identification of RASAL1 as a major tumor suppressor gene in thyroid cancer. *J. Natl. Cancer Inst.* **105**, 1617–27 (2013).

29 M. Ohta *et al.*, Decreased expression of the RAS-GTPase activating protein RASAL1 is associated with colorectal tumor progression. *Gastroenterology*. **136**, 206–16 (2009).

30 H. Chen *et al.*, Hypermethylation and clinicopathological significance of RASAL1 gene in gastric cancer. *Asian Pac. J. Cancer Prev.* **14**, 6261–5 (2013).

31 V. Afanassiev, Preparation of DNA and protein micro arrays on glass slides coated with an agarose film. *Nucleic Acids Res.* **28**, 66e–66 (2000).

32 M. Terweij *et al.*, Recombination-Induced Tag Exchange (RITE) Cassette Series to Monitor Protein Dynamics in Saccharomyces cerevisiae. *G3: Genes|Genomes|Genetics*. **3**, 1261–1272 (2013).

33 M. Smits *et al.*, EZH2-regulated DAB2IP is a medulloblastoma tumor suppressor and a positive marker for survival. *Clin. Cancer Res.* **18**, 4048–58 (2012).

34 Antitumor effects of pharmacological EZH2 inhibition on malignant peripheral nerve sheath tumor through the miR-30a and KPNB1 pathway. *Mol. Cancer* (available at http://apps.webofknowledge.com/full_record.do?product=UA&search_mode=GeneralSearch&qid=10&SID=Y27COxiSLVb1MbCZ5DP&page=1&doc=1).

35 Ribavirin as a tri-targeted antitumor repositioned drug. *Oncol. Rep.* (available at http://apps.webofknowledge.com/full_record.do?product=UA&search_mode=GeneralSearch&qid=12&SID=Y27COxiSLVb1MbCZ5DP&page=1&doc=2).

36 L. Cong *et al.*, Multiplex genome engineering using CRISPR/Cas systems. *Science*. **339**, 819–23 (2013).

8 SUMMARY

FUNCTIONAL MOLECULAR IMAGING OF CANCER DEVELOPMENT AND STEM CELL REGENERATION IN THE NERVOUS SYSTEM

Brain tumors are devastating diseases that have a great impact on patients. Glioblastomas are high-grade gliomas with poor prognosis while medulloblastoma patients have a better outcome. Despite this, cognitive effects as a consequence of the treatment significantly reduce medulloblastoma patient quality of life. While lower back pain is considered a pathology that has significantly less impact on patients compared to brain tumors, a relatively high incidence makes it a disease with great socio-economic impact.

It is hypothesized that brain tumors may arise from aberrant stem cells and clonal selection, resulting in heterogeneous tumor development. Tumor heterogeneity and clonal selection remains to be one of the foremost challenges in developing adequate therapies. While in brain tumors, stem cells may prove to be the cause of progressive disease, stem cell transplantation might also be beneficial in tissue regeneration in, for example, degenerated intervertebral disc.

In an effort to develop a method to study tumor heterogeneity we developed a series of functional bioluminescent reporters that can be used in multiplex. Therefore, we fused epitope tags to the naturally secreted functional bioluminescent reporter *Gaussia* luciferase. We then used a tag-specific antibody binding assay to separately measure each secreted reporter from cell culture medium or blood. We showed that by using this method we were able to follow multiple brain tumor cell lines, each expressing a reporter with different tag, in co-culture *in vitro* and *in vivo*. We then used this method to study the function of putative tumor suppressors in glioblastomas.

First, we compiled a comprehensive list of putative tumor suppressor genes and compared this list with gene expression data of medulloblastoma to identify putative tumor suppressor genes that are down regulated. Here we identified DAB2IP, a RAS-GTPase activating protein that is suppressed by EZH2-induced methylation. We also showed that DAP2IP expression in medulloblastoma is a positive marker for patient survival. We then used this list to identify down regulated putative tumor suppressor genes in glioblastoma. We then created neural precursor cell lines expressing short hairpin RNA against selected putative tumor suppressor genes and expressing a specific tagged reporter. We then co-injected these cells in the mouse striatum and analyzed tumor development. We found that RASAL1 might act as a tumor suppressor in neural precursor cells and that knock down can possibly result in tumor induction.

Then, we used luciferase reporters to image adipose derived mesenchymal stem cells over prolonged periods of time inside large mammal intervertebral discs to study stem cell regeneration. We therefore injected luciferase-expressing adipose derived mesenchymal stem cells in intervertebral discs and cultured them over time under simulated loading conditions to mimic physical load. We were able to do bioluminescent imaging of stem cells in goat intervertebral discs, despite confounding

factors that might induce interference. We also found that *Gaussia* luciferase is more suited to image cells in intervertebral discs compared to *Firefly* luciferase.

This research may provide new insights into brain tumor development and heterogeneity and in stem cell biology, providing novel approaches for therapeutic modalities.

9

NEDERLANDSE SAMENVATTING
LIST OF PUBLICATIONS
CURRICULUM VITAE
DANKWOORD

FUNCTIONELE MOLECULAIRE BEELDVORMING VAN DE ONTWIKKELING VAN KANKER EN REGENERATIE DOOR STAMCELLEN IN HET CENTRAAL ZENUWSTELSEL

Een hersentumor is een ernstige ziekte die een grote impact heeft op patiënten. Een glioblastoom is een hooggradig glioom met een uiterst slechte prognose, terwijl patiënten met een medulloblastoom een beter vooruitzicht hebben. Desondanks zijn cognitieve effecten als gevolg van de behandeling aanzienlijk en vermindert de kwaliteit van leven van een patiënt met een medulloblastoom aanzienlijk. Terwijl de pijn in de onderrug (lumbago) wordt beschouwd als een ziekte die aanzienlijk minder invloed heeft op patiënten in vergelijking met hersentumoren, maakt de relatief hoge incidentie het een ziekte met grote sociaaleconomische gevolgen.

Er wordt verondersteld dat hersentumoren kunnen voortvloeien uit afwijkende stamcellen en klonale selectie, wat resulteert in heterogene tumorontwikkeling. Tumor heterogeniteit en klonale selectie blijft een van de belangrijkste uitdagingen bij het ontwikkelen van geschikte therapieën. Terwijl in hersentumoren de stamcellen de oorzaak van ziekte progressieve kunnen zijn, is stamceltransplantatie een mogelijke oplossing voor weefselregeneratie in bijvoorbeeld gedegenereerde tussenwervelschijven.

Om een methode te ontwikkelen om tumor heterogeniteit te bestuderen hebben we een serie functionele bioluminescente reporters gemaakt die gebruikt kunnen worden in een multiplex analyse. Daarom hebben we de van nature gesecreteerde *Gaussia* luciferase reporter gefuseerd met epitoop labels. Vervolgens hebben we gebruik gemaakt van een immuun-bindingsassay waarmee we met label-specifieke antilichamen elke uitgescheiden reporter van cel medium of bloed afzonderlijk kunnen meten. We hebben aangetoond dat we met deze methode meerdere hersentumorcellijnen konden volgen, elk met expressie van een ander gelabelde reporter in co-culture *in vitro* en *in vivo*. Vervolgens hebben we deze methode gebruikt om de functie van potentiële tumor suppressorgenen in glioblastomen te bestuderen.

Eerst hebben we een uitgebreide lijst samengesteld met mogelijke tumor suppressor genen en deze vergeleken met genexpressiedata van medulloblastomen om vermeende tumor suppressor genen te identificeren die lager tot expressie worden gebracht. Op deze manier hebben we DAB2IP geïdentificeerd, een RAS-GTPase activerend eiwit dat wordt onderdrukt door EZH2-geïnduceerde methylatie. We hebben ook aangetoond dat DAP2IP expressie in medulloblastomen een positieve marker is voor overleving van de patiënt. Vervolgens hebben we deze lijst gebruikt om in glioblastomen naar beneden gereguleerde, vermeende, tumor suppressor genen te identificeren. We hebben vervolgens neurale voorloper cellijnen gemaakt die short hairpin RNA tegen geselecteerde vermeende tumor suppressor genen en een specifieke gelabelde reporter tot expressie brachten. Vervolgens hebben we deze

cellen samen geïnjecteerd in het striatum van de muis en hebben we de ontwikkeling van tumoren geanalyseerd. We vonden dat RASAL1 mogelijk kan fungeren als een tumor suppressor in neurale voorloper cellen en dat het verminderen van de expressie ervan mogelijk kan leiden tot tumorinductie.

Vervolgens hebben we luciferase reporters gebruikt om uit vetweefsel geïsoleerde mesenchymale stamcellen over langere tijd te imagen in tussenwervelschijven van grote zoogdieren om stamcelregeneratie te bestuderen. We hebben daarom uit vetweefsel geïsoleerde mesenchymale stamcellen een luciferase reporter tot expressie laten brengen en geïnjecteerd in tussenwervelschijven van de geit en ze gekweekt onder gesimuleerde beladingscondities om fysieke belasting na te bootsen. We waren in staat om bioluminescente beeldvorming van stamcellen in geit tussenwervelschijven toe te passen, ondanks bijkomende factoren die hierin verstoringen kunnen veroorzaken. We vonden ook dat Gaussia luciferase beter geschikt is voor bioluminescente beeldvorming van cellen in tussenwervelschijven in vergelijking met Firefly luciferase.

Dit onderzoek kan nieuwe inzichten in de ontwikkeling van hersentumoren en tumorheterogeniteit en in stamcelbiologie geven, waarmee het aanknopingspunten zou kunnen geven voor nieuwe mogelijkheden voor therapeutische toepassingen.

LIST OF PUBLICATIONS

Van Rijn, S., Peeters, M., Vergroesen, P. P., Paul, C. P., Noske, D. P., Vandertop W. P., Wurdinger, T. & Helder, M. N. Bioluminescence-mediated longitudinal monitoring of adipose-derived stem cells in a large mammal ex vivo organ culture. *Sci Rep.* **5,** 13960 (2015).

Van Rijn, S., Würdinger, T. & Nilsson, J. Multiplex functional bioluminescent reporters using Gaussia luciferase fused to epitope tags in an immunobinding assay. *Methods Mol Biol.* **1098,** 231-47 (2014).

Van Rijn, S., Nilsson, J., Noske, D. P., Vandertop, W. P., Tannous, B. A. & Würdinger, T. Functional multiplex reporter assay using tagged Gaussia luciferase. *Sci Rep.* **3,** 1046 (2013).

Smits, M., **van Rijn, S.**, Hulleman, E., Biesmans, D., van Vuurden, D. G., Kool, M., Haberler, C., Aronica, E., Vandertop, W. P., Noske, D. P. & Würdinger, T. EZH2-regulated DAB2IP is a medulloblastoma tumor suppressor and a positive marker for survival. *Clin Cancer Res.* **18,** 4048-58 (2012).

Nilsson, R. J., Balaj, L., Hulleman, E., **van Rijn, S.**, Pegtel, D. M., Walraven, M., Widmark, A., Gerritsen, W. R., Verheul, H. M., Vandertop, W. P., Noske, D. P., Skog, J. & Würdinger, T. Blood platelets contain tumor-derived RNA biomarkers. *Blood* **118,** 3680-3 (2011).

Skog, J., Würdinger, T., **van Rijn, S.**, Meijer, D. H., Gainche, L., Sena-Esteves, M., Curry, W. T. Jr, Carter, B. S., Krichevsky, A. M. & Breakefield XO. Glioblastoma microvesicles transport RNA and proteins that promote tumour growth and provide diagnostic biomarkers. *Nat Cell Biol.* **10,** 1470-6 (2008).

CURRICULUM VITAE

Sjoerd van Rijn was born in the city of Leiden on March 14, 1981. He lived his early life in the coastal town of Noordwijk and did his primary education at De Witte School and pre-university secondary education at Northgo College in this town. After a brief detour at Delft University of Technology and the Amsterdam University of Applied Sciences, Sjoerd started with the bachelor's program in Biomedical Sciences at VU University in Amsterdam. There, he also did his first scientific internship with Dr. Joen Luirink and Dr. Edwin van Bloois in the department of molecular microbiology of VU University, working on the elucidation of Sec and YidC dependent membrane protein integration. He obtained his bachelor's degree in 2005. After a year of working and travelling to New Zealand, Australia and Indonesia he commenced with the master's program in Oncology at the VU University Medical Center. He then completed his first master's program scientific internship in the laboratory of professor Victor van Beusechem at the genetherapy unit of the VU University Medical Center department of Medical Oncology. He there worked on the enhancement of oncolytic potency of conditionally replicative adenoviruses. The last scientific internship was accomplished in Massachusetts General Hospital in Boston, were he joined the Breakefield lab to work together with Dr. Johan Skog on the development of microvesicle biology and diagnostics. He then returned to Amsterdam to start a PhD training in the newly established Neuro-oncology Research Group of the Department of Neurosurgery at the VU University Medical Center Cancer Center Amsterdam. He worked there together with professor Thomas Würdinger and Dr. David Noske on the development and application of functional molecular imaging tools in tumors and regenerative stem cells in the central nervous system. Sjoerd has now accepted a postdoc position at the DKFZ in Heidelberg, in the Pediatric Neuro-oncology group of Professor Stefan Pfister and Dr. Marcel Kool.

DANKWOORD

Ik hou het kort…

Mijn promotietraject is me best zwaar gevallen. Ik begon heel ambitieus aan mijn projecten en werkte hard om zo snel mogelijk data te krijgen. Het nadeel van een, toen nog, jong lab met over de breedte en de diepte weinig ervaring is dat de onderzoeksinfrastructuur nog opgebouwd moet worden. Hierdoor ging er veel tijd zitten in het opzetten van methoden in plaats van het genereren van data, hetgeen zo belangrijk is om publicaties te maken. Dit kwam bovenop het gebrek aan mijn eigen onderzoekservaring, de reden waarom je een promotietraject doorloopt.

Zeker de laatste twee jaren zijn me zwaar gevallen. Door tegenvallende vorderingen in mijn onderzoek kreeg ik steeds meer het gevoel heel veel in mijn onderzoek te stoppen maar er steeds minder uit terug te krijgen. Mijn motivatie was bij tijd en wijle tanende naar niveau Marianentrog. Maar zonder dalen geen pieken. Het zit er op! Ik heb met hangen en wurgen en een hoop getreuzel toch een proefschrift bij elkaar weten te schrijven en het resultaat ligt hier voor je. Waar mijn onderzoek mij menigmaal op het randje van wanhoop heeft gedreven, zijn jullie het die mij net zo vaak weer van die rand weggehaald hebben. Mijn promotie heb ik daarom vooral aan jullie te danken. Met het risico om mensen tekort te doen ga ik toch een aantal mensen in het bijzonder noemen.

Beste Tom, ik zal het nooit vergeten toen ik je voor het eerst ontmoette bij de koffiemachine in het CCA, waarna je me naar Mass General in Boston hebt gehaald voor een stage bij Xandra en Johan. Een avontuur dat ik voor geen goud had willen missen! Nadat jij in Amsterdam de NRG met David hebt opgezet, heb jij mij de kans gegeven om mijn promotie bij jullie te doen. Wat hebben we veel meegemaakt en wat zijn we in de loop van de tijd veranderd! Gegroeid, kan ik wel zeggen. Onderzoek doen is zoveel meer dan alleen maar pipetteren. Het is onderhandelen met partners, het is je resultaten verkopen, het is je zaak verdedigen, het is politiek bedrijven. Jij snapt dat spel als geen ander en, hoewel sommige elementen misschien niet mijn tweede natuur zijn, ik heb enorm veel van je geleerd. Ook heb je nooit je vertrouwen in mij verloren, zelfs niet toen daar misschien alle reden voor was. Jij hebt mij uiteindelijk alle kansen gegeven om mijn promotie tot een mooi einde te brengen en zelfs daarna nog steek je je hand voor mij in het vuur. Ik ben je daar zo dankbaar voor. Ik zal je niet teleurstellen in Heidelberg!

Beste David, jij bent de laconieke vaste rots in de branding van de NRG. Als "Onze man in de Kliniek" ben je achter de schermen waarschijnlijk de reden dat de organisatie draaiende bleef. Ook wij hebben samen het hele NRG avontuur meegemaakt en ik vind het knap dat je altijd zo ontspannen en goedlachs bleef, ook als er soms wat kreukels gladgestreken moesten worden. Volgens mij heb ik je nog nooit uit je slof zien schieten. Je relativisme kon ik goed hebben en je had toch altijd een aardig woordje over als ik er even doorheen zat met mijn motivatie.

Ook jij hebt het vertrouwen in mij nooit verloren en mede dankzij jou is mijn promotie alsnog tot een goed einde gekomen. Veel dank voor alles wat je voor me gedaan hebt!

Beste professor Vandertop, hoewel onze concrete samenwerking zich voornamelijk de laatste tijd, rond mijn promotie, heeft afgespeeld wil ik u ook graag bedanken voor de kans die u mij heeft gegeven om deze promotie bij neurochirurgie succesvol af te ronden. Ik hou van uw efficiëntie, zowel in uw woorden als uw daden. De snelheid waarmee u altijd handelt met revisies van manuscripten en dergelijke is alom geroemd! Als u bij gelegenheden de hele club toesprak, bleek wel degelijk dat u op de hoogte was van het reilen en zeilen binnen de NRG en u wist dat toch altijd subtiel maar raak aan te stippen. Ongetwijfeld is uw rol achter de schermen groter dan ik kan vermoeden en ik dank u daarvoor hartelijk.

Hoog- en Zeergeleerde opponenten van de leescommissie, Ik dank u hartelijk dat u mijn proefschrift op wetenschappelijke waarde heeft willen beoordelen en met mij van gedachten wilt wisselen over mijn werk. Professor Van Beusechem, beste Victor, ook aan jou heb ik veel te danken. Ik heb mijn eerste masterstage bij je mogen lopen en jij hebt me bij Tom voorgedragen om naar Boston te gaan. Het verloop van mijn wetenschappelijke carrière heb ik dus in eerste instantie aan jou te danken. Ik waardeer je nuchtere kijk op de zaken en dank je voor alles wat je voor me hebt betekend.

Ik bedank stichting STOPhersentumoren.nl en stichting VUMC CCA voor het financieel mogelijk maken van mijn onderzoek en hun onaflatende inzet om onderzoek naar kanker, en hersentumoren in het bijzonder, op alle mogelijke fronten te steunen. Jullie hulp is onontbeerlijk voor ons onderzoek. Klaske en Nico, de energie en het enthousiasme waarmee jullie stichting STOPhersentumoren.nl en alle gerelateerde evenementen vorm geven is werkelijk ongelofelijk!

Beste Esther, Bart, Daniëla, Xi Wen, Postdocs zijn de pijler waar het onderzoek op bouwt. Nu ben ik zelf ook aan de beurt om een serieuze duit in het zakje van de wetenschap te doen. Ik heb veel van jullie geleerd en had nog meer willen leren maar nu kan ik jullie alleen nog maar bedanken voor jullie hulp en samenwerking. Jullie zijn mijn voorbeeld. Esther, we zijn nu meer in elkaars onderzoeksrichting gevaren. Ik hoop dat we in de toekomst nog eens een leuk project met elkaar kunnen gaan opzetten!

Beste Laurine, jij bent de labmoeder. Dat dekt, denk ik, de gehele lading wel. Ida, als Laurine de labmoeder is, ben jij onze tante. Zonder jullie zou er van onderzoeken weinig terecht komen. Niemand zou weten waar 'ie wat moest vinden. Jullie staan altijd klaar voor iedereen met raad en daad en ik kan jullie niet genoeg bedanken voor alle hulp die jullie me in al die jaren hebben gegeven.

Tjabba Jonas! Jij hebt mij op sleeptouw genomen in de eerste anderhalf jaar van mijn promotie. Door jou weet ik hoe gek je moet zijn voor de wetenschap. Elke nacht had je weer een nieuw, gek plan in je ideeënboek gekrabbeld en ik moest dan

uit jouw verhaal een soort eenvoudig destillaat hiervan zien te ontcijferen. Ik heb veel van je geleerd, en jouw creativiteit heeft een blijvende invloed gehad op mijn wetenschappelijke denkraam. Naast werk zijn we ook bevriend geraakt en hebben we vele avonturen beleefd, waarvan ik onze tocht op de Kungsleden en het bezoek aan de sauna's aldaar het meeste herinner. Je bent een man van weinig woorden maar met een groot hart en hoewel je nu weer ver weg woont, hoop ik dat we elkaar bij gelegenheden blijven zien.

Beste Chris, Ciao Viola! jullie waren mijn eerste collega PhD-lotgenoten en ik ben blij dat ik jullie heb mogen leren kennen. Jullie hebben mij laten zien hoe je een goede PhD student wordt en daarmee een goede postdoc. Ik heb natuurlijk ook van jullie veel geleerd op werk maar misschien nog meer daarbuiten. Dank voor jullie vriendschap en ik hoop jullie nog veel te zien in de toekomst. Het gaat jullie goed en ik wen jullie natuurlijk heel veel geluk met jullie kids (nee, niet van elkaar)!

Beste collega's in Boston e.o., Xandra, Bakhos, Johan, Casey, Jon en Flavia, dank voor een onvergetelijke en leerzame tijd in Boston. Hopelijk tot snel weer!

Beste Myron, Susanna, Nik, Tonny, Ellen, Jasmina, Heleen, Edward, Francois, Piotr en Sjors. Met jullie is het altijd en overal gezellig en jullie hebben me vaak door een dalletje heengetrokken. Fijn dat jullie mijn collega's wilden zijn!

Hey Ravi, Olà Jordi, Rogier, Topper! Joe Pep, Goedemiddag Hans. Ciao Rubina! Hai Maxime, vrienden. Jullie zijn zoveel meer dan collega's. Zonder jullie had ik deze promotie nooit gered. Gelukkig (of misschien wel niet) konden we altijd op elkaar bouwen om onze ellende te verdrinken en weg te lachen. We hebben veel beleefd samen en ik ben blij dat ik jullie tot mijn vrienden mag beschouwen. Jullie zijn de besten!

Beste Michiel, ze noemen ons Waldorf en Statler. Laten we het opnemen als een compliment. Desalniettemin, ik heb enorm met je kunnen lachen en ben blij dat we elkaar nog vaak zien en spreken. Zijn we toch nog goed terecht gekomen! Fijn dat we goede vrienden zijn geworden! Dank voor alle wijze lessen en mooie uitdrukkingen (tanende).

Beste Majid, Christiane, Paul, Kelly, Juriaan, Priya, Jeroen, Leonoor, Jeroen, Marjella, Arthur, Rifka, Kevin, Marieke, Matthijs, Elske. Vrienden van de peuterspeelzaal tot en met de middelbare school, enkelen erna pas. Jullie zijn mijn beste vrienden en hoewel we langzaamaan allemaal uitwaaien is onze vriendschap blijvend en, zoals ik het laatst aan Majid omschreef, heeft weinig onderhoud nodig. Als we elkaar weer zien na een lange tijd is het alsof de tijd heeft stilgestaan. Ouwe-jongens-krentenbrood!

Lieve Tomas en Marloes, mijn enige, echte broer en zus. Wat zijn we verschillend, maar wat lijken we verdomd veel op elkaar! Ik kan me mijn leven zonder jullie niet voorstellen. Hoewel we op onze eigen manier met elkaar omgaan, weet ik dat jullie er altijd voor me zijn en vergeet niet dat ik er ook altijd voor jullie zal zijn. Suzanne en Marc, jullie zijn ook leuk! Ik ben heel blij met jullie allemaal!

Lieve Oma, wat gaat het goed met u! Al 92 jaar, of was het alweer 93 jaar? En nog in zulke goede doen. Ik ben blij dat u hier in goede gezondheid bij ons bent en dat we nog zo goed kunnen praten en leuke dingen kunnen doen. U en opa hebben ons hele leven voor ons klaar gestaan en ik ben net zo blij met u, als u met ons. Dank voor alle steun en liefde!

Lieve Pappa, zouden de meesten zeggen. Ik zeg Henk. Dat heb ik altijd gedaan. Jij hebt ons altijd onvoorwaardelijk gesteund met alles wat we deden en doen. Je staat altijd klaar, komt altijd helpen met vanalles en doet altijd je best voor ons. We mopperen wel op je als je misschien wat onbehouwen bent, maar uiteindelijk mogen we in onze handen knijpen met jou als vader. Ik zal ook wel moeten, want ik lijk toch veel op je! Carla, ik ben blij dat Henk en jij elkaar hebben gevonden. Ook jij zet je onvoorwaardelijk voor mij en mijn broer en zus in en ook voor Henk ben je de enige juiste. Ik wens dat jullie nog lang gelukkig zijn met elkaar en lekker genieten van het leven als volleerde pensionado's. Ok, nog net niet helemaal voor jou dan, Carla. Dank voor al jullie steun.

Lieve Mamma, zouden de meesten zeggen. Ik zei Mieke. Dat heb ik altijd gedaan. Ik denk niet elke dag meer aan je. Zo gaat dat, alles slijt met de tijd. Toch blijf je altijd bij me en ben ik je dankbaar omdat ik door Henk en jou ben geworden wie ik ben. Ik denk ook dat ik door jou gefascineerd ben geraakt van de verwoestende gevolgen van kanker. Door jou sta ik hier nu. Wat zou je trots geweest zijn.

Lieve Lotte, jij bent het beste wat ik aan mijn promotie heb overgehouden! Ik geloof in jou en mij!

Is het toch nog een lang verhaal geworden…
Sjoerd